Integrated Ocean Drilling Program Expedition 346 Scientific Prospectus

Asian Monsoon

Onset and evolution of millennial-scale variability of Asian monsoon and its possible relation with Himalaya and Tibetan Plateau uplift

Ryuji Tada
Co-Chief Scientist
Department of Earth and Planetary Science
Graduate School of Science
The University of Tokyo
7-3-1 Hongo, Bunkyo-ku
Tokyo 113-0033
Japan

Richard W. Murray
Co-Chief Scientist
Department of Earth and Environment
Boston University
685 Commonwealth Avenue
Boston MA 02215
USA

Carlos Andrés Alvarez Zarikian
Expedition Project Manager/Staff Scientist
Integrated Ocean Drilling Program
Texas A&M University
College Station TX 77845
USA

Published by
Integrated Ocean Drilling Program Management International, Inc.,
for the Integrated Ocean Drilling Program

Publisher's notes

Citation:
Tada, R., Murray, R.W., and Alvarez Zarikian, C.A., 2013. Asian Monsoon: onset and evolution of millennial-scale variability of Asian Monsoon and its possible relation with Himalaya and Tibetan plateau uplift. *IODP Sci. Prosp.,* 346. doi:10.2204/iodp.sp.346.2013

Distribution:
Electronic copies of this series may be obtained from the Integrated Ocean Drilling Program (IODP) Scientific Publications homepage on the World Wide Web at **www.iodp.org/scientific-publications/.**

This publication was prepared by the Integrated Ocean Drilling Program U.S. Implementing Organization (IODP-USIO): Consortium for Ocean Leadership, Lamont-Doherty Earth Observatory of Columbia University, and Texas A&M University, as an account of work performed under the international Integrated Ocean Drilling Program, which is managed by IODP Management International (IODP-MI), Inc. Funding for the program is provided by the following agencies:

National Science Foundation (NSF), United States

Ministry of Education, Culture, Sports, Science and Technology (MEXT), Japan

European Consortium for Ocean Research Drilling (ECORD)

Ministry of Science and Technology (MOST), People's Republic of China

Korea Institute of Geoscience and Mineral Resources (KIGAM)

Australian Research Council (ARC) and GNS Science (New Zealand), Australian/New Zealand Consortium

Ministry of Earth Sciences (MoES), India

Coordination for Improvement of Higher Education Personnel, Brazil

Disclaimer

This IODP *Scientific Prospectus* is based on precruise Science Advisory Structure panel discussions and scientific input from the designated Co-Chief Scientists on behalf of the drilling proponents. During the course of the cruise, actual site operations may indicate to the Co-Chief Scientists, the Staff Scientist/Expedition Project Manager, and the Operations Superintendent that it would be scientifically or operationally advantageous to amend the plan detailed in this prospectus. It should be understood that any proposed changes to the science deliverables outlined in the plan presented here are contingent upon the approval of the IODP-USIO Science Services, TAMU, Director in consultation with IODP-MI.

January 2013

Abstract

Integrated Ocean Drilling Program Expedition 346 will core and log seven sites covering a wide latitudinal range in the Japan Sea and one site in the northern East China Sea to test the hypothesis that Pliocene–Pleistocene uplift of the Himalaya and Tibetan Plateau, and the consequent emergence of the two discrete modes of Westerly Jet circulation, caused the amplification of millennial-scale variability of the East Asian summer monsoon (EASM) and East Asian winter monsoon (EAWM) and provided teleconnection mechanism(s) for Dansgaard–Oeschger cycles.

Specific scientific objectives are

- To address the timing of onset of orbital- and millennial-scale variability of the EASM and EAWM and their relation with variability of Westerly Jet circulation;
- To reconstruct orbital- and millennial-scale changes in surface and deepwater circulations and surface productivity in the Japan Sea during at least the last 5 m.y.;
- To reconstruct the history of the Yangtze River discharge using cores from the northern end of the East China Sea, as it reflects variation and evolution in EASM and exerts an impact on the paleoceanography of the Japan Sea; and
- To examine the interrelationship among the EASM, EAWM, nature and intensity of the influx through the Tsushima Strait, the intensity of winter cooling, surface productivity, ventilation, and bottom water oxygenation in the Japan Sea and their changes during the last 5 m.y.

A latitudinal transect of the Japan Sea will be cored to monitor the behaviors of the Westerly Jet, EAWM, and the Tsushima Warm Current. The southern part of the transect also will be used to reconstruct the behavior of the Subpolar Front and examine its relationship with the Westerly Jet and sea level changes, whereas the northern part of the transect will be used to identify ice-rafted debris events and reconstruct temporal variation in its southern limit. In addition, a depth transect of sites will reconstruct the ventilation history of the Japan Sea and examine the relation between ventilation and the nature of the influx through the Tsushima Strait and/or the intensity of winter cooling. We also will drill in the northern part of the East China Sea to monitor the Yangtze River discharge history that should reflect variations in EASM intensity.

Expedition 346 will potentially recover ~6060 m of sediment. Drilling strategies will include triple advanced piston corer, single or double extended core barrel, and single rotary core barrel (East China Sea) drilling. We will drill in 316–3435 m water depth.

Considering the significant transit time at the beginning of the expedition (~2 weeks), this coring schedule within the remaining 6 weeks of the expedition is indeed ambitious and will require tight operational planning and flexibility. The final operations plan and number of sites to be cored is contingent upon the R/V *JOIDES Resolution* operations schedule, operational risks, and the outcome of requests for territorial permission to occupy particular sites.

All relevant IODP sampling and data policies will be in effect. On board sampling will be restricted to acquiring ephemeral data and to limited low-resolution sampling of parameters that may be affected by even short-term core storage. Most sampling will be deferred to a postcruise sampling party at the Kochi Core Center (KCC; Japan). An onshore "X-ray fluorescence (XRF) scanning plan" will be developed in consultation with scientific participants.

Schedule for Expedition 346

Expedition 346 is based on Integrated Ocean Drilling Program (IODP) drilling Proposal 605-Full2-Addendum 3 (**iodp.tamu.edu/scienceops/expeditions/asian_monsoon.html**). Following ranking by the IODP Scientific Advisory Structure, the expedition was scheduled for the R/V *JOIDES Resolution,* operating under contract with the U.S. Implementing Organization (USIO).

At the time of publication of this *Scientific Prospectus,* the expedition is scheduled to start in Valdez, Alaska (USA), on 29 July 2013 and to end in Busan, Korea, on 28 September. A total of 60 days (61 calendar days due to the crossing of the International Date Line) will be available for the transit, drilling, coring, and downhole measurements described in this report (for the current detailed schedule, see **iodp.tamu.edu/scienceops/**). Further details about the facilities aboard the *JOIDES Resolution* and the USIO can be found at **www.iodp-usio.org/.**

Introduction

The overall goal of Expedition 346 is to core and log sites on a latitudinal transect in the Japan Sea and one site in the northern East China Sea to test the hypothesis that Pliocene–Pleistocene uplift of the Himalaya and Tibetan Plateau (HTP) and the consequent emergence of the two discrete modes of Westerly Jet circulation caused the

amplification of millennial-scale variability of the East Asian monsoon and provided teleconnection mechanism(s) for Dansgaard–Oeschger cycles (DOCs).

The research is oriented toward exploring the relationships between atmospheric processes (e.g., positioning of Westerly Jet circulation), rainfall (e.g., Yangtze River discharge), and oceanic processes (e.g., surface water circulation into and out of the Japan Sea and deepwater convection within the sea). Multiple timescales are targeted, and assessing climate sensitivity variations through time and space are an important component of the research plan. Results from this expedition will enable reconstruction of the onset and evolution of orbital- and millennial-scale variations of summer monsoon, winter monsoon, Westerly Jet position and intensity, desertification in East and Central Asia, and their interrelationships during the last 5 m.y. We will also be exploring the linkages between orbital- and millennial-scale variations of the East Asian summer monsoon (EASM) and East Asian winter monsoon (EAWM), discharge of the Yangtze and Yellow Rivers, and the paleoceanography of the Japan Sea.

Specific scientific objectives are

- To address the timing of onset of orbital- and millennial-scale variability of the EASM and EAWM and their relation with variability of Westerly Jet circulation;
- To reconstruct orbital- and millennial-scale changes in surface and deepwater circulation and surface productivity in the Japan Sea during at least the last 5 m.y.;
- To reconstruct the history of the Yangtze River discharge using cores from the northern end of the East China Sea as it reflects variation and evolution in EASM and exert an impact on the paleoceanography of the Japan Sea; and
- To examine the interrelationship among EASM, EAWM, the nature and intensity of the influx through the Tsushima Strait, the intensity of winter cooling, surface productivity, ventilation, and the bottom water oxygenation in the Japan Sea and their changes during the last 5 m.y.

During Expedition 346, we aim to collect the geological evidence necessary to address these objectives by drilling and coring at seven sites in the Japan Sea and one site in the northern part of the East China Sea (Fig. **F1**). We plan to drill a latitudinal transect of the Japan Sea (proposed Sites JB-3, JB-2, JB-1, YR-1, UB-1, YB-2, and YB-1) to monitor the behaviors of the Westerly Jet, EAWM, and the Tsushima Warm Current (TWC). The southern part of the transect (proposed Sites YR-1, UB-1, and YB-2) also will be used to reconstruct the behavior of the Subpolar Front and examine its relationship with the Westerly Jet and sea level changes, whereas the northern part of the

transect (proposed Sites JB-3, JB-2, JB-1, and YR-1) will be used to identify ice-rafted debris (IRD) events and reconstruct temporal variation in its southern limit. In addition, a depth transect (proposed Sites YB-1, YB-2, JB-1, JB-2, and JB-3) will reconstruct the ventilation history of the Japan Sea and examine the relation between ventilation and the nature of the influx through the Tsushima Strait and/or the intensity of winter cooling. We also will drill in the northern part of the East China Sea (proposed Site ECS-1B) to monitor the Yangtze River discharge history, which should reflect variations in EASM intensity (Kubota et al., 2010).

Paleoclimatology and paleoceanography of the East Asian monsoon system, the Japan Sea, and marginal basins

Onset and evolution of millennial-scale variability of Asian monsoon and its possible linkage with uplift of the Himalaya and Tibetan Plateau

Elucidation of the processes and mechanisms of millennial-scale abrupt climatic changes (e.g., DOCs) is one of the most important subjects outlined in the IODP Initial Science Plan "Earth, Oceans, and Life." Such millennial-scale climatic variability is a global phenomenon and is characterized by complex interactions among the atmosphere, ocean, cryosphere, and biosphere (e.g., Bond et al., 1993; Broecker et al., 1990). However, the spatial patterns, amplification, and propagation mechanisms and ultimate driving forces of DOCs are still not well understood. Reconstructing the evolution of DOCs within a precise temporal and spatial context is necessary to solve these problems.

The East Asian and Indian summer monsoon have varied significantly in association with DOCs (Schulz et al., 1998; Tada et al., 1999; Wang et al., 2001, 2008; Tada, 2004). In addition, climate and oceanography in the western Mediterranean Sea and surrounding areas varied in association with DOCs, with the variation characterized by a northward shift and intensification of the Westerly Jet during the Dansgaard–Oeschger stadials (Moreno et al., 2002; Cacho et al., 2002; Sánchez Goñi et al., 2002). Shifts in circulation of the Westerly Jet are also reported from North America, with its southward shift during Dansgaard–Oeschger stadials (Asmerom et al., 2010; Wagner et al., 2010).

Nagashima et al. (2007, 2011) showed that the Westerly Jet path over the Japan Sea also shifted southward during Dansgaard-Oeschger stadials. Together with the west-

ern Mediterranean and North American results described above, this suggests that the Westerly Jet circulation mode changed in association with DOCs. Because the inferred movement of the Westerly Jet axis is opposite between the Mediterranean Sea and what is documented in North America and the Japan Sea (Fig. **F2**), the shift could be characterized by different mode of meandering rather than a simple north–south shift analogous to the seasonal cycle (Fig. **F3**). Ono et al. (1998) suggested that the Westerly Jet flowed along the southern side of the HTP during marine isotope stage (MIS) 2, based on eolian quartz provenance in East Asia inferred from electron spin resonance (ESR) signal intensity. If correct, the topographic effect of the HTP could be critical for causing a different course of the Westerly Jet circulation and its shift in association with DOCs. It is even possible that HTP uplift could have created multiple stable modes of Westerly Jet circulation and triggered the onset of DOC-type climatic variability (Tada, 2004).

According to the study of IRD in the North Atlantic, millennial-scale IRD events are recognized at least since 1.4 Ma (Jansen et al., 2000; Raymo et al., 1998) and could be as old as 2.5 Ma (Mc Intyre et al., 2001; Becker et al., 2006). However, it is not well constrained when such millennial-scale variability started, how it evolved through time, and what is its relationship with the onset and evolution of the orbital-scale variability. Furthermore, the timing and mode of uplift of the HTP is still being debated (e.g., Copeland, 1997; Tapponnier et al., 2001; Royden et al., 2008; Wang et al., 2008), but results of recent studies suggest that HTP uplift started as early as 50 Ma and that the southern and central parts of Tibet approximately reached their present height by 34 Ma (e.g., Rowley and Currie, 2006). Records from inland Asia also demonstrate that uplift of northern Tibet started around 3.6 Ma (Zheng et al., 2000; Li et al., 1997) and that uplift of Himalaya restarted during the late Pliocene to Pleistocene and continued until the present (Jain et al., 2000; Sakai et al., 2002; Vance et al., 2003; Wobus et al., 2003). Because uplift of these areas should have enhanced the extent and altitude of the topographic barrier against the Westerly Jet, it is possible that the course and intensity of the Westerly Jet were also influenced significantly (Rea et al., 1998). Thus, results of recent paleoclimatic and tectonic studies seem concordant with the idea that HTP uplift amplified the DOC-type millennial-scale variability of Westerly Jet circulation through the topographic effect.

Recent climatic model simulation studies that evaluate the impact of HTP uplift on the onset and evolution of Asian monsoon and its variability suggest that desertification in inland Asia and the EASM and EAWM and their orbital-scale variability neither started nor evolved simultaneously (An et al., 2001; Liu and Yin, 2002; Abe et al.,

2003, 2004; Kitoh, 2004). According to the models, the Indian monsoon and EASM intensified from 3.6 to 2.6 Ma and were stronger than the modern monsoon during the relatively early stage of the uplift. Intensities slightly decreased during the later stages of uplift, whereas the EAWM intensified only after ~50% of the present height of Tibet was attained and increased from 3.6 Ma, continuing to do so after 2.6 Ma. Temporal variations of the summer and winter monsoon proxies in Chinese loess seem consistent with these climatic simulation results (An et al., 2001), although questions remain about the validity of the winter monsoon proxies used (grain size of loess and paleosol) (Ding et al., 2005).

In addition, the behavior of the Westerly Jet and its relation with East Asian monsoon during the last 2.6 m.y. has been discussed on the basis of the grain size of Chinese loess (Sun et al., 2003). However, the relation between the Westerly Jet and the East Asian monsoon before 2.6 Ma, as well as the onset timing and evolution process of millennial-scale variability of EASM and EAWM, have never been fully explored.

Potential contributions from Expedition 346

We aim to reconstruct the axial position and intensity of the Westerly Jet through examination and comparison of the eolian dust provenance, flux, and grain size along the latitudinal transect of the Japan Sea. Eolian dust grain size and flux are considered as useful parameters to evaluate the intensity of transport wind and aridity of source areas (e.g., Rea et al., 1985), and reconstruction of the westerly jet axis position may be possible through examination of eolian dust grain size variation along the north–south transect (e.g., Rea and Leinen, 1988). Additionally, approaches such as ESR and quartz crystallinity (e.g., Nagashima et al., 2007, 2011) are likely to be able to resolve contrasts between quartz respectively sourced from Mongolian Gobi (Siberia–Northeastern China), Taklimakan, and the Japanese arc. Application of end-member modeling (e.g., Prins et al., 2000) to the grain size distribution data combined with eolian dust provenance data may further improve our estimation of the relative contribution and grain size distribution of eolian dust from different sources as well as detrital particles delivered from rivers by suspension in the surface water. Other approaches focusing on geochemistry and radiogenic isotopic tracers of terrigenous provenance (e.g., Irino and Tada, 2000, 2002) are likely to be fruitful as well.

We hope to reconstruct the winter monsoon intensity through examination of IRD abundance and distribution along the northern latitudinal transect in the Japan Sea. At present, stronger winter monsoon wind produces deep water, called Japan Sea

Proper Water (JSPW), through sea ice formation in the northwestern part of the Japan Sea (Talley et al., 2003). Consequently, sea ice formation and deepwater ventilation could reflect winter monsoon intensity. Ikehara (2003) described the occurrence of millennial-scale IRD events in the northern part of the Japan Sea during the last 160 k.y. Correlation of these IRD data with the lightness (L*) profile of Core MD01-2407 suggests that many of these IRD events coincide with the intervals of high L* values, further suggesting intense deepwater ventilation that in turn coincides with Heinrich events (Fig. **F4**). Grain size studies of the loess–paleosol sequence in China also suggest intensification of winter monsoon during Heinrich events (e.g., Porter and An, 1995).

We aim to reconstruct summer monsoon intensity through examination of surface water temperature and salinity changes and variation in chemistry, mineralogy, and mass accumulation rate of the terrigenous sediment delivered from the Yangtze River at proposed Site ECS-1 on the northeastern margin of the East China Sea. Ijiri et al. (2005) reported the occurrence of light $\delta^{18}O$ spikes of planktonic foraminifer *Globigerinoides ruber* that seem to correspond to interstadials of the DOC. They interpret these spikes as reflecting low-salinity events caused by increased discharge from the Yangtze and Yellow Rivers and subsequent expansion of East China Sea Coastal Water (ECSCW) because no changes in alkenone temperature are observed during these events. It is possible to estimate salinity changes associated with these events more precisely by combining $\delta^{18}O$ with Mg/Ca measurements (Kubota et al., 2010). Recent geochemical studies of Ocean Drilling Program (ODP) Site 1145 in the northern South China Sea have also shown the potential usefulness of K/Al and Ba/Si ratios as proxy indicators for summer and winter monsoon intensities, respectively (Wehausen and Brumsack, 2002).

Collectively, these approaches targeting allied aspects of abrupt climate behavior will allow unprecedented reconstruction of the interrelationships between the EASM, EAWM, and Westerly Jet axis movement through the Pliocene–Pleistocene. Assuming appropriate age control, we further aim to compare our enhanced understanding of the East Asian monsoon from the Japan Sea and East China Sea with marine records from the northwestern Atlantic and ice cores from Antarctica as well as with data from the Okhotsk Sea to examine when the millennial-scale climatic linkage between North Atlantic and East Asia began and how it evolved.

Land-ocean linkage through monsoon variability in the East Asian continental margin

With increasing awareness of the human impact on our environment, the public is paying more attention to the impact of discharge from large rivers on the environment of continental margins and marginal seas. Society is also becoming increasingly concerned about the impact of the consequent oceanographic changes on terrestrial climate. For example, the effect of the construction of the Three Gorges Dam, and the consequent decrease in Yangtze River discharge, on the oceanographic conditions in the East China Sea and the Japan Sea and regional climate in their surrounding area has been noted (e.g., Chen, 2002; Yang et al., 2011). As described above, EASM intensity varied significantly on orbital and millennial scales (Tada et al., 1999; Wang et al., 2001, 2008; Tada, 2004; Cheng et al., 2009), which should have caused significant variation in the discharges from the Yangtze and Yellow Rivers. Tada et al. (1999) speculated that such variation in Yangtze River discharge could have been responsible for the dramatic changes in paleoceanography of the Japan Sea, leading to deposition of distinct alternations of the organic carbon–rich dark laminated layers and organic carbon–poor light bioturbated layers. However, this hypothesis has never been tested rigorously. Thus, the process(es) and mechanism(s) linking the EASM, Yangtze River discharge, and Japan Sea paleoceanography are still not fully understood in spite of their importance to evaluate the ongoing and near-future changes in the oceanography of the Japan and East China Seas as well as to climate in the surrounding land area.

The oceanography of the Japan Sea is very sensitive to the nature and amount of the influx of seawater through the Tsushima Strait. This is important because in the present East China Sea, dissolved phosphorous is mainly supplied through upwelling of the subsurface Kuroshio water to the edge of the East China Sea shelf. The upwelling is basically induced by outflow of the low-salinity water from the shelf area (Chen et al., 1999) (Fig. **F5**). Consequently, the increase in freshwater discharge from the Yangtze River enhances nutrient supply to the East China Sea through enhancement of upwelling of the nutrient-rich subsurface Kuroshio water. Because nutrient supply to the Japan Sea is dominantly carried by the TWC, it is reasonable to consider that surface productivity in the Japan Sea is controlled by nutrient flux through the Tsushima Strait, especially in timescales greater than 100 y (Fig. **F6**). In this way, variations in the summer monsoon intensity may be recorded as variations in organic phospho-

rous and carbon burial rate in the Japan Sea, and documenting variability in this system may provide an important additional constraint on behavior of the EASM.

Sedimentary deposits in the Japan Sea indicate that such changes in nutrient cycling have also happened in the past and indeed may have changed in concert with abrupt climate change. For example, Quaternary hemipelagic sediments of the Japan Sea are characterized by centimeter- to decimeter-scale alternations of organic carbon–rich dark and organic carbon–poor light layers (e.g., Tada et al., 1992) that are associated with DOCs (Tada et al., 1995, 1999) (Fig. **F7**). Based on the increase in the relative abundance of *Paralia sulcata,* a sublittoral diatom species characteristic of ECSCW, in these dark layers, Tada et al. (1999) argued that deposition of these dark layers resulted from the increasing contribution of low-salinity and nutrient-rich ECSCW to the TWC. This would in turn have caused an increase in surface biological productivity and a reduction in vertical mixing. Tada et al. (1999) further argued that the increase in relative contribution of the ECSCW to the TWC could have been caused by increased discharge from the Yangtze and Yellow Rivers in response to intensified summer monsoon. This proposed mechanism is consistent with high-resolution records of $\delta^{18}O$ in the Hulu Cave stalagmite, which suggests summer monsoon intensification during the DOC (Wang et al., 2001; Ijiri et al., 2005). These collected observations suggest an additional link between monsoonal dynamics (rainfall into the Yangtze/Yellow watersheds), ocean currents (ECSCW to the TWC), paleoproductivity (nutrients and upwelling), and sediment deposition (organic cycles).

Glacio-eustatic sea level changes may also have a profound influence on the paleoceanographic condition of the Japan Sea from orbital to millennial timescales. The sill depth of the sea became shallower than 20 m and the surface water salinity decreased drastically as a result of increasing contribution from precipitation and, thus, of the freshwater input from the surrounding rivers relative to the seawater influx through the Tsushima Strait during the Last Glacial Maximum (e.g., Oba et al., 1991, 1995; Matsui et al., 1998) (Fig. **F8**). The low-salinity surface water strengthened density stratification, causing euxinic deepwater conditions similar to the present Black Sea and resulted in deposition of a finely laminated thick, dark layer (Oba et al., 1991; Tada et al., 1999). According to a salt- and water-budget calculation using a simple box model, freshening of the surface water salinity of the Japan Sea becomes evident when the sill depth of the Tsushima Strait decreased below 30 m (Matsui et al., 1998). These studies further confirm the linkage among glacio-eustatic sea level decreases, the decrease in the surface-water salinity, development of euxinic deep water, and deposition of finely laminated dark layers.

On the other hand, periods other than glacial maxima are characterized by deposition of centimeter- to decimeter-scale alternations of dark laminated layers and light bioturbated layers, with the dark layers corresponding to the DOC interstadials (Tada et al., 1999), suggesting a link between the EASM, Yangtze River discharge, and paleoceanographic conditions of the Japan Sea. Thus, deconvolving sea level influences, driven by global climate variability (that is, ice volume), from those variables driven by EASM (such as local nutrient supply) will be critical. This requires an increased understanding of the physical dynamics of the oceanic circulation and the relationship to biogeochemical responses.

Potential contributions from Expedition 346

We aim to examine the paleoceanographic responses of the Japan Sea to variations in glacio-eustatic sea level changes and Asian monsoon dynamics through a multiproxy approach that will assess changes in surface and deepwater parameters. Site locations have been selected to record water masses in the eastern and western sides of the Japan Sea and through a near-complete depth gradient. Such reconstructions can be based on Mg/Ca and $\delta^{18}O$ (and other isotopic systems) of benthic and planktonic foraminifers, organic biomarkers (e.g., alkenones, TEX86, etc.), and other proxies, including $CaCO_3$ concentration and preservation. Deepwater oxygenation levels can be assessed by documenting the degree of lamina preservation, C/S ratio, concentrations and accumulations of redox-sensitive elements (e.g., Mo), S, U isotopes, and $\delta^{13}C$ (planktonic–benthic) (e.g., Tada et al., 1999; Crusius et al., 1999). We plan to reconstruct temporal variation in the carbonate compensation depth based on the comparison of burial flux of biogenic carbonate between the shallower and deeper sites. We also plan to reconstruct burial fluxes of biogenic silica, biogenic carbonate, and organic carbon to examine temporal changes in the nature and intensity of surface production. Geochemical proxies of export production (e.g., Ba) and terrigenous provenance are also likely to prove beneficial.

Geological and oceanographic setting of the Japan Sea and northern East China Sea

Physiographic and tectonic setting

The Japan Sea is a semi-enclosed marginal sea with an area of ~1×10^6 km^2 and an average depth of 1350 m. The sea consists of three major basins: the Japan Basin to

the north, the Yamato Basin to the southeast, and the Tsushima (Ulleung) Basin to the southwest (Fig. **F1**). The Japan, Yamato, and Tsushima (Ulleung) Basins are separated by the Yamato Rise. The Japan Sea is connected with other seas by shallow, narrow straits, namely to the East China Sea to the south through the Tsushima Strait (130 m water depth), to the North Pacific to the east through the Tsugaru Strait (130 m water depth), and to the Okhotsk Sea to the north through the Soya (55 m water depth) and Mamiya (20 m water depth) Straits. The shallow depths of these passages figures prominently in the Japan Sea's sensitivity to glacially driven sea level change.

The Japan Sea and East China Sea are backarc basins in the western margin of the North Pacific. Whereas the Japan Sea has a relatively long geological history, the history of the East China Sea (Okinawa Trough) is relatively short. The Japan Sea opened as a pull-apart basin triggered by the collision of India and Asia (Kimura and Tamaki, 1986; Tamaki et al., 1992) (Fig. **F9**). The opening started at ~32 Ma and ceased at ~15 Ma (Tamaki et al., 1992; Jolivet et al., 1994). The Japan Basin has oceanic crust especially in its eastern part and opening started at ~32 Ma, whereas the Yamato Basin has thinned continental crust with basaltic sill intrusions and opening started at ~20 Ma (Tamaki et al., 1992; Jolivet et al., 1994; Tada, 1994). The Tsushima (Ulleung) Basin is most likely floored with thinned continental crust as well, although no drilling to the acoustic basement has been conducted. A tectonically quiet "transitional interval" spanned from 10 to 7 Ma, and the east–west compressional stage started at ~7 Ma (Tamaki et al., 1992; Jolivet et al., 1994). Compression became intense, and deformation was focused on the eastern margin of the Japan Sea, where the new plate boundary seems to have formed at ~3 Ma.

The East China Sea is composed of continental shelf in its northwestern part and the Okinawa Trough in its southwestern part. The Okinawa Trough is a backarc basin behind the Ryukyu arc and is one of the rare examples of an incipient continental backarc basin (Gungor et al., 2012; Fournier et al., 2001) (Fig. **F10**). Whereas the southern Okinawa Trough is formed by focused rifting, the northern Okinawa Trough is characterized by diffuse rifting of thinned continental crust (e.g., Gungor et al., 2012).

The northern part of the Okinawa Trough began to open in the late Miocene (Kimura, 1996; Fournier et al., 2001), whereas the main phase of southern Okinawa Trough opening started at ~2 Ma (Gungor et al., 2012; Sibuet et al., 1998). Fournier et al. (2001) proposed three episodes of opening of the Okinawa Trough. The first episode is late Miocene N40W to N20E extension, the second episode is late Pliocene to early Pleistocene N20E extension, and the third episode is latest Pleistocene to present

N20W extension. The northern Ryukyu arc and southern Kyushu Island have rotated ~30° counterclockwise (Kodama and Nakayama, 1993), which probably occurred during the last 3 m.y. and was caused by termination of the opening process toward both extremities of the basin (the tapered extension model of Fournier et al., 2012). From a geometric point of view, it is possible to regard the present stage of opening of the Okinawa Trough as being similar to that of the opening of the Japan Basin 25 m.y. ago, except for the lack of a dextral strike-slip zone along the westernmost margin of the Okinawa Trough (Fournier et al., 2001).

Oceanographic setting

In the East China Sea, the Taiwan Warm Current, a branch of the Kuroshio Current, mixes with Changjiang (also known as the Yangtze) River Diluted Water to form the TWC (Ichikawa and Beardsley, 2002) (Fig. **F11**). More than 70% of the fresh water discharged from the Yangtze River is carried into the Japan Sea with the TWC (Isobe et al., 2002). As a result, the salinity of the surface water in the Japan Sea is strongly influenced by the freshwater discharge from the Yangtze River. Because the EASM supplies a large amount of fresh water to the catchment area of the Yangtze River, it is likely that the EASM influences the surface waters of the Japan Sea through the TWC. The East China Sea shelf is known as a high-productivity area, sustained by nutrients provided by upwelling of Kuroshio subsurface water (Chen and Wang, 1999) that is probably induced by estuary circulation driven by Yangtze River discharge. Thus, it is possible that productivity and bottom water oxygenation level are also controlled by the Yangtze River discharge.

The East China Sea and the Japan Sea are inextricably linked to each other. At present, the TWC, a branch of the Kuroshio Current, is the only current flowing into the Japan Sea (Fig. **F1**). After entering the Japan Sea, the TWC is divided into three branches. The first branch of the TWC flows into the Japan Sea through the eastern channel of the Tsushima Strait (Katoh, 1993; Hase et al., 1999) and moves northeastward along the Japanese coast. Its flow path is trapped within a narrow zone on the inner shelf (Hase et al., 1999; Watanabe et al., 2006) and exists throughout the year (Hase et al., 1999). This first branch is characterized by a relatively stable flow of 1–2 Sv (1 Sv = 10^6 m^3/s) (e.g., Isobe, 1994; Watanabe et al., 2006). The second branch of the TWC flows into the Japan Sea through the western channel of the Tsushima Strait (Kawabe, 1982; Hase et al., 1999) and flows northward along the continental shelf and slope with high variability (Hase et al., 1999). Its flow path is located to the west of the first branch of the TWC and is characterized by eddies associated with its own meander

(Kim and Yoon, 1999; Hase et al., 1999). This second branch of the TWC becomes distinct during late spring to early fall when the total volume transport of the TWC increases (Kawabe, 1982; Kim and Yoon, 1999; Hase et al., 1999), and the seasonal variation of its flux is relatively large (between 1 and 4 Sv) (Takikawa et al., 2005). The third branch of the TWC, called the East Korea Warm Current, flows into the Japan Sea through the western channel of the Tsushima Strait from late spring to fall and flows northward along the eastern margin of the Korean Peninsula to ~38°N. This third branch then deflects eastward to cross the central part of the Japan Sea, forming the Subpolar Front. It then merges with the first and second branches at ~40°N along the western margin of Honshu Island.

The majority of the TWC exits the Japan Sea through the Tsugaru Strait, whereas the rest flows further north along the western margin of Hokkaido Island and subsequently flows out through the Soya Strait into the Okhotsk Sea. As a result, the TWC carries heat as far north as 45°N, compared with the Kuroshio Current that penetrates only to 38°N, and gives a significant influence on the climate not only in Honshu and Hokkaido but further north in the southern part of Sakhalin.

The Japan Sea has its own deep water, JSPW. JSPW is present below ~300 m water depth and is characterized by a nearly constant salinity of 34.06‰–34.08‰, rather cold temperatures of 0.0°–0.6°C, and high dissolved oxygen concentrations of 5–7 mL/L (Sudo, 1986) (Fig. **F12**). This high oxygenation level reflects vigorous ventilation of the deep water with a residence time of a few hundred years (e.g., Gamo and Horibe, 1983; Harada and Tsunogai, 1986; Watanabe et al., 1991; Tsunogai et al., 1993).

JSPW is formed in the northwestern part of the Japan Sea as a result of severe winter cooling and consequent formation of sea ice (Talley et al., 2003) (Fig. **F13**). Consequently, deepwater ventilation could be influenced by winter monsoon intensity (Gamo, 1999). Production of JSPW is roughly balanced with inflow of the TWC during winter (Yanagi, 2002), suggesting a possible link between the influx of the TWC and ventilation in the deeper part of the Japan Sea. The concentration of dissolved oxygen in Japan Sea deep water has been significantly reduced below 1500 m water depth during the last 70 y. If this trend continues, dissolved oxygen may be eliminated within 300 y, and it has been suggested that global warming and a subsequent weakening of the winter monsoon is responsible (Gamo, 1999).

The modern Japan Sea is rather poor in nutrients partly because of the high ventilation rate and consequent short residence time of the deep water. The concentration of dissolved phosphorous in JSPW is 2.3 mM (Yanagi, 2002). The major source of phosphorous to the Japan Sea is the TWC through the Tsushima Strait, with a flux estimated at 2.1×10^{10} mol/y (Fig. **F6**). This is more than an order of magnitude greater than the influxes from surrounding rivers and eolian input. In the modern Japan Sea, ~90% of the phosphorous influx exits through the Tsugaru and Soya Straits. This is because the sill depth of the Tsugaru Strait is ~130 m, which is deeper than the thermocline depth and thus allowing nutrient-rich subsurface water to leave the Japan Sea. The remaining ~10% of the phosphorous influx is buried in the form of organic phosphorous and inorganic phosphorous adsorbed on iron oxides.

At present, significant amounts of eolian dust falls over the Japan Sea, especially during early spring. Sediment trap studies estimate annual eolian dust fluxes of 45 g/m^2/y in the western Japan Basin and 23 g/m^2/y in the Yamato Basin (Otosaka et al., 2004). These values are comparable to average mass accumulation rates of Quaternary sediments of 41 g/m^2/y at ODP Site 797 (Irino and Tada, 2000), suggesting a significant contribution of eolian dust to the bulk Quaternary hemipelagic sediments of the Japan Sea. Nagashima et al. (2007) demonstrated that quartz in the silt fraction (>4 µm) of hemipelagic sediments of the Japan Sea is dominantly eolian, whereas quartz in the clay fraction (<4 µm) is a mixture of eolian and detrital grains derived from the Japanese islands.

Seismic studies and site survey data

Seismic and acoustic profiles of the sediments to be drilled in the Japan and East China Seas were surveyed during Cruise KR05-09 to the northern part of the Japan Sea (26–31 July 2005), Cruise KY07-04 to the northern part of the East China Sea (24 February–1 March 2007), Cruise KR07-12 to the northern part of the East China Sea and southern to central part of the Japan Sea (8–25 September 2007), and Cruise KT08-10 to the northern part of the East China Sea (24–29 May 2008). During the KR05-09 cruise, four single-channel seismic (SCS) lines (including one cross line over the site), subbottom profiling (SBP), multibeam, and one piston core (PC-1) were taken at proposed Site JB-2A, and five SCS lines (including one cross line over the site), SBP, multibeam, and one piston core (PC-2) were taken at proposed Site JB-3A. During the KY07-04 cruise, eight SCS lines (including two cross lines over the two sites), SBP, and multibeam were taken at proposed Sites ECS-1A and ECS-1B, and two piston cores

(PC-01 and PC-02) were taken at proposed Site ECS-1A. During the KR07-12 cruise, five multichannel seismic (MCS) lines (including one cross line over the site), SBP, multibeam, and one piston core (PC-01) were taken at proposed Site ECS-1B; three SCS lines (including one cross line over the site), SBP, multibeam, and one piston core (PC-03) were taken at proposed Site YB-1A; three SCS lines (including one cross line over the site), SBP, multibeam, and one piston core (PC-07) were taken at proposed Site YB-3A; and four SCS lines including 1 cross line over the site, SBP, multibeam, and two piston cores (PC-05, 08) were taken at Site YR-1A. During the KT08-10 cruise, dredge and three piston cores (PC-01, PC-02, and PC-03) were taken at proposed Site ECS-1B. About 2530 line-km of MCS data were obtained in 2004 aboard the R/V *Tamhae II* (Korea Institute of Geoscience and Mineral Resources) in the eastern part of the South Korea Plateau using an 80-channel streamer and air gun sources. An east–west seismic line (04GH-12) of MCS crosses over proposed Site UB-1. Detailed multibeam bathymetry and SBP data over the site were obtained by the National Oceanographic Research Institute of Korea from 1996 to 1997. A few piston cores (05GCRP-21, 05GCRP1-9, and 05GCRP1-18) were retrieved from the eastern part of the South Korea Plateau aboard the *Tamhae II* in 2005.

Proposed Sites JB-1, YB-3, and YB-2 will be re-drills of ODP Legs 127 and 128 Sites 794, 797, and 798, respectively. The supporting site survey data for this expedition are archived in the **IODP Site Survey Data Bank.**

Operations plan and drilling strategy

Expedition 346 aims to achieve an ambitious coring program that prioritizes eight primary sites and two alternate sites in 316–3435 m of water depth (Tables **T1, T2**). Eight of the sites are in Japanese and Korean territorial waters in the Japan Sea and two are in Japanese waters in the East China Sea. The final operations plan and number of sites to be cored is contingent upon the *JOIDES Resolution* operations schedule, operational risks (see below), and the outcome of requests for territorial permission to occupy these sites. Of particular relevance is the planned ~13–14 day transit from Valdez, Alaska, prior to beginning coring operations in the Japan Sea. Should ship speed be less than the estimated average of 10.5 kt, the drilling schedule could be significantly impacted.

Coring strategy will consist of APC coring using nonmagnetic core barrels in three holes (A, B, and C) at each site to ~200 meters below seafloor (mbsf) or APC refusal,

with the exception of proposed Site JB-1, which has slightly shallower depth objectives (150 mbsf). As described below and pending further discussions, at this point only cores in Hole A at each site will be oriented.

For planning purposes, the APC refusal depth is estimated at 200 mbsf, although we anticipate that this may be exceeded at some of the more mud-rich sites with target depths greater than 200 mbsf. APC refusal is conventionally defined in two ways: (1) a complete stroke (as determined from the standpipe pressure after the shot) is not achieved because the formation is too hard and (2) excess force (>100,000 lb) is required to pull the core barrel out of the formation because the sediment is too cohesive or "sticky." In cases where a significant stroke can be achieved but excessive force cannot retrieve the barrel, the core barrel can be "drilled over" (i.e., after the inner core barrel is successfully shot into the formation, the bit is advanced to some depth to free the APC barrel). When APC refusal occurs in a hole before the target depth is reached, the XCB technique may be used to advance the hole.

The target depth at the five primary proposed sites (YR-1 [450 mbsf], YB-1 [500 mbsf], YB-2 [400 mbsf], UB-1 [285 mbsf], and ECS-1B [800 mbsf]) is greater than the APC refusal depth. The deeper sections will be advanced by XCB coring on one or two of the holes, time permitting. If the target depth at proposed Site ECS-1B cannot be reached by XCB coring, RCB coring may be employed, time permitting, to reach 800 mbsf. Rotary coring will allow penetration through a significant portion of the Pliocene and possibly into the upper Miocene at proposed Site YR-1 (see Tables **T2** and **T3** for operations details per site). All target depths in the current operations plan have been approved by the IODP Environmental Protection and Safety Panel (EPSP) and the Texas A&M University Safety Panel, but a request to extend the penetration depths at all sites (except proposed Site ECS-1B) by 50 m will be submitted after publication of this *Scientific Prospectus*. Triple APC holes will allow us to build a composite stratigraphic section at each site for the upper ~200 mbsf.

According to the current operations plan, Expedition 346 will core ~6820 m of sediment and potentially recover ~6060 m of core. Considering the significant transit time at the beginning of the expedition (~2 weeks), this coring schedule within the remaining 6 weeks of the expedition is indeed ambitious and will require tight operational planning and flexibility. The estimate of the amount of core recovered is based on 100% recovery with the APC system and 65% recovery with the XCB system.

Downhole logging measurements strategy

Because of the high priority of completing the coring operations at all primary sites and the limited operational time of Expedition 346, sites previously logged during ODP Legs 127 and 128 (Sites 794, 795, 797, and 798) are not in the current logging plan (proposed Sites JB-1, JB-3, YB-3, and YB-2, respectively). Wireline logging is planned for the deepest hole at proposed Sites JB-2, YR-1, YB-1, UB-1, and ECS-1B and at alternate proposed Site ECS-1A. Because we expect 100% core recovery with the APC in the upper 200 m of the sediment sections, downhole logging at shallow penetration sites (200 mbsf or less) is not a priority for the expedition.

The downhole measurement plan aims to provide a broad set of parameters that can be used for the characterization of in situ formation properties (lithologies, structures, and petrophysics) and orbital- and millennial-scale cyclicities (Fig. **F14**). The plan includes the use of as many as four different tool strings (details may be found at **iodp.ldeo.columbia.edu/TOOLS_LABS/tools.html**):

1. The triple combination (triple combo) tool string, which logs formation resistivity, density, porosity, natural gamma radiation (NGR), and borehole diameter. A diameter log is provided by the caliper on the density tool to allow assessment of hole conditions (e.g., washouts of sandy beds), log quality, and the potential for success of the following runs. NGR data gathered by the triple combo may prove useful to correlate with the ship-based NGR measurements.
2. The paleo-combo tool string, which is a modified triple combo in which a newly built Magnetic Susceptibility Sonde (MSS) will replace the porosity sonde. Results can be correlated with magnetic susceptibility measurements from whole-round cores. As with the triple combo, NGR data gathered by the paleo-combo may prove useful to correlate with the ship-based NGR instrument.
3. The Formation MicroScanner (FMS)-sonic tool string, which provides an oriented 360° high-resolution resistivity image of the borehole wall and logs of formation acoustic velocity and borehole diameter. Sonic logs can be combined with the density logs from the triple combo to generate synthetic seismograms and provide high-resolution seismic-well integration. A NGR tool will also be run in the FMS-sonic tool string in order to depth-match the different logging runs, and perhaps correlate to the ship-based NGR instrument.
4. The Versatile Seismic Imager (VSI) tool string, which is used to acquire a zero-offset vertical seismic profile (VSP) for high-resolution integration of borehole stratigraphy and seismic profile, may be used at some sites, in particular proposed

Site ECS-1B, pending time availability as well as permission from the National Science Foundation to conduct the operation in compliance with IODP marine mammal protection policy. A check shot survey planned with ~25 m spacing of stations over the entire open hole interval will give depth to seismic-traveltime conversions. The seismic source for the check shots will be a generator-injector air gun, and its deployment is also subject to the IODP marine mammal policy. The check shot survey would have to be postponed or cancelled if policy conditions are not met.

Two IODP tool string configurations will be deployed in each logging hole. At proposed Sites JB-2, YR-1, and UB-1, the first run will be the triple combo tool string. At proposed Sites YB-1 and ECS-1, the first run will be the paleo-combo tool string. At each logged site, the second run will be the FMS-sonic tool string. At proposed Site ECS-1B, a third run may include using the VSI tool string. The deployment order for the tool strings at this site may be adjusted to ensure that the VSP is acquired during daylight operations. Logging time estimates for each site are given in **"Operations plan and drilling strategy."**

Downhole measurements will be the only data available where core recovery is incomplete. Moreover, the data will provide common measurements for core-log integration (density, NGR, and magnetic susceptibility) and to establish the link between borehole and core features and reflectors on seismic profiles by synthetic seismograms and VSP.

Formation temperature measurements and core orientation

Temperature measurements are planned for all sites to reconstruct the thermal gradient at each location. Four measurements are planned at one hole per site using the advanced piston corer temperature tool. The thermal gradient at each site will help constrain the history of burial diagenesis of the sediments encountered.

In addition, the FlexIt orientation tool will be used in the first hole cored at each site to orient all APC cores as needed. This instrument uses three orthogonally mounted fluxgate magnetometers to record the orientation with respect to magnetic north of the double lines scribed on the core liner. The tool also has three orthogonally mounted accelerometers that monitor the movement of the drill assembly and help determine when the most stable, and thus most useful, core orientation data are gath-

ered. Declination, inclination, and temperature are recorded internally at regular intervals until the tool's memory capacity is filled.

Risks and contingency

The principal operational risks identified for this expedition include

- Shallow water coring (at proposed Site YB-1);
- Weather. Although the expedition has been scheduled take place in late summer, which is the optimum weather window, severe weather (e.g., typhoons) may still occur and could adversely impact operations;
- The presence of gas-prone sediments at some sites and depths leading to a potential for core expansion on deck. Moreover, potentially high H_2S contents may require degassing of the cores on the catwalk after they are recovered;
- Alternating lithologies that may lead to hole instability;
- Commercial fishing operations and normal marine traffic; and
- An extremely ambitious operations plan for the time available. Good time management will be extremely important to mitigate this risk.

All of these factors may affect coring and drilling operations.

Sampling and data sharing strategy

Shipboard and shore-based researchers should refer to the IODP Sample, Data, and Obligations Policy (**www.iodp.org/program-policies/**). This document outlines the policy for distributing IODP samples and data. It also defines the obligations incurred by sample and data recipients. All requests for data and core samples must be approved by the Sample Allocation Committee (SAC). The SAC is composed of the Co-Chief Scientists, Staff Scientist, and the IODP Curator on shore (on board the ship, the curatorial representative serves in place of the Curator).

Every member of the science party is obligated to carry out scientific research for the expedition and publish the results. For this purpose, shipboard and shore-based scientists are expected to submit sample requests (at **smcs.iodp.org/**) detailing their science plan 3 months before the beginning of the expedition. Based on sample requests (shore-based and shipboard) and input from the scientific party, the SAC will prepare a tentative sampling plan, which will be revised on the ship as dictated by recovery

and cruise objectives. The sampling plan will be subject to modification depending upon the actual material recovered and collaborations that may evolve between scientists during the expedition. Given the specific objectives of Expedition 346, great care will be taken to maximize shared sampling to promote integration of data sets and enhance scientific collaboration among members of the scientific party. This planning process is necessary to coordinate the research to be conducted and to ensure that the scientific objectives are achieved. Modifications to sample requests and access to samples and data during the expedition and the 1 y postexpedition moratorium period require approval of the SAC.

All sampling frequencies and sample sizes must be justified on a scientific basis and will depend on core recovery, the full spectrum of other requests, and the expedition objectives. Some redundancy of measurement is unavoidable, but minimizing the duplication of measurements among the shipboard party and identified shore-based collaborators will be a factor in evaluating sample requests. Success will require collaboration, integration of complementary data sets, and consistent methods of analysis. Substantial collaboration and cooperation are highly encouraged.

Shipboard sampling will be restricted to acquiring ephemeral data types and to limited low-resolution sampling (e.g., for stratigraphic purposes [biostratigraphy, magnetostratigraphy, optically stimulated luminescence dating], physical properties, and geochemical and microbiological analyses). Shipboard biostratigraphic and paleomagnetostratigraphic sampling will also be restricted to rapidly produce age models that are critical to the overall objectives of the expedition and to the planning for higher resolution postcruise sampling. In addition, selected postexpedition-related sampling may be conducted during the cruise to minimize the effect of sediment oxidation and dissolution of certain sedimentary components (e.g., carbonate microfossils) caused by oxidation of pyrite in sediment. Additionally, because Quaternary sediments of the Japan Sea frequently alternate organic carbon– and pyrite-rich layers, half-split cores should be vacuum sealed in aluminum-coated plastic-pack and preserved cool until the sampling party.

Sampling for the majority of individual scientist's personal research will be postponed until a shore-based sampling party implemented between 2 and 4 months after the expedition at the KCC at Kochi University, Kochi, Japan. The KCC repository houses cores from the Pacific Ocean (west of the western boundary of the Pacific plate), the Indian Ocean (north of 60°), Kerguelen Plateau, and the Bering Sea.

The KCC includes an XRF scanner as part of its facilities. Pending further discussion with shipboard and shore-based participants, we will develop an XRF scanning plan, whereby initial low-resolution scanning at the KCC may occur for all recovered material and for a select suite of chemical elements. These data would be considered as part of the data subject to the moratorium policy and be available to all participants. Individual scientists, as part of their sampling request, are encouraged to propose additional XRF scanning, either at the KCC or in their own laboratories.

There may be considerable demand for samples from a limited amount of cored material for some critical intervals at certain sites. Critical intervals may require special handling that includes a higher sampling density, reduced sample size, or continuous core sampling for a set of particular high-priority research objectives. The SAC may require a revision of the approved sampling plan before critical intervals are sampled, and a special sampling plan shall be developed to maximize scientific return and participation and to preserve some material for future studies. The SAC can decide at any stage during the expedition or during the one year moratorium period which recovered intervals should be considered as critical.

All collected data and samples will be protected by a 1 y postcruise moratorium, during which time data and samples are available only to the Expedition 346 science party and approved shore-based participants. This moratorium will extend 1 y following the completion of the postcruise sampling party (note, not 1 y from the end of the time at sea). We anticipate that specific shipboard and shore-based scientific party members may require specific sampling methods. For example, Rhizon sampling may be requested for high-resolution or trace metal clean pore water sampling; for optically stimulated luminescence dating sampling, appropriate storage mechanisms must be employed to minimize exposure to sunlight; and microbiological sampling often requires rapid sample processing. Additionally, as of this point in time, we plan to employ "LL-channel sampling" (Nakagawa et al., 2012; **youtube.com/watch?v=SsgYG6VNW5Q**) to assist in the generation of high-resolution data sets. Wherever possible, techniques and methodologies such as these (or others not listed here) will be used, and participants are encouraged to specifically identify their needs in their requests.

References

Abe, M., Kitoh, A., and Yasunari, T., 2003. An evolution of the Asian summer monsoon associated with mountain uplift—simulation with the MRI atmosphere–ocean coupled GCM. *J. Meteorol. Soc. Jpn.,* 81(5):909–933. **doi:10.2151/jmsj.81.909**

Abe, M., Yasunari, T., and Kitoh, A., 2004. Effects of large-scale orography on the coupled atmosphere-ocean system in the tropical Indian and Pacific Oceans in boreal summer. *J. Meteorol. Soc. Jpn.,* 82(2):745–759. **doi:10.2151/jmsj.2004.745**

An, Z., Kutzbach, J.E., Prell, W.L., and Porter, S.C., 2001. Evolution of Asian monsoons and phased uplift of the Himalaya–Tibetan Plateau since late Miocene times. *Nature (London, U. K.),* 411(6833):62–66. **doi:10.1038/35075035**

Asmerom, Y., Polyak, V.J., and Burns, S.J., 2010. Variable winter moisture in the southwestern United States linked to rapid glacial climate shifts. *Nat. Geosci.,* 3(2):114–117. **doi:10.1038/ngeo754**

Becker, J., Lourens, L.J., and Raymo, M.E., 2006. High-frequency climate linkages between the North Atlantic and the Mediterranean during marine oxygen isotope Stage 100 (MIS100). *Paleoceanography,* 21(3):PA3002. **doi:10.1029/2005PA001168**

Bond, G., Broecker, W., Johnsen, S., McManus, J., Labeyrie, L., Jouzel, J., and Bonani, G., 1993. Correlations between climate records from North Atlantic sediments and Greenland ice. *Nature (London, U. K.),* 365(6442):143–147. **doi:10.1038/365143a0**

Broecker, W.S., Bond, G., Klas, M., Bonani, G., and Wolfli, W., 1990. A salt oscillator in the glacial Atlantic? 1. The concept. *Paleoceanography,* 5(4):469–477. **doi:10.1029/PA005i004p00469**

Cacho, I., Grimalt, J.O., and Canals, M., 2002. Response of the Western Mediterranean Sea to rapid climatic variability during the last 50,000 years: a molecular biomarker approach. *J. Mar. Sys.,* 33–34:253–272. **doi:10.1016/S0924-7963(02)00061-1**

Chen, C.-T.A., 2002. The impact of dams on fisheries: case of the Three Gorges Dam. *In* Steffen, W., Jaeger, J., Carson, D.J., and Bradshaw, C. (Eds.), *Challenges of a Changing Earth:* Berlin (Springer-Verlag), 97–99.

Chen, C.-T.A., and Wang, S.-L., 1999. Carbon, alkalinity and nutrient budgets on the East China Sea continental shelf. *J. Geophys. Res., [Oceans],* 104(C9):20675–20686. **doi:10.1029/1999JC900055**

Cheng, H., Edwards, R.L., Broecker, W.S., Denton, G.H., Kong, X., Wang, Y., Zhang, R., and Wang, X., 2009. Ice age terminations. *Science,* 326(5950):248–252. **doi:10.1126/science.1177840**

Copeland, P., 1997. The when and where of the growth of the Himalaya and the Tibetan Plateau. *In* Ruddiman, W.F. (Ed.), *Tectonic Uplift and Climatic Change:* New York (Plenum Press), 19–40.

Crusius, J., Pedersen, T.F., Calvert, S.E., Cowie, G.L., and Oba, T., 1999. A 36 kyr geochemical record from the Sea of Japan of organic matter flux variations and changes in intermediate water oxygen concentrations. *Paleoceanography,* 14(2):248–259. **doi:10.1029/1998PA900023**

deMenocal, P.B, Bristow, J.F., and Stein, R., 1992. Paleoclimatic applications of downhole logs: Pliocene–Pleistocene results from Hole 798B, Sea of Japan. *Proc. ODP Sci. Results,* 127/128 (Pt. 1): College Station, TX (Ocean Drilling Program), 337–353. **doi:10.2973/odp.proc.sr.127128-1.143.1992**

Ding, Z.L., Derbyshire, E., Yang, S.L., Sun, J.M., and Liu, T.S., 2005. Stepwise expansion of desert environment across northern China in the past 3.5 Ma and implications for monsoon evolution. *Earth Planet. Sci. Lett.,* 237(1–2):45–55. **doi:10.1016/j.epsl.2005.06.036**

Fournier, M., Fabbri, O., Angelier, J., and Cadet, J.-P., 2001. Regional seismicity and on-land deformation in the Ryukyu arc: implications for the kinematics of opening of the Okinawa Trough. *J. Geophys. Res., [Solid Earth],* 106(B7):13751–13768. **doi:10.1029/2001JB900010**

Fujine, K., 2004. Fluctuation of the alkenone SST in the Japan Sea during the last 160 kys. [Ph.D. thesis]. Univ. Tokyo.

Gamo, T., 1999. Global warming may have slowed down the deep conveyor belt of a marginal sea of the northwestern Pacific: Japan Sea. *Geophys. Res. Lett.,* 26(20):3137–3140. **doi:10.1029/1999GL002341**

Gamo, T., and Horibe, Y., 1983. Abyssal circulation in the Japan Sea. *J. Oceanogr.,* 39(5):220–230. **doi:10.1007/BF02070392**

Guo, Z.T., Peng, S.Z., Hao, Q.Z., Biscaye, P.E., and Liu, T.S., 2001. Origin of the Miocene–Pliocene Red-Earth Formation at Xifeng in northern China and implications for paleoenvironments. *Palaeogeogr., Palaeoclimatol., Palaeoecol.,* 170(1–2):11–26. **doi:10.1016/S0031-0182(01)00235-8**

Gungor, A., Lee, G.H., Kim, H.-J., Han, H.-C., Kang, M.-H., Kim, J., and Sunwoo, D., 2012. Structural characteristics of the northern Okinawa Trough and adjacent areas from regional seismic reflection data: geologic and tectonic implications. *Tectonics,* 522–523:198–207. **doi:10.1016/j.tecto.2011.11.027**

Hao, Q., and Guo, Z., 2004. Magnetostratigraphy of a late Miocene–Pliocene loess-soil sequence in the western Loess Plateau in China. *Geophys. Res. Lett.,* 31(9):L09209. **doi:10.1029/2003GL019392**

Harada, K., and Tsunogai, S., 1986. ^{226}Ra in the Japan Sea and temporal variations of water characteristics in the Japan Sea bottom water. *J. Mar. Res.,* 44:781–793.

Hase, H., Yoon, J.-H., and Koterayama, W., 1999. The current structure of the Tsushima Warm Current along the Japan coast. *J. Oceanogr.,* 55(2):217–235. **doi:10.1023/A:1007894030095**

Ichikawa, H., and Beardsley, R.C., 2002. The current system in the Yellow and East China Seas. *J. Oceanogr.,* 58(1):77–92. **doi:10.1023/A:1015876701363**

Ijiri, A., Wang, L., Oba, T., Kawahata, H., Huang, C.-Y., and Huang, C.-Y., 2005. Paleoenvironmental changes in the northern area of the East China Sea during the past 42,000 years. *Palaeogeogr., Palaeoclimatol., Palaeoecol.,* 219(3–4):239–261. **doi:10.1016/j.palaeo.2004.12.028**

Ikehara, K., 2003. Late Quaternary seasonal sea-ice history of the northeastern Japan Sea. *J. Oceanogr.,* 59(5):585–593. **doi:10.1023/B:JOCE.0000009588.49944.3d**

Irino, T., and Tada, R., 2000. Quantification of aeolian dust (Kosa) contribution to the Japan Sea sediments and its variation during the last 200 ky. *Geochem. J.,* 34(1):59–93. **doi:10.2343/geochemj.34.59**

Irino, T., and Tada, R., 2003. High-resolution reconstruction of variation in aeolian dust (Kosa) deposition at ODP Site 797, the Japan Sea, during the last 200 ka. *Global Planet. Change,* 35(1–2):143–156. **doi:10.1016/S0921-8181(02)00135-2**

Isobe, A., Ando, M., Watanabe, T., Senjyu, T., Sugihara, S., and Manda, A., 2002. Freshwater and temperature transports through the Tsushima-Korea Straits. *J. Geophys. Res., [Oceans],* 107(C7):3065. **doi:10.1029/2000JC000702**

Jain, A.K., Kumar, D., Singh, S., Kumar, A., and Lal, N., 2000. Timing, quantification, and tectonic modeling of Pliocene–Quaternary movements in the NW Himalaya: evidence from fission track dating. *Earth Planet. Sci. Lett.,* 179(3–4):437–451. **doi:10.1016/S0012-821X(00)00133-3**

Jansen, E., Fronval, T., Rack, F., and Channell, J.E.T., 2000. Pliocene–Pleistocene ice rafting history and cyclicity in the Nordic Seas during the last 3.5 Myr. *Paleoceanography,* 15(6):709–721. **doi:10.1029/1999PA000435**

Jolivet, L., Tamaki, K., and Fournier, M., 1994. Japan Sea, opening history and mechanism: a synthesis. *J. Geophys. Res., [Solid Earth],* 99(B11):22237–22259. **doi:10.1029/93JB03463**

Katoh, O., 1993. Detailed current structures in the eastern channel of the Tsushima Strait in summer. *J. Oceanogr.,* 49(1):17–30. **doi:10.1007/BF02234005**

Kawabe, M., 1982. Branching of the Tsushima Current in the Japan Sea, Part I. Data analysis. *J. Oceanogr.,* 38(2):95–107. **doi:10.1007/BF02110295**

Kido, Y., Minami, I., Tada, R., Fujine, K., Irino, T., Ikehara, K., and Chun, J.-H., 2007. Orbital-scale stratigraphy and high-resolution analysis of biogenic components and deep-water oxygenation conditions in the Japan Sea during the last 640 kyr. *Palaeogeogr., Palaeoclimatol., Palaeoecol.,* 247(1–2):32–49. **doi:10.1016/j.palaeo.2006.11.020**

Kim, C.-H., and Yoon, J.-H., 1999. A numerical modeling of the upper and the intermediate layer circulation in the East Sea. *J. Oceanogr.,* 55(2):327–345. **doi:10.1023/A:1007837212219**

Kimura, G., and Tamaki, K., 1986. Collision, rotation, and back-arc spreading in the region of the Okhotsk and Japan Seas. *Tectonics,* 5(3):389–401. **doi:10.1029/TC005i003p00389**

Kimura, M., 1996. Active rift system in the Okinawa Trough and its northern continuation. *Bull. Disaster Prev. Res. Inst., Kyoto Univ.,* 45(2–3):389. **http://repository.kulib.kyoto-u.ac.jp/dspace/bitstream/2433/125010/1/b45p2-3n389p03.pdf**

Kitoh, A., 2004. Effects of mountain uplift on East Asian summer climate investigated by a coupled atmosphere–ocean GCM. *J. Clim.,* 17:783–802. **doi:10.1175/1520-0442(2004)017<0783:EOMUOE>2.0.CO;2**

Kodama, K., and Nakayama, K., 1993. Paleomagnetic evidence for post-late Miocene intra-arc rotation of South Kyushu, Japan. *Tectonics,* 12(1):35–47. **doi:10.1029/92TC01712**

Kondo, M., 1985. Oceanographic investigations of fishing grounds in the East China Sea and the Yellow Sea—I. Characteristics of the mean temperature and salinity distributions measured at 50 m and near the bottom. *Bull. Seikai Reg. Fish. Res. Lab.,* 62:19–55. (in Japanese with abstract in English)

Kong, F., Lawver, L.A., and Lee, T.-Y., 2000. Evolution of the southern Taiwan–Sinzi Folded Zone and opening of the southern Okinawa Trough. *J. Asian Earth Sci.,* 18(3):325–341. **doi:10.1016/S1367-9120(99)00062-0**

Kubota, Y., Kimoto, K., Tada, R., Oda, H., Yokoyama, Y., and Matsuzaki, H., 2010. Variations of East Asian summer monsoon since the last deglaciation based on Mg/Ca and oxygen isotope of planktic foraminifera in the northern East China Sea. *Paleoceanography,* 25(4):PA4205. **doi:10.1029/2009PA001891**

Li, J.-J., Fang, X.-M., Van der Voo, R., Zhu, J.-J., Mac Niocaill, C., Cao, J.-X., Zhong, W., Chen, H.-L., Wang, J., and Wang, J.-M., and Zhang, Y.-C., 1997. Late Cenozoic magnetostratigraphy (11–0 Ma) of the Dongshanding and Wangjiashan sections in the Longzhong Basin, western China. *Geol. Mijnbouw,* 76(1–2):121–134. **doi:10.1023/A:1003153717799**

Liu, X., and Yin, Z.-Y., 2002. Sensitivity of East Asian monsoon climate to the uplift of the Tibetan Plateau. *Palaeogeogr., Palaeoclimatol., Palaeoecol.,* 183(3–4):223–245. **doi:10.1016/S0031-0182(01)00488-6**

Matsui, H., Tada, R., and Oba, T., 1998. Low-salinity isolation event in the Japan Sea in response to eustatic sea-level drop during LGM: reconstruction based on salinity-balance model. *Quat. Res. (Daiyonki-Kenkyu),* 37(3):221–233. (in Japanese with abstract in English) **doi:10.4116/jaqua.37.221**

Mc Intyre, K., Delaney, M.L., and Ravelo, A.C., 2001. Millennial-scale climate change and oceanic processes in the late Pliocene and early Pleistocene. *Paleoceanography,* 16(5):535–543. **doi:10.1029/2000PA000526**

Moreno, A., Cacho, I., Canals, M., Prins, M.A., Sánchez-Goñi, M.-F., Grimalt, J.O., and Weltje, G.J., 2002. Saharan dust transport and high-latitude glacial climatic variability: the Alboran Sea record. *Quat. Res.,* 58:(3):318–328. **doi:10.1006/qres.2002.2383**

Nagashima, K., 2005. Reconstruction of millennial-scale variation in eolian dust transport path to the Japan Sea based on grain size and ESR analyses [Ph.D. thesis]. Univ. Tokyo.

Nagashima, K., Tada, R., Matsui, H., Irino, T., Tani, A., and Toyoda, S., 2007. Orbital- and millennial-scale variations in Asian dust transport path to the Japan Sea. *Palaeogeogr., Palaeoclimatol., Palaeoecol.,* 247(1–2):144–161. **doi:10.1016/j.palaeo.2006.11.027**

Nagashima, K., Tada, R., Tani, A., Sun, Y., Isozaki, Y., Toyoda, S., and Hasegawa, H., 2011. Millennial-scale oscillations of the westerly jet path during the last glacial period. *J. Asian Earth Sci.,* 40(6):1214–1220. **doi:10.1016/j.jseaes.2010.08.010**

Nakagawa, T., Gotanda, K., Haraguchi, T., Danhara, T., Yonenobu, H., Brauer, A., Yokoyama, Y., Tada, R., Takemura, K., Staff, R.A., Payne, R., Ramsey, C.B., Bryant, C., Brock, F., Schlolaut, G., Marshall, M., Tarasov, P., Lamb, H., and Suigetsu 2006 Project Members, 2012. SG06, a fully continuous and varved sediment core from Lake Suigetsu, Japan: stratigraphy and potential for improving the radiocarbon calibration model and understanding of late Quaternary climate changes. *Quat. Sci. Rev.,* 36:164–176. **doi:10.1016/j.quascirev.2010.12.013**

Oba, T., Kato, M., Kitazato, H., Koizumi, I., Omura, A., Sakai, T., and Takayama, T., 1991. Paleoenvironmental changes in the Japan Sea during the last 85,000 years. *Paleoceanography,* 6(4):499–518. **doi:10.1029/91PA00560**

Oba, T., Murayama, M., Matsumoto, E., and Nakamura, T., 1995. AMS-^{14}C ages of the Japan Sea cores from the Oki Ridge. *Quat. Res. (Daiyonki-Kenkyu),* 34(4):289–296. (in Japanese with abstract in English) **doi:10.4116/jaqua.34.4_289**

Ono, Y., Naruse, T., Ikeya, M., Kohno, H., and Toyoda, S., 1998. Origin and derived courses of eolian dust quartz deposited during marine isotope Stage 2 in East Asia, suggested by ESR signal intensity. *Global Planet. Change,* 18(3–4):129–135. **doi:10.1016/S0921-8181(98)00012-5**

Otosaka, S., Togawa, O., Baba, M., Karasev, E., Volkov, Y.N., Omata, N., and Noriki, S., 2004. Lithogenic flux in the Japan Sea measured with sediment traps. *Mar. Chem.,* 91(1–4):143–163. **doi:10.1016/j.marchem.2004.06.006**

Porter, S.C., and An, Z., 1995. Correlation between climatic events in the North Atlantic and China during the last glaciation. *Nature (London, U. K.),* 375(6529):305–308. **doi:10.1038/375305a0**

Prins, M.A., Postma, G., and Weltje, G.J., 2000. Controls on terrigenous sediment supply to the Arabian Sea during the late Quaternary: the Makran continental slope. *Mar. Geol.,* 169(3–4):351–371. **doi:10.1016/S0025-3227(00)00087-6**

Raymo, M.E., Ganley, K., Carter, S., Oppo, D.W., and McManus, J., 1998. Millenial-scale climate instability during the early Pleistocene epoch. *Nature (London, U. K.),* 392(6677):699–702. **doi:10.1038/33658**

Rea, D.K., and Leinen, M., 1988. Asian aridity and the zonal westerlies: late Pleistocene and Holocene record of eolian deposition in the northwest Pacific Ocean. *Palaeogeogr., Palaeoclimatol., Palaeoecol.,* 66(1–2):1–8. **doi:10.1016/0031-0182(88)90076-4**

Rea, D.K., Leinen, M., and Janecek, T.R., 1985. Geologic approach to the long-term history of atmospheric circulation. *Science,* 227(4688):721–725. **doi:10.1126/science.227.4688.721**

Rea, D.K., Snoeckx, H., and Joseph, L.H., 1998. Late Cenozoic eolian deposition in the North Pacific: Asian drying, Tibetan uplift, and cooling of the Northern Hemisphere. *Paleoceanography,* 13(3):215–224. **doi:10.1029/98PA00123**

Rowley, D.B., and Currie, B.S., 2006. Palaeo-altimetry of the late Eocene to Miocene Lunpola Basin, central Tibet. *Nature (London, U. K.),* 439(7077):677–681. **doi:10.1038/nature04506**

Royden, L.H., Burchfiel, B.C., and van der Hilst, R.D., 2008. The geological evolution of the Tibetan Plateau. *Science,* 321(5892):1054–1058. **doi:10.1126/science.1155371**

Sakai, H., Fujii, R., and Kuwahara, Y., 2002. Changes in the depositional system of the paleo-Kathmandu Lake caused by uplift of the Nepal Lesser Himalayas. *J. Asian Earth Sci.,* 20(3):267–276. **doi:10.1016/S1367-9120(01)00046-3**

Sánchez Goñi, M.-F., Cacho, I., Turon, J.-L., Guiot, J., Sierro, F.J., Peypouquet, J.-P., Grimalt, J.O., and Shackleton, N.J., 2002. Synchroneity between marine and terrestrial responses to millennial scale climatic variability during the last glacial period in the Mediterranean region. *Clim. Dyn.,* 19(1):95–105. **doi:10.1007/s00382-001-0212-x**

Schiemann, R., Lüthi, D., and Schär, C., 2009. Seasonality and interannual variability of the Westerly Jet in the Tibetan Plateau region. *J. Clim.,* 22(11):2940–2957. **doi:10.1175/2008JCLI2625.1**

Schulz, H., von Rad, U., and Erlenkeuser, H., 1998. Correlation between Arabian Sea and Greenland climate oscillations of the past 110,000 years. *Nature (London, U. K.),* 393(6680):54–57. **doi:10.1038/31750**

Sibuet, J.-C., Deffontaines, B., Hsu, S.-K., Thareau, N., Le Formal, J.-P., Liu, C.-S., and the ACT Party, 1998. Okinawa Trough backarc basin: early tectonic and magmatic evolution. *J. Geophys. Res., [Solid Earth],* 103(B12):30245–30267. **doi:10.1029/98JB01823**

Sudo, H., 1986. A note on the Japan Sea Proper Water. *Prog. Oceanogr.,* 17(3–4):313–336. **doi:10.1016/0079-6611(86)90052-2**

Sun, D., An, Z., Su, R., Lu, H., and Sun, Y., 2003. Eolian sedimentary records for the evolution of monsoon and westerly circulations of northern China in the last 2.6 Ma. *Sci. China, Ser. D: Earth Sci.,* 46(10):1049–1059. **doi:10.1007/BF02959400**

Tada, R., 1994. Paleoceanographic evolution of the Japan Sea. *Palaeogeogr., Palaeoclimatol., Palaeoecol.,* 108(3–4):487–508. **doi:10.1016/0031-0182(94)90248-8**

Tada, R., 2004. Onset and evolution of millennial-scale variability in the Asian monsoon and its impact on paleoceanography of the Japan Sea. *In* Clift, P., Kuhnt, W., Wang, P., and Hayes, D. (Eds.), *Continent-Ocean Interactions within East Asian Marginal Seas*. Geophys. Monogr., 149:283–298. **doi:10.1029/149GM15**

Tada, R., and Iijima, A., 1992. Lithostratigraphy and compositional variation of Neogene hemipelagic sediments in the Japan Sea. *In* Tamaki, K., Suyehiro, K., Allan, J., McWilliams, M., et al., *Proc. ODP, Sci. Results,* 127/128 (Pt. 2): College Station, TX (Ocean Drilling Program), 1229–1260. **doi:10.2973/odp.proc.sr.127128-2.188.1992**

Tada, R., Irino, T., and Koizumi, I., 1995. Possible Dansgaard–Oeschger oscillation signal recorded in the Japan Sea sediments. *In* Tsunogai, S., Iseki, K., Koike, I., and Oba, T. (Eds.),

Global Fluxes of Carbon and Its Related Substances in the Coastal Sea-Ocean-Atmosphere Systems: Yokohama, Japan (M & J International), 517–522.

Tada, R., Irino, T., and Koizumi, I., 1999. Land-ocean linkages over orbital and millennial timescales recorded in late Quaternary sediments of the Japan Sea. *Paleoceanography,* 14(2):236–247. **doi:10.1029/1998PA900016**

Tada, R., Koizumi, I., Cramp, A., and Rahman, A., 1992. Correlation of dark and light layers, and the origin of their cyclicity in the Quaternary sediments from the Japan Sea. *In* Pisciotto, K.A., Ingle, J.C., Jr., von Breymann, M.T., Barron, J., et al., *Proc. ODP, Sci. Results,* 127/128 (Pt. 1): College Station, TX (Ocean Drilling Program), 577–601. **doi:10.2973/odp.proc.sr.127128-1.160.1992**

Takikawa, T., Yoon, J.-H., and Cho, K.-D., 2005. The Tsushima Warm Current through Tsushima Straits estimated from ferryboat ADCP data. *J. Phys. Oceanogr.,* 35(6):1154–1168. **doi:10.1175/JPO2742.1**

Talley, L.D., Lobanov, V., Ponomarev, V., Salyuk, A., Tishchenko, P., Zhabin, I., and Riser, S., 2003. Deep convection and brine rejection in the Japan Sea. *Geophys. Res. Lett.,* 30(4):1159. **doi:10.1029/2002GL016451**

Tamaki, K., Suyehiro, K., Allan, J., Ingle, J.C., Jr., and Pisciotto, K.A., 1992. Tectonic synthesis and implications of Japan Sea ODP drilling. *In* Tamaki, K., Suyehiro, K., Allan, J., McWilliams, M., et al., *Proc. ODP, Sci. Results,* 127/128 (Pt. 2): College Station, TX (Ocean Drilling Program), 1333–1348. **doi:10.2973/odp.proc.sr.127128-2.240.1992**

Tapponnier, P., Zhiqin, X., Roger, F., Meyer, B., Arnaud, N., Wittlinger, G., and Jingsui, Y., 2001. Oblique stepwise rise and growth of the Tibet Plateau. *Science,* 294(5547):1671–1677. **doi:10.1126/science.105978**

Tsunogai, S., Watanabe, Y.W., Harada, K., Watanabe, S., Saito, S., and Nakajima, M., 1993. Dynamics of the Japan Sea Deep Water studied with chemical and radiochemical tracers. *In* Teramato, T. (Ed.), *Deep Ocean Circulation—Physical and Chemical Aspects*. Elsevier Oceanogr. Ser. (Amsterdam), 59:105–119. **doi:10.1016/S0422-9894(08)71321-7**

Vance, D., Bickle, M., Ivy-Ochs, S., and Kubik, P.W., 2003. Erosion and exhumation in the Himalaya from cosmogenic isotope inventories of river sediments. *Earth Planet. Sci. Lett.,* 206(3–4):273–288. **doi:10.1016/S0012-821X(02)01102-0**

Wagner, J.D.M., Cole, J.E., Beck, J.W., Patchett, P.J., Henderson, G.M., and Barnett, H.R., 2010. Moisture variability in the southwestern United States linked to abrupt glacial climate change. *Nat. Geosci.,* 3:(2):110–113. **doi:10.1038/ngeo707**

Wang, C., Zhao, X., Liu, Z., Lippert, P.C., Graham, S.A., Coe, R.S., Yi, H., Zhu, L., Liu, S., and Li, Y., 2008. Constraints on the early uplift history of the Tibetan Plateau. *Proc. Natl. Acad. Sci. U. S. A.,* 105(13):4987–4992. **doi:10.1073/pnas.0703595105**

Wang, Y.J., Cheng, H., Edwards, R.L., An, Z.S., Wu, J.Y., Shen, C.-C., and Dorale, J.A., 2001. A high-resolution absolute-dated late Pleistocene monsoon record from Hulu Cave, China. *Science,* 294(5580):2345–2348. **doi:10.1126/science.1064618**

Watanabe, Y.W., Watanabe, S., and Tsunogai, S., 1991. Tritium in the Japan Sea and the renewal time of the Japan Sea Deep Water. *Mar. Chem.,* 34(1–2):97–108. **doi:10.1016/0304-4203(91)90016-P**

Wehausen, R., and Brumsack, G.-J., 2002. Astronomical forcing of the East Asian monsoon mirrored by the composition of Pliocene South China Sea sediments. *Earth Planet. Sci. Lett.,* 201(3–4):621–636. **doi:10.1016/S0012-821X(02)00746-X**

Wobus, C.W., Hodges, K.V., and Whipple, K.X., 2003. Has focused denudation sustained active thrusting at Himalayan topographic front? *Geology,* 31(10):861–864. **doi:10.1130/G19730.1**

Yanagi, T., 2002. Water, salt, phosphorus and nitrogen budgets of the Japan Sea. *J. Oceanogr.,* 58(6):797–804. **doi:10.1023/A:1022815027968**

Yang, S.L., Milliman, J.D., Li, P., and Xu, K., 2011. 50,000 dams later: erosion of the Yangtze River and its delta. *Global Planet. Change,* 75(1–2):14–20. **doi:10.1016/j.gloplacha.2010.09.006**

Yokoyama, Y., Kido, Y., Tada, R., Minami, I., Finkel, R.C., and Matsuzaki, H., 2007. Japan Sea oxygen isotope stratigraphy and global sea-level changes for the last 50,000 years recorded in sediment cores from the Oki Ridge. *Palaeogeogr., Palaeoclimatol., Palaeoecol.,* 247(1–2):5–17. **doi:10.1016/j.palaeo.2006.11.018**

Yuan, D., Cheng, H., Edwards, R.L., Dykoski, C.A., Kelly, M.J., Zhang, M., Qing, J., Lin, Y., Wang, Y., Wu, J., Dorale, J.A., An, Z., and Cai, Y., 2004. Timing, duration, and transitions of the last interglacial Asian monsoon. *Science,* 304(5670):575–578. **doi:10.1126/science.1091220**

Zheng, H., Powell, C.M., An, Z., Zhou, J., and Dong, G., 2000. Pliocene uplift of the northern Tibetan Plateau. *Geology,* 28(8):715–718. **doi:10.1130/0091-7613(2000)28<715:PUOTNT>2.0.CO;2**

Table T1. Primary and alternate proposed sites, Expedition 346.

Site	Latitude	Longitude	Water depth (m)	Penetration depth (mbsf)	Estimated bottom age
Primary:					
YB-1	35°57.92′N	134°26.06′E	316	500	Pleistocene
YB-2	37°02.00′N	134°48.00′E	930	400	Pliocene
YR-1	39°29.44′N	134°26.55′E	1917	450	Pliocene–Miocene
JB-1	40°11.40′N	138°13.90′E	2811	150	Pliocene
JB-2	41°41.95′N	139°04.98′E	1785	250	Pliocene
JB-3	43°45.99′N	138°49.99′E	3435	200	Pliocene
ECS-1B	31°40.64′N	129°02.00′E	746	800	Pliocene
UB-1	37°54.16′N	131°32.25′E	1064	285	Pliocene–Miocene
Alternate:					
YB-3	38°37.00′N	134°32.00′E	2874	200	Pliocene
ECS-1A	31°38.30′N	128°56.60′E	746		Pliocene

All penetration depths shown have been approved by the Environmental Protection and Safety Panel. A new request to extend the approved depths by 50 m at all sites, except proposed Sites JB-2 and ECS-1A, is pending.

Table T2. Operations plan for primary proposed sites, Expedition 346.

Site No.	Location (Latitude Longitude)	Seafloor Depth (mbrf)	Operations Description		Transit (days)	Drilling Coring (days)	LWD/MWD Log (days)
Valdez			Begin Expedition	5.0	port call days		
			Transit ~3277 nmi to JB-3 @ 10.5 knots (+17 hours of time change)		13.7		
JB-3	43° 45.99' N	3446	Hole A - APC to ~200 mbsf w/APCT3 measurements and orientation			1.9	
EPSP	138° 49.99' E		Hole B - APC to ~200 mbsf			1.1	
to 200 mbsf			Hole C - APC to ~200 mbsf			1.5	
			Sub-Total Days On-Site:	4.5			
			Transit ~125 nmi to JB-2 @ 10.5 knots		0.5		
JB-2	41° 41.95' N	1796	Hole A - APC to 200 mbsf w/APCT3 measurements and orientation			1.1	
EPSP	139° 4.98' E		Hole B - APC to 200 mbsf			0.7	
to 250 mbsf			Hole C - APC to 200 mbsf and Log with triple combo and FMS-sonic			1.0	0.6
			Sub-Total Days On-Site:	3.4			
			Transit ~98 nmi to JB-1 @ 10.5 knots		0.4		
JB-1	40° 11.40' N	2822	Hole A - APC to ~150 mbsf w/APCT3 measurements and orientation			1.3	
EPSP	138° 13.90' E		Hole B - APC to ~150 mbsf			0.8	
to 150 mbsf			Hole C - APC to ~150 mbsf			1.1	
			Sub-Total Days On-Site:	3.2			
			Transit ~180 nmi toYR-1 @ 10.5 knots		0.7		
YR-1	39° 29.44' N	1928	Hole A - APC to 200 mbsf w/APCT3 measurements and orientation			1.3	
EPSP	134° 26.55' E		Hole B - APC/XCB to 450 mbsf			2.2	
to 450 mbsf			Hole C - APC/XCB to 450 mbsf and log with triple combo and FMS-sonic			2.3	1.0
			Sub-Total Days On-Site:	6.8			
			Transit ~148 nmi to YB-2 @ 10.5 knots		0.6		
YB-2	37° 2.00' N	941	Hole A - APC to 200 mbsf w/APCT3 measurements and orientation			1.0	
EPSP	134° 48.00' E		Hole B - APC to 200 mbsf			0.6	
to 400 mbsf			Hole C - APC/XCB to 400 mbsf			1.6	
			Sub-Total Days On-Site:	3.2			
			Transit ~66 nmi to YB-1 @ 10.5 knots		0.3		
YB-1	35° 57.92' N	327	Hole A - APC to 200 mbsf w/APCT3 measurements and orientation			0.8	
EPSP	134° 26.06' E		Hole B - APC to 200 mbsf			0.4	
to 500 mbsf			Hole C - APC/XCB to 500 mbsf and log with paleo combo and FMS-sonic			1.7	1.0
			Sub-Total Days On-Site:	3.9			
			Transit ~181 nmi to UB-1 @ 10.5 knots		0.7		
UB-1	37° 54.16' N	1075	Hole A - APC to 200 mbsf w/APCT3 measurements and orientation			1.0	
EPSP	131° 32.25' E		Hole B - APC/XCB to 285 mbsf			1.0	
to 285 mbsf			Hole C - APC/XCB to 285 mbsf and log with triple combo and FMS-sonic			1.2	0.7
			Sub-Total Days On-Site:	3.9			
			Transit ~397 nmi to ECS-1B @ 10.5 knots		1.6		
ECS-1B	31° 40.64' N	747	Hole A - APC to 200 mbsf w/APCT3 measurements			0.9	
EPSP	129° 2.00' E		Hole C - APC/XCB to 800 mbsf and log with paleo combo and FMS-sonic			3.2	1.3
to 800 mbsf			Hole C - APC/XCB to 600 mbsf			2.4	
			Sub-Total Days On-Site:	7.8			
			Transit ~220 nmi to Busan @ 10.5 knots		0.9		
Busan			End Expedition		19.3	32.1	4.6

Port Call:	5.0	Total Operating Days:	56.0
Sub-Total On-Site:	36.7	Total Expedition:	61.0

Note: Pending request to EPSP to extend approved depth by 50 m on all sites.

EPSP = Environmental Protection and Safety Panel. APC = advanced piston corer, XCB = extended core barrel, APCT3 = advanced piston corer temperature tool, triple combo = triple combination tool string, FMS-sonic = Formation MicroScanner-sonic tool string.

Table T3. Operations plan for alternate proposed sites, Expedition 346.

Site No.	Location (Latitude Longitude)	Seafloor Depth (mbrf)	Operations Description	Drilling Coring (days)	LWD/MWD Log (days)
YB-3	38° 37.00' N	2885	Hole A - APC to ~200 mbsf w/APCT3 measurements and orientation	1.5	
EPSP	134° 32.00' E		Hole B - APC to ~200 mbsf	1.1	
to 200 mbsf			Hole C - APC to 200 mbsf and Log with Triple combo and FMS Sonic	1.5	0.7
			Sub-Total Days On-Site: 4.8		
ECS-1A	31° 38.30' N	757	Hole A - APC to 200 mbsf w/APCT3 measurements and orientation	0.9	
EPSP	128° 56.60' E		Hole B - APC to 200 mbsf	0.5	
TBD			Hole C - APC to 200 mbsf and Log with Paleo combo and FMS Sonic	0.8	0.7
			Sub-Total Days On-Site: 2.9		

Note 1: Pending request to EPSP to extend approved depth by 50 m on YB-3.

Note 2: Pending request to EPSP to approve alternate site ECS-1A to 500 mbsf.

EPSP = Environmental Protection and Safety Panel. APC = advanced piston corer, APCT3 = advanced piston corer temperature tool, triple combo = triple combination tool string, FMS-sonic = Formation MicroScanner-sonic tool string.

Figure F1. Bathymetric map with locations of proposed sites, previously drilled DSDP and ODP sites, and surface current systems within and surrounding the Expedition 346 operations area in the Japan Sea.

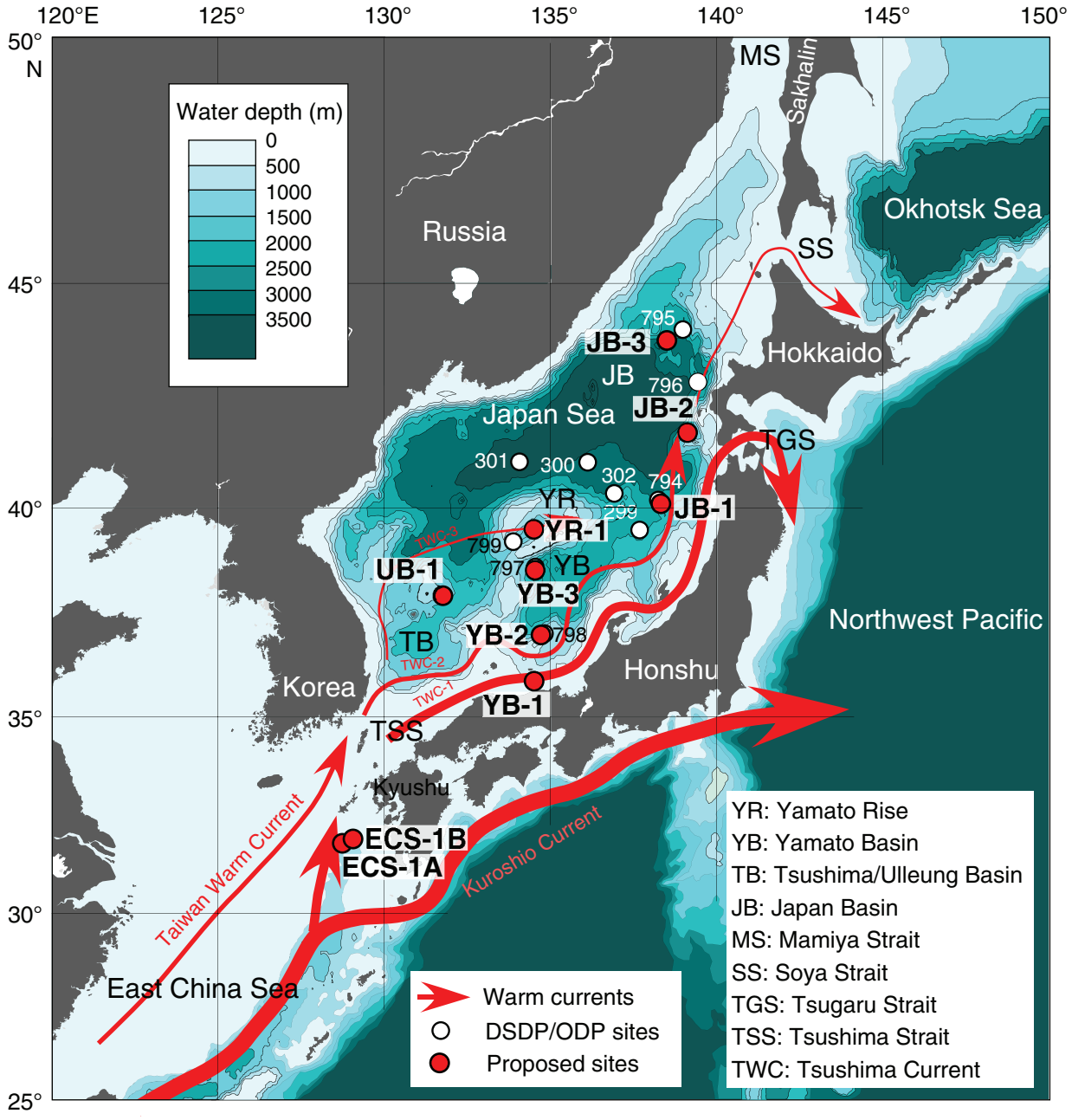

Figure F2. Map with two hypothesized modes of Westerly Jet circulation patterns in the northern hemisphere corresponding to stadials and interstadials of Dansgaard–Oeschger cycles. The sense of shifts seems to have been opposite between EastAsia and Mediterranean areas. The Himalaya and Tibetan Plateau should play the role of topographic barrier.

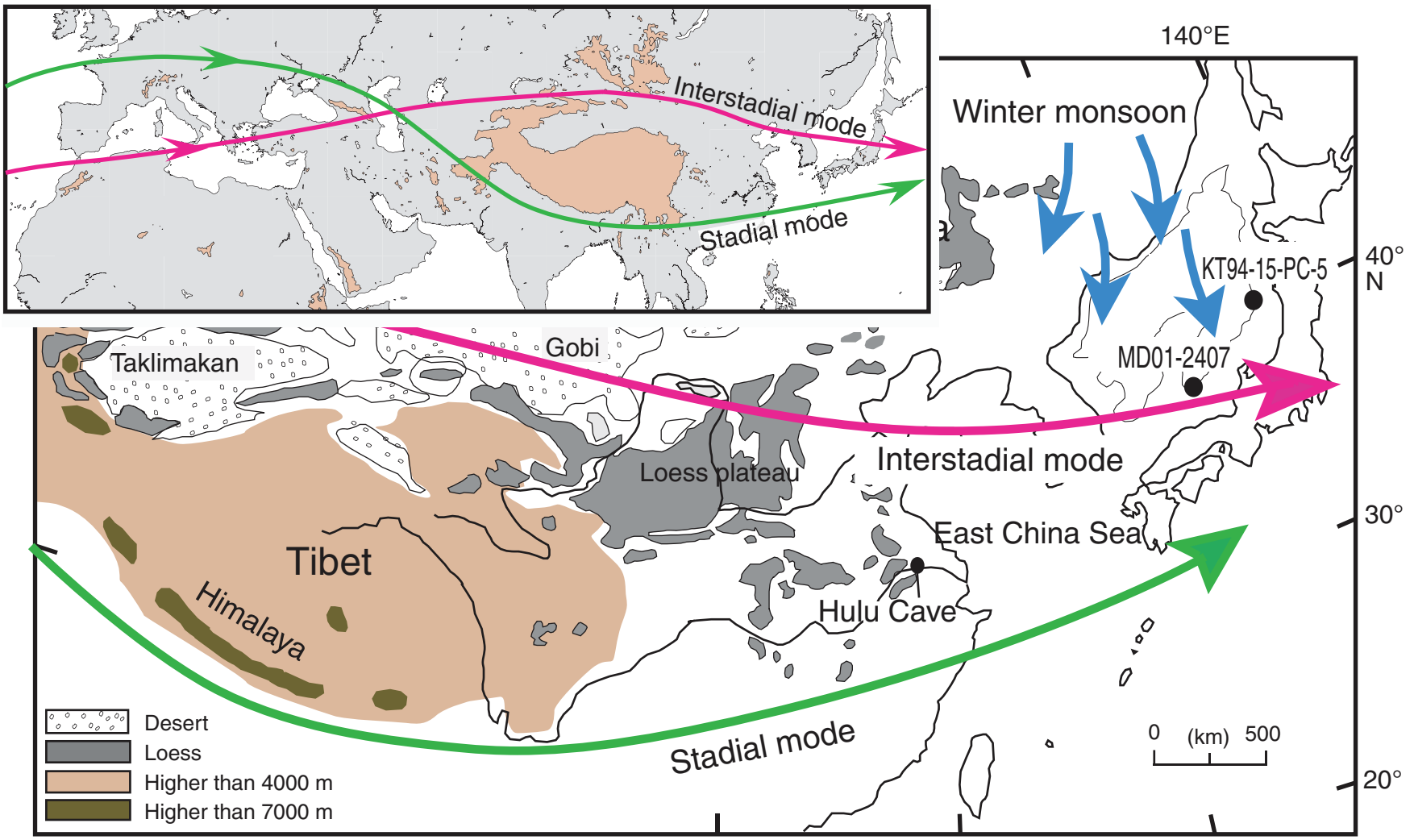

Figure F3. Plot of the seasonal cycle of the daily jet latitude at 80°–90°E (open circles) and the jet latitude obtained after low-pass filtering with a cutoff period of 30 days (solid line) for A.D. 2000. Shaded area is the latitude range corresponding to the Himalaya and Tibetan Plateau.

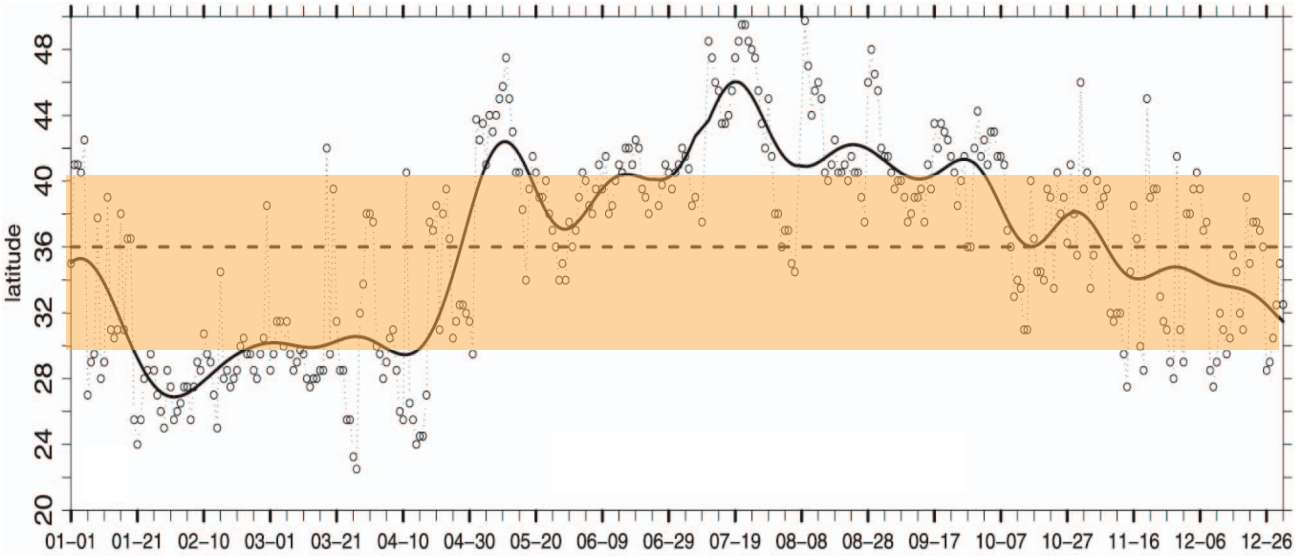

Figure F4. Plots of temporal variation in ice-rafted debris content at GH95-1208 (proposed Site JB-3) during the last 160 k.y. correlated to L* profile at MD01-2407 (proposed Site YB-2). Sharp ice-rafted debris events tend to agree with horizons of high L* values that tends to coincide with Heinrich events.

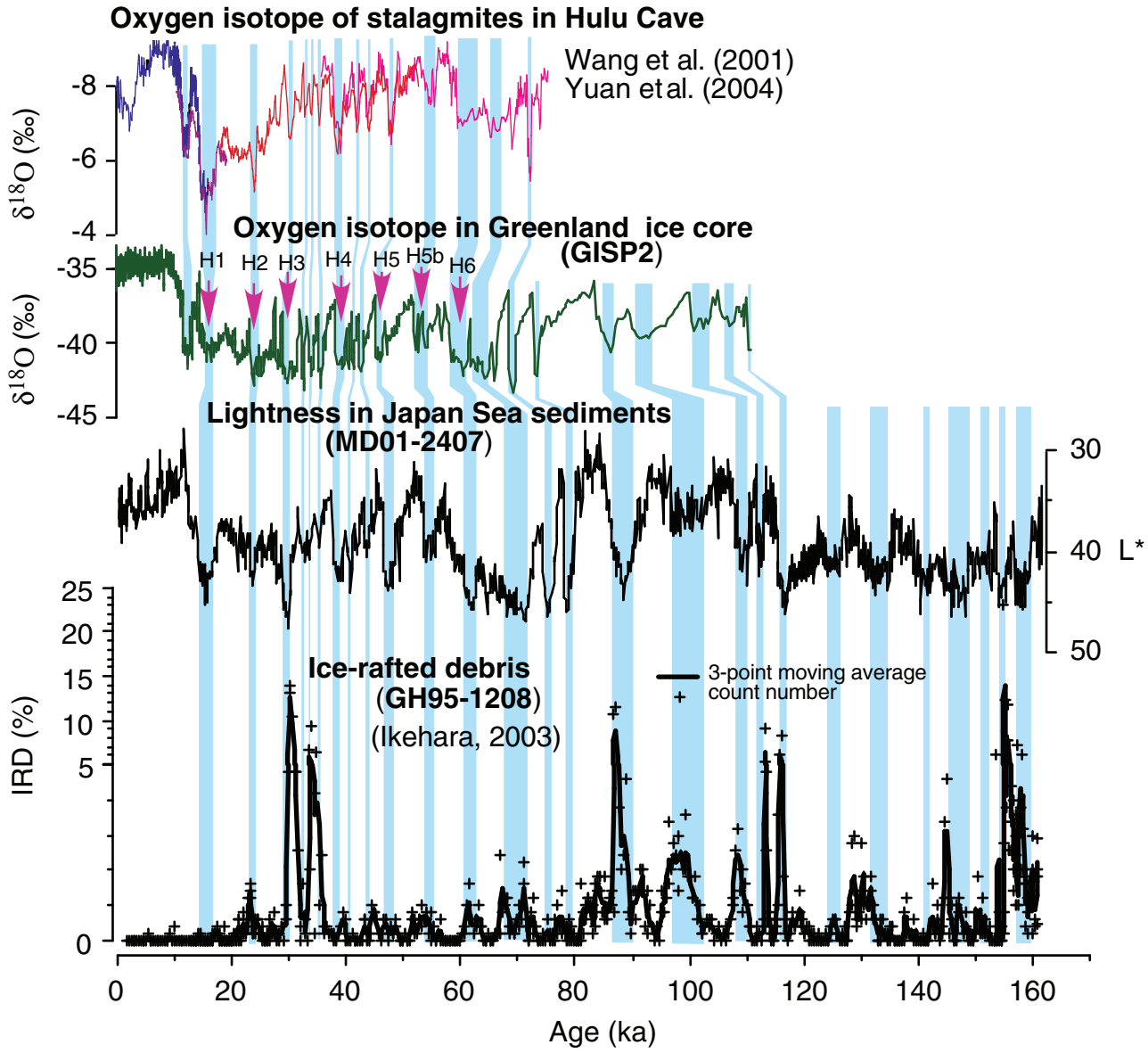

Figure F5. Diagram of phosphorus (Q) and water (in parentheses) budgets in the northern part of the East China Sea shelf and its margin. Modified from Chen and Wang (1999).

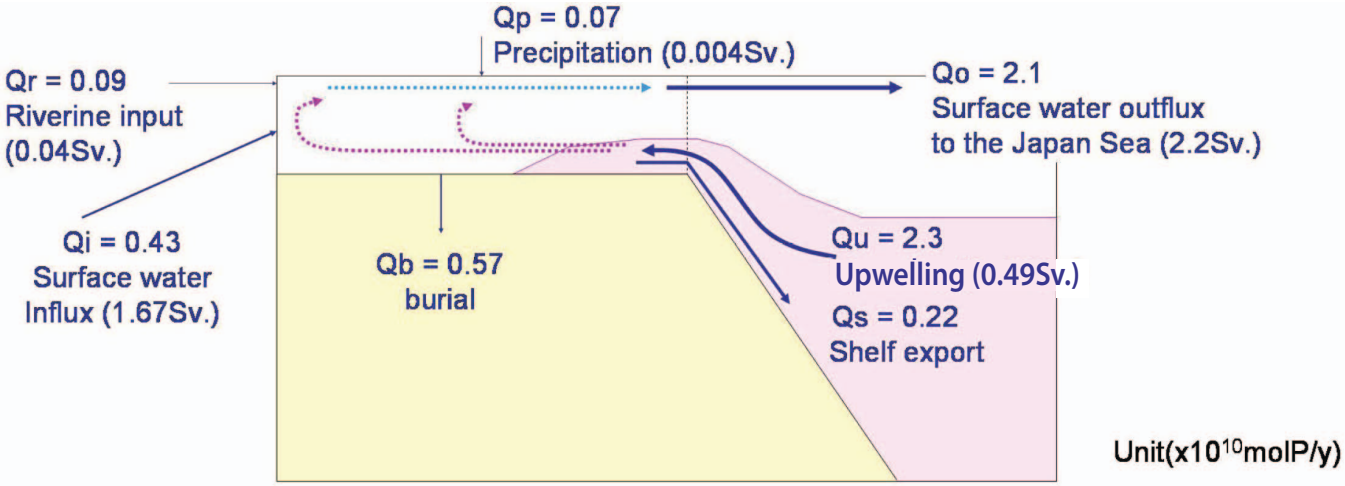

Figure F6. Diagram of phosphorus (Q) and water (in parentheses) budgets in the Japan Sea (Tada, 2003).

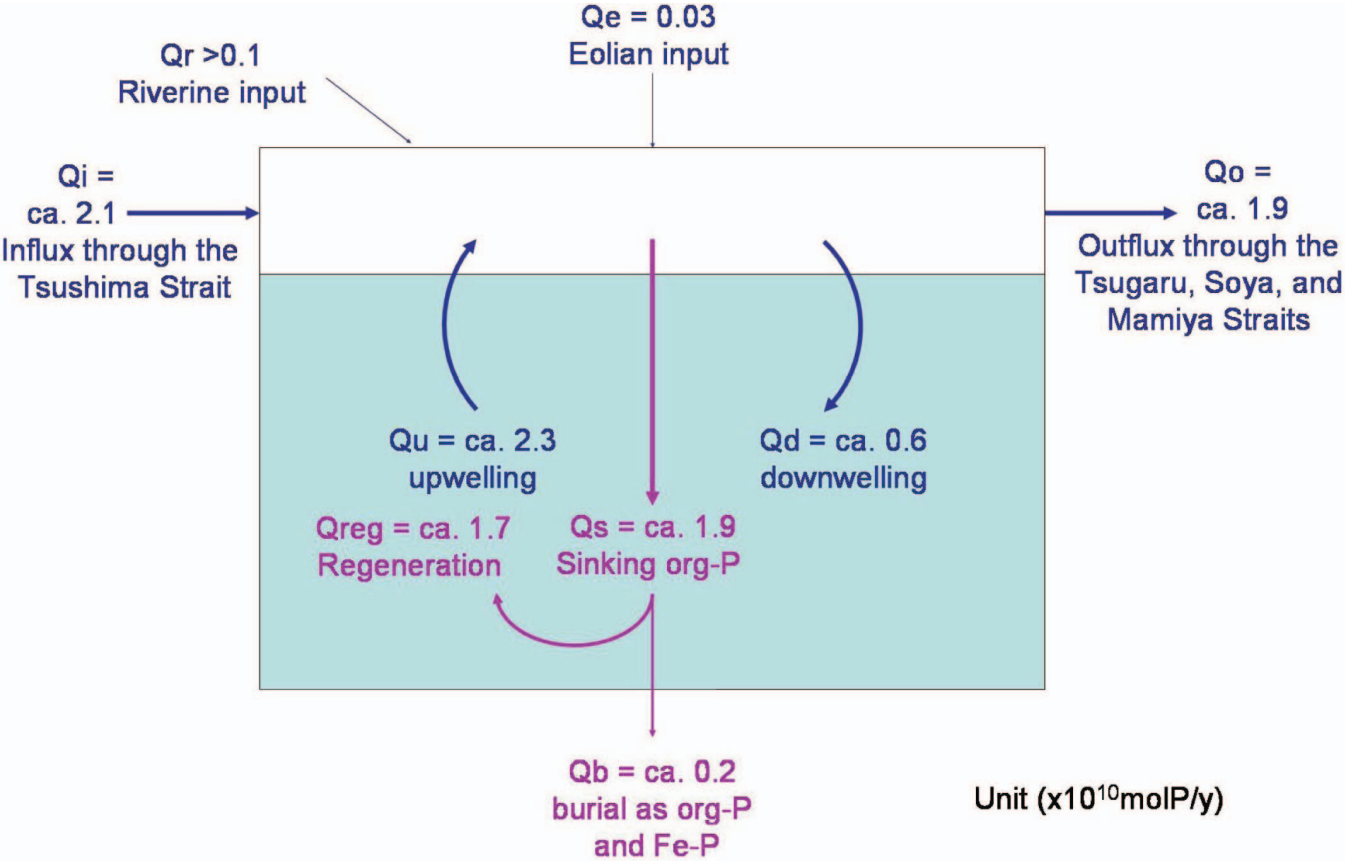

Figure F7. Plots showing the correlation between $\delta^{18}O$ records of GISP2 ice core and L* of MD01-2407 (proposed Site YB-2) in the Japan Sea. The age model is after Yokoyama et al. (2007).

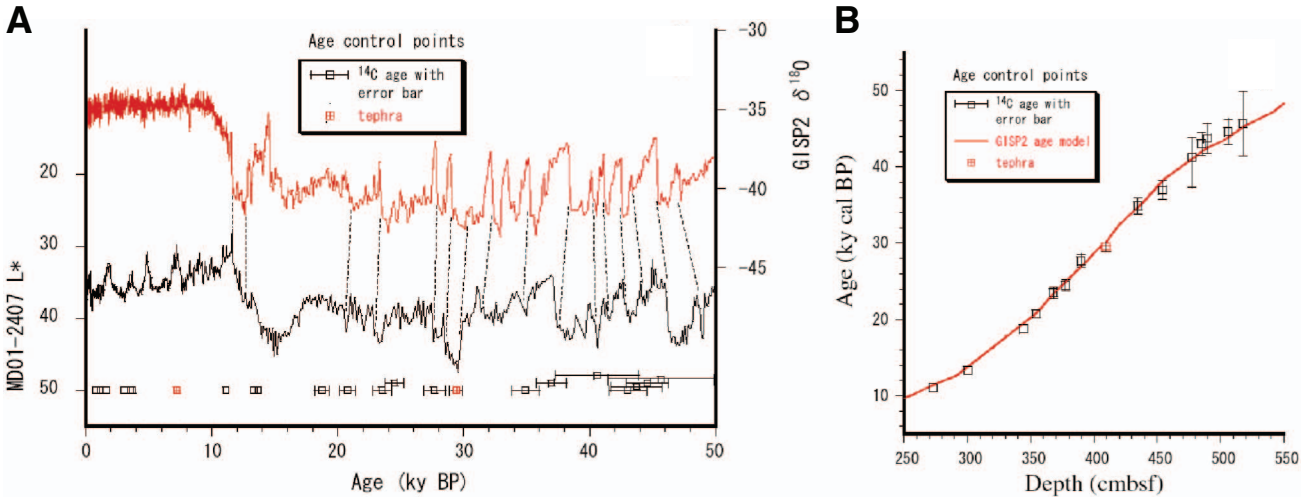

Figure F8. Plot of oxygen isotope ratio of planktonic foraminifers in sediment from MD01-2407 core during the last 250 k.y. Age model is based on 14 ^{14}C dates and 3 tephra layers (AT, Aso-4,and Ata-Th, of which ages are well constrained). Shaded areas indicate stratigraphic intervals characterized by thinly laminated thick dark layers. Modified from Kido et al. (2007).

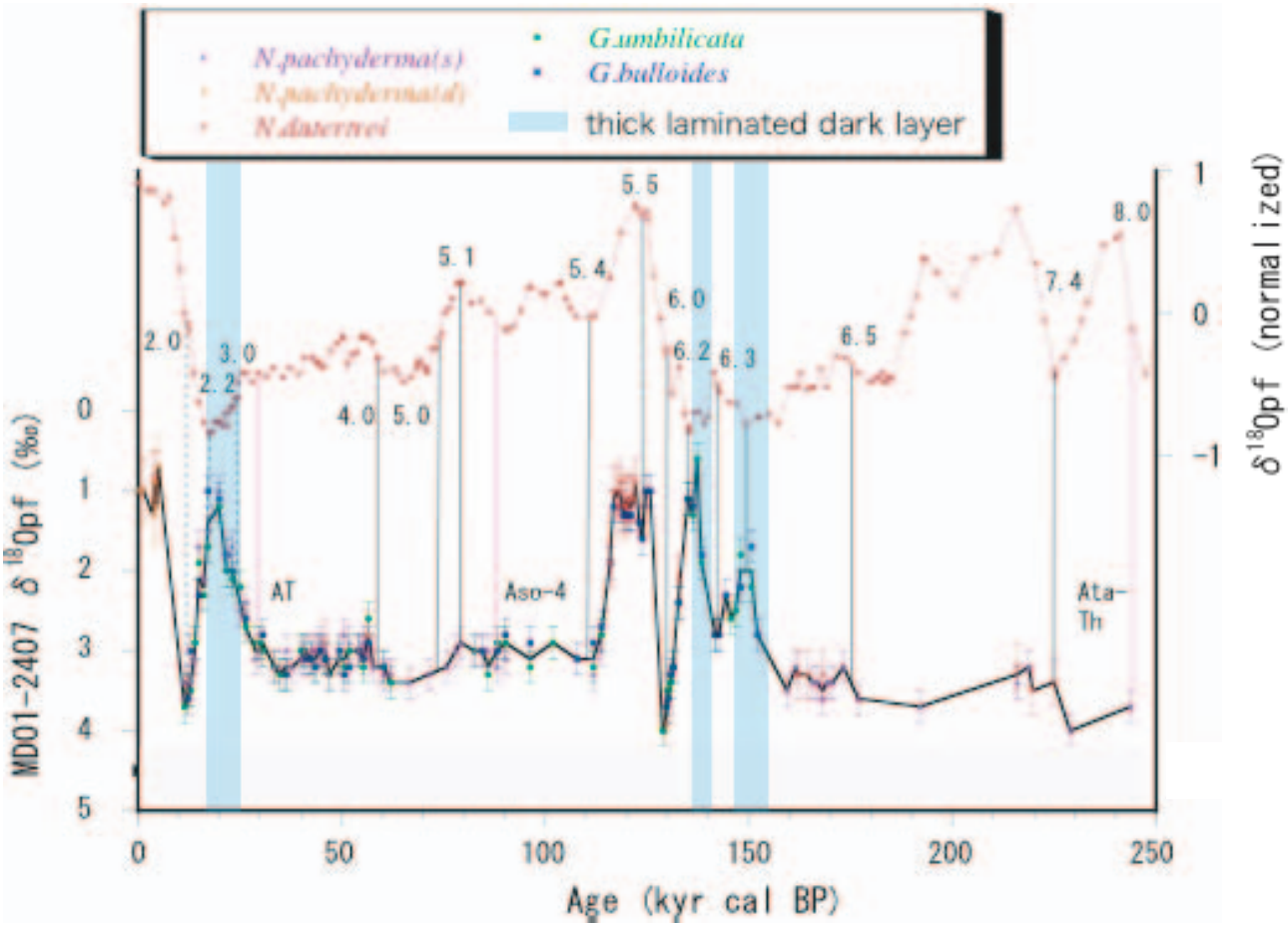

Figure F9. Simplified cartoon of the opening of the Japan Sea (modified from Tamaki et al., 1992). Crustal thinning and extension prevails at the initial stage. Seafloor spreading was triggered by the breakup of the lithosphere along the strike-slip margin at the eastern side of the Japan Sea. The spreading center propagated southwestward to increase the area of the oceanic crust while the southern Japan Sea was undergoing thinning.

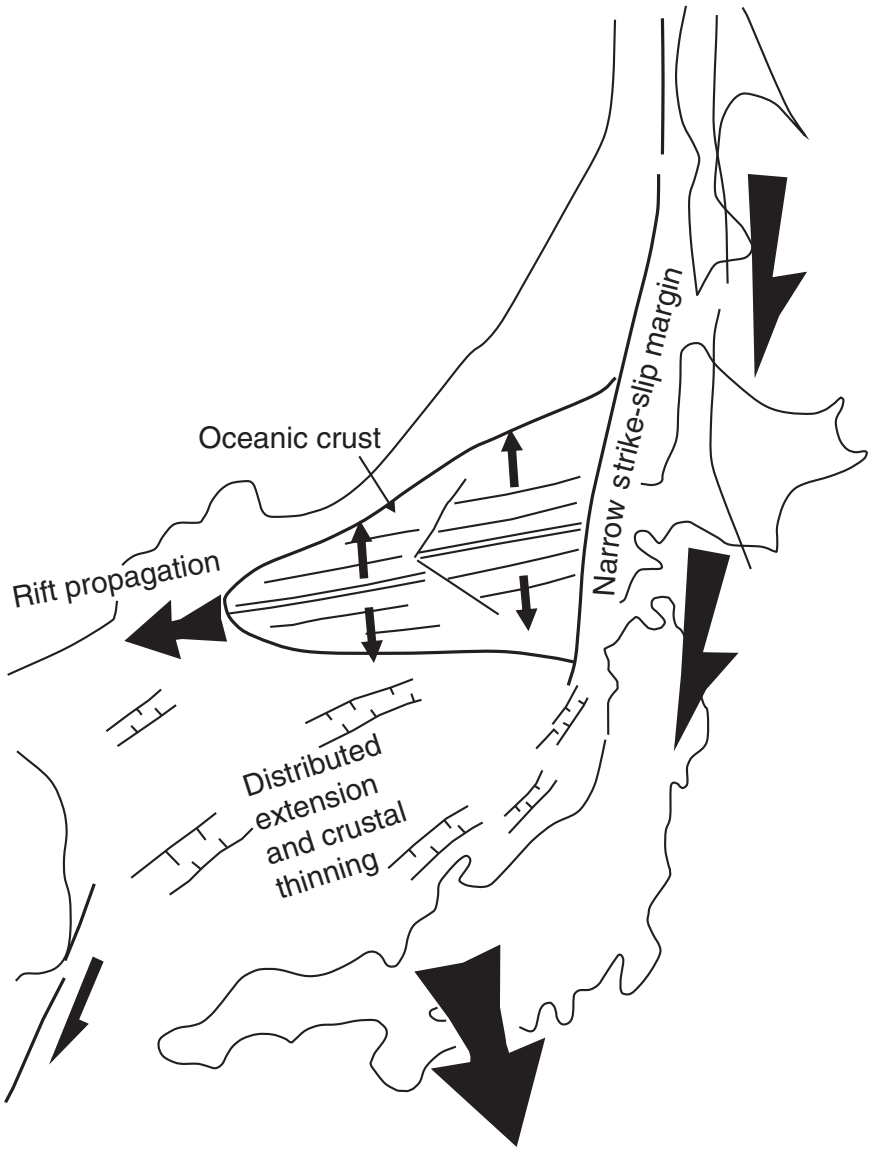

Figure F10. Drawing of the tectonic framework in the East China Sea area. CNTSFZ = central-northern Taiwan-Sinzi folded zone, GR = Guanyin Rise, NB = Nanjihtao Basin, NPB = North Pengchiahsu Basin, PH = Penghu Basin, PP = Pengchiahsu Platform, SPB = South Pengchiahsu Basin, STSFZ = southern Taiwan-Sinzi folded zone, TOB = Taiwan orogenic belt, TR = Tungyintao Ridge. From Kong et al. (2000).

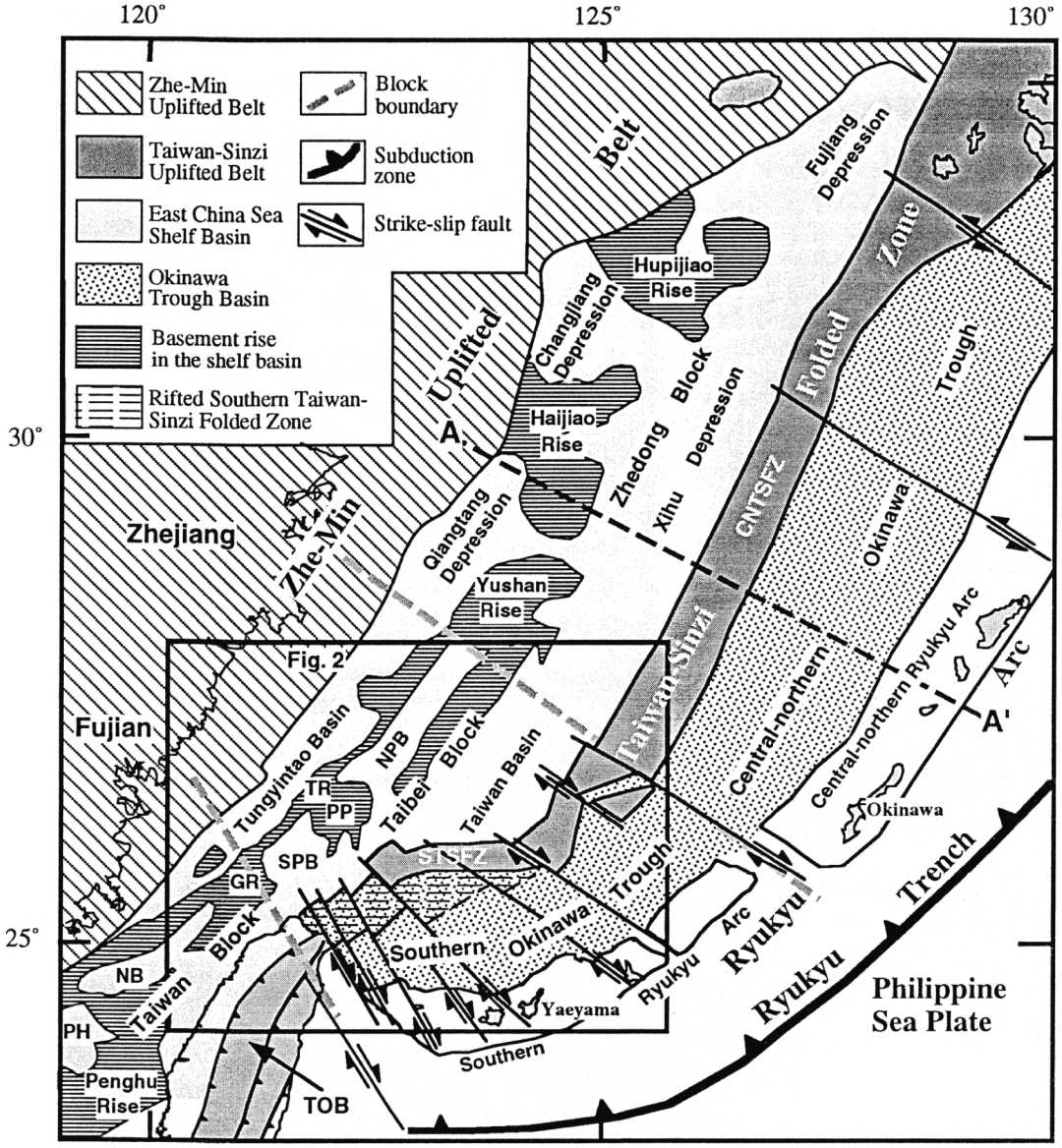

Figure F11. Schematics of winter and summer horizontal circulation patterns near 50 m water depth together with the distributions of water masses and oceanic fronts (after Kondo, 1985). The 200 m isobath is also shown. YSCCW = Yellow Sea Central Cold Water, YSWC = Yellow Sea Warm Current, TSWC = Tsushima Warm Current, CRDW = Changjiang River Diluted Water, KBCWK = Kuroshio Branch Current west of Kyushu, KBCNT = Kuroshio Branch Current north of Taiwan, TWWC = Taiwan Warm Current.

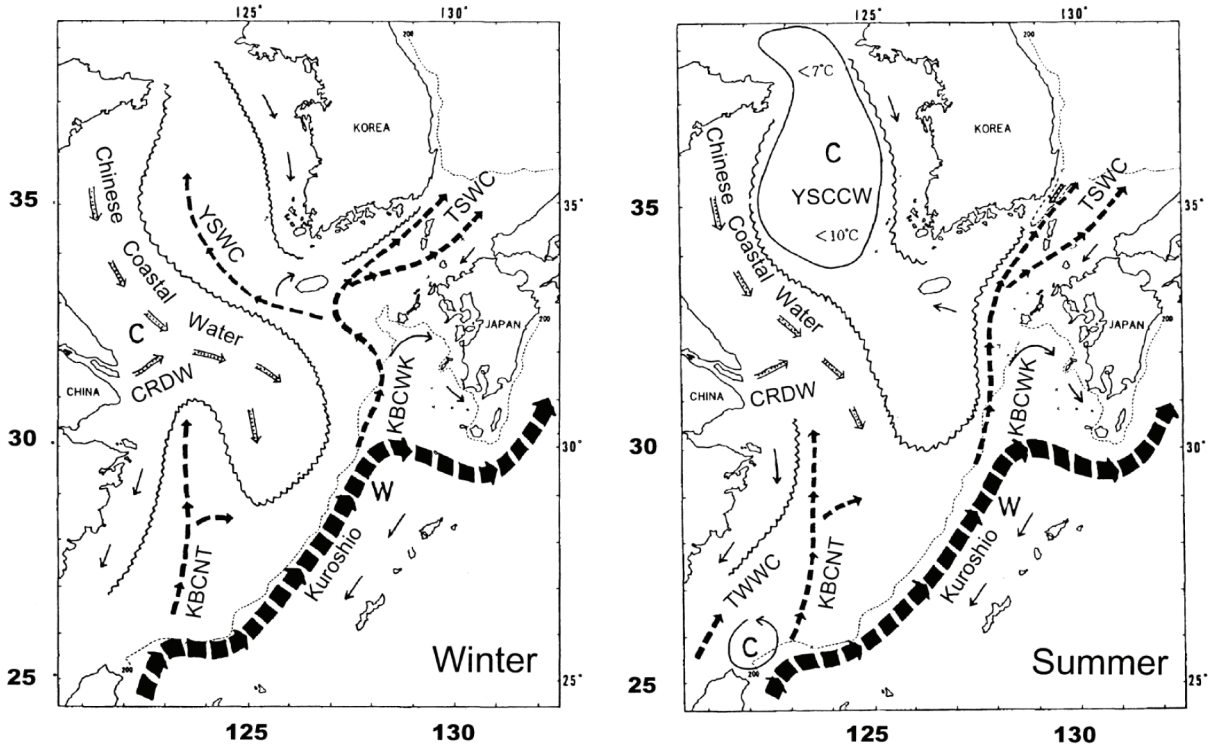

Figure F12. Vertical profiles of potential temperature, salinity, and dissolved oxygen of the Japan Sea.

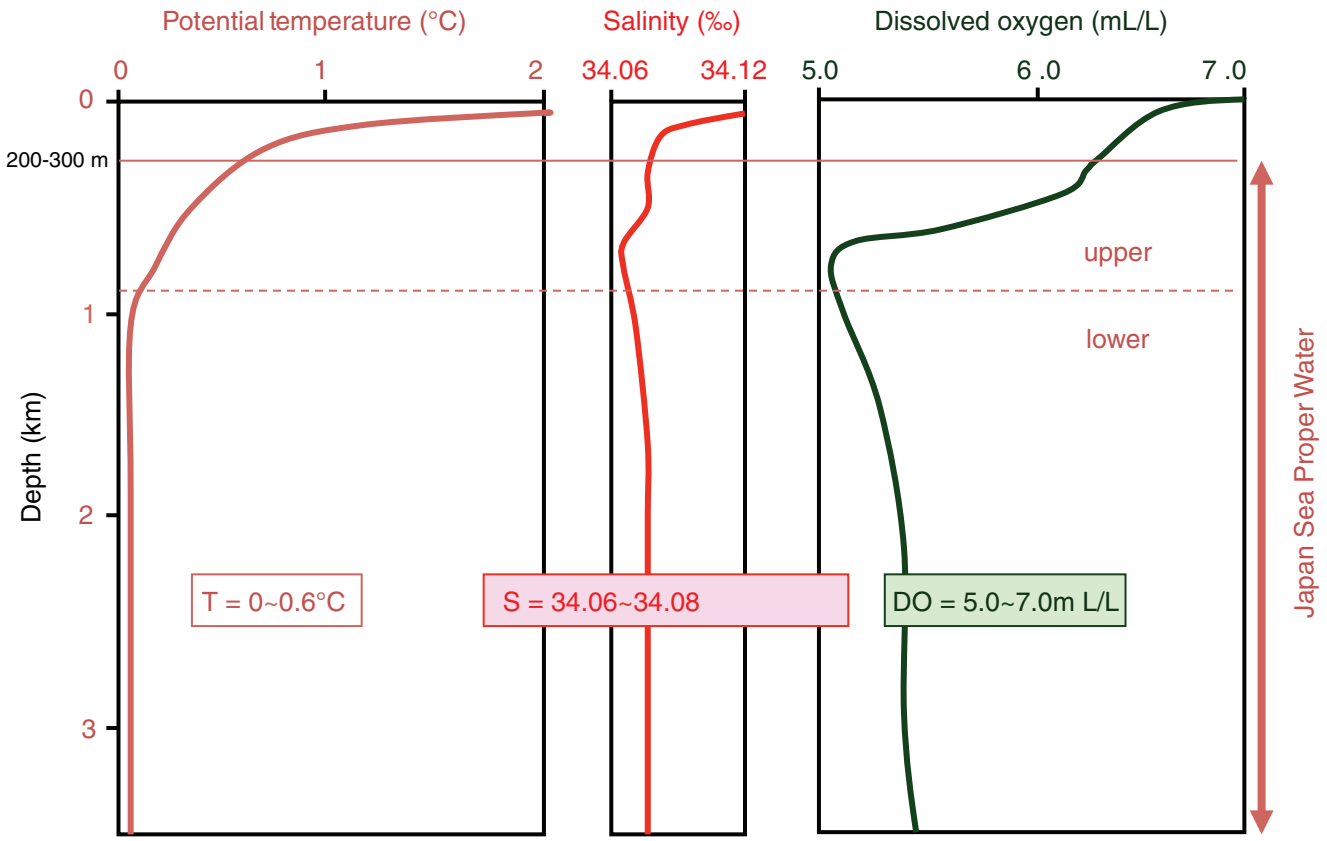

Figure F13. A, B. Graphic representations of oxygen content along 131°–300°E. Episodic formation of Japan Sea Proper Water sinking to the bottom of the Japan Sea during severe winter of 2001 is shown in B.

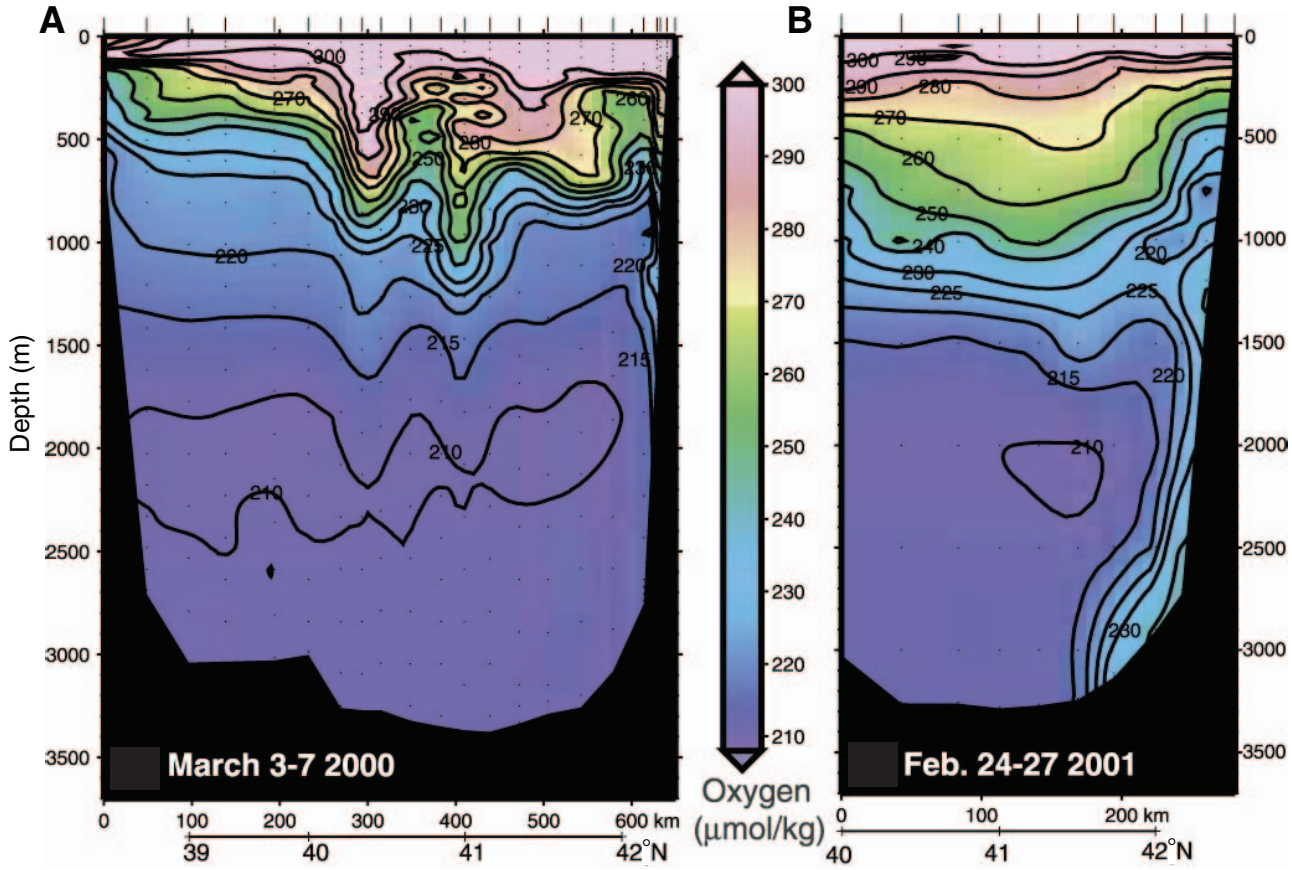

Figure F14. Downhole logs of an interval with cyclic alternations from ODP Leg 128 Site 798B. SFLU = focused induction resistivity, IMPH = medium induction resistivity, RHOM = bulk density, HSGR = standard (total) gamma radiation, FMS = Formation MicroScanner (resistivity image of the borehole wall). The cyclic nature of alternating dark and light intervals in cores is related to orbital-scale variability of paleoceanographic conditions in the Japan Sea. Gray areas correspond to dark clay- and organic matter–rich intervals in cores and correlate with high values in gamma ray, density, and resistivity logs and low conductivity values in FMS images.

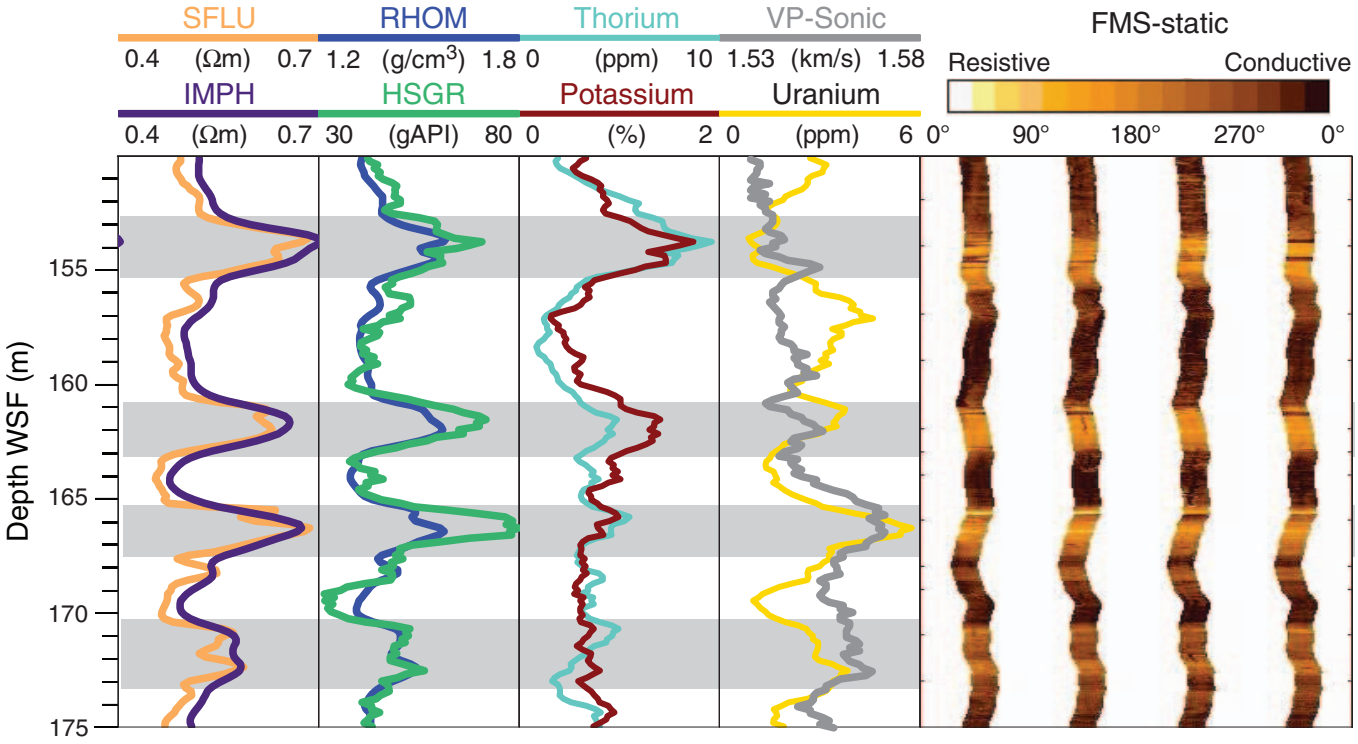

Site summaries

Site JB-3 (Japan Basin, Japan Sea)

Priority:	Primary (medium)
Position:	43°45.99′N, 138°49.99′E (WGS 84)
Water depth (m)	3435
Target drilling depth (mbsf):	200
Approved maximum penetration (mbsf):	200 [EPSP 2008] *Pending request to EPSP for 250
Previous drilling in area:	ODP Site 795 drilled ~40 km NE of this proposal site Piston core: GH95-1208
Comments:	Old site name: JS-5B Jurisdiction: Japan EEZ Potential hazards: typhoon season (June to October)
Survey coverage (track map, seismic profile):	Bathymetric sketch and site track map (Fig. **AF1**) High-resolution seismic reflection: • Primary line(s): KR05-09, Line 5N4346 (SP321) (Fig. **AF2**) • Crossing lines(s): KR05-09, Line 5E13850 (SP487) (Fig. **AF3**) 3.5 kHz: R05-09: Line 5N4346, Line 5E13850
Objectives (see text for complete details):	High-resolution reconstruction of dust flux, as well as other paleoceanographic records, in the southern part of the Japan Sea during the last 4 m.y.
Drilling, coring, and downhole measurements program:	Triple APC to 200 mbsf Temperature measurements: APCT-3 Orientation on first hole: FlexIt
Downhole logging program:	NA
Anticipated lithology:	Diatomaceous clay to silt

Site summaries (continued)

Site JB-2 (Japan Basin, Matsumae Plateau, Japan Sea)

Priority:	Primary (high)
Position:	41°41.95′N, 139°04.98′E (WGS 84)
Water depth (m)	1785
Target drilling depth (mbsf):	250
Approved maximum penetration (mbsf):	250 [EPSP 2008] *Pending request for 300 to EPSP
Previous drilling in area:	ODP Site 796 drilled ~170 km N Piston core: GH96-1217
Comments:	Old site name: JS-4 Jurisdiction: Japan EEZ Potential hazards: typhoon season (June to October)
Survey coverage (track map, seismic profile):	Bathymetric sketch and site track map (Fig. **AF4**) High-resolution seismic reflection: • Primary line(s): KR05-09, Line 7E13905 (SP444) (Fig. **AF5**) • Crossing lines(s): KR05-09, Line 7N4142 (SP680) (Fig. **AF6**) 3.5 kHz: KR05-09: Line 7E13905, Line 7N4142
Objectives (see text for complete details):	High-resolution reconstruction of dust flux, as well as other paleoceanographic records, in the southern part of the Japan Sea during the last 4 m.y.
Drilling, coring, and downhole measurements program:	Triple APC to 200 mbsf Temperature measurements: APCT-3 Orientation on first hole: FlexIt
Downhole logging program:	Standard tools: triple combo, FMS-sonic
Anticipated lithology:	Diatomaceous clay to silt

Site summaries (continued)

Site JB-1 (Japan Basin, Japan Sea)

Priority:	Primary
Position:	40°11.40′N, 138°13.90′E (WGS 84)
Water depth (m):	2811
Target drilling depth (mbsf):	150
Approved maximum penetration (mbsf):	150 [EPSP 2008] *Pending request to EPSP for 200
Previous drilling in area:	Redrill of ODP Site 794
Comments:	Old site name: JS-7B Jurisdiction: Japan EEZ Potential hazards: typhoon season (June to October)
Survey coverage (track map, seismic profile):	Bathymetric sketch and site track map (Fig. **AF7**) Deep penetration seismic reflection: • Primary line(s): KT88-9, Line 108 (SP1262) (Fig. **AF8**) • Crossing lines(s): DELP′85, Line E (SP3895) (Fig. **AF9**)
Objectives (see text for complete details):	High-resolution reconstruction of dust flux, as well as other paleoceanographic records, in the southern part of the Japan Sea during the last 4 m.y.
Drilling, coring, and downhole measurements program:	Triple APC to 150 mbsf Temperature measurements: APCT-3 Orientation on first hole: FlexIt
Downhole logging program:	NA
Anticipated lithology:	Diatomaceous clay to silt

Site summaries (continued)

Site YR-1 (Yamato Ridge, Japan Sea)

Priority:	Primary (very high)
Position:	39°29.44′N, 134°26.55′E (WGS 84)
Water depth (m)	1917
Target drilling depth (mbsf):	450
Approved maximum penetration (mbsf):	450 [EPSP 2008] *Pending request to EPSP for 500
Previous drilling in area:	ODP Site 799 Piston cores: KR07-12, St. 7′′, PC-05 and PC-08
Comments:	Old Site Number: JS-3B Jurisdiction: Japan EEZ Potential hazards: typhoon season (June to October)
Survey coverage (track map, seismic profile):	Bathymetric sketch and site track map (Fig. **AF10**) High-resolution seismic reflection: • Primary line(s): KR07-12, Line st7′′-1-2 (SP100) (Fig. **AF11**) • Crossing lines(s): KR07-12, Line st7′′-5-6 (SP510) (Fig. **AF12**) 3.5 kHz and swath bathymetry: KR07-12, Lines st7′′-1-2, st7′′-5-6
Objectives (see text for complete details):	High-resolution reconstruction of dust flux, as well as other paleoceanographic records, in the southern part of the Japan Sea during the last 5 m.y.
Drilling, coring, and downhole measurements program:	Triple APC to 200 mbsf; double XCB to 450 mbsf Temperature measurements: APCT-3 Orientation on first hole: FlexIt
Downhole logging program:	Standard tools: triple combo, FMS-sonic
Anticipated lithology:	Diatomaceous clay to silt

Site summaries (continued)

Site YB-2 (Yamato Basin, Oki Ridge, Japan Sea)

Priority:	Primary
Position:	37°02.00'N, 134°48.00'E (WGS 84)
Water depth (m)	930
Target drilling depth (mbsf):	400
Approved maximum penetration (mbsf):	400 [EPSP 2008] *Pending request to EPSP for 450
Previous drilling in area:	Redrill of ODP Site 798
Comments:	Old site name: JS-1 Jurisdiction: Japan EEZ Potential hazards: typhoon season (June to October)
Survey coverage (track map, seismic profile):	Deep-penetration seismic reflection: • Primary line(s): GH86-4, Line JS-2 (SP2049) (Fig. **AF13**) 3.5 kHz: GH874, 23:50 September 19 Site track location (Fig. **AF14**)
Objectives (see text for complete details):	High-resolution reconstruction of dust flux, as well as other paleoceanographic records, in the southern part of the Japan Sea during the last 4 m.y.
Drilling, coring, and downhole measurements program:	Triple APC to 200 mbsf; single XCB to 400 mbsf Temperature measurements: APCT-3 Orientation on first hole: FlexIt
Downhole logging program:	NA
Anticipated lithology:	Diatomaceous clay to silt

Site summaries (continued)

Site YB-1 (Yamato Basin, Japan Sea)

Priority:	Primary (high)
Position:	35°57.92′N, 134°26.06′E (WGS 84)
Water depth (m)	316
Target drilling depth (mbsf):	500
Approved maximum penetration (mbsf):	500 [EPSP 2008] *Pending request to EPSP for 550
Previous drilling in area:	ODP Site 798; piston Core GH872-308
Comments:	Old site name: JS-10B Jurisdiction: Japan EEZ Potential hazards: typhoon season (June to October)
Survey coverage (track map, seismic profile):	High-resolution seismic reflection: • Primary line(s): KR07-12, Line St4-3-4 (SP1140) (Fig. **AF15**) • Crossing lines(s): KR07-12, Line St4-1-2 (SP1250) (Fig. **AF16**) 3.5 kHz: KR07-12: Line St4-3-4, Line St4-1-2 Swath bathymetry: KR07-12, Line St4-3-4, Line St4-1-2 (Fig. **AF17**)
Objectives (see text for complete details):	High-resolution reconstruction of dust flux, as well as other paleoceanographic records, in the southern part of the Japan Sea during the last 2 m.y.
Drilling, coring, and downhole measurements program:	Triple APC to 200 mbsf; single XCB to 500 mbsf Temperature measurements: APCT-3 Orientation on first hole: FlexIt
Downhole logging program:	Standard tools: paleo combo, FMS-sonic
Anticipated lithology:	Diatomaceous clay to silt

Site summaries (continued)

Site UB-1 (Ullung Basin, South Korean Plateau)

Priority:	Primary (high)
Position:	37°54.16′N, 131°32.25′E (WGS 84)
Water depth (m)	1064
Target drilling depth (mbsf):	285
Approved maximum penetration (mbsf):	285 [EPSP 2008] *Pending request to EPSP for 335
Previous drilling in area:	
Comments:	Old site name: JS-11C Jurisdiction: Korea EEZ Potential hazards: typhoon season (June to October)
Survey coverage (track map, seismic profile):	Bathymetric sketch and site track map (Fig. **AF18**) Deep-penetration seismic reflection: • Primary line(s): Line_04GH-12 (Fig. **AF19**) • Crossing line(s): Line_04GH-20 (Fig. **AF20**)
Objectives (see text for complete details):	High-resolution analyses of dust flux, SST, SSS, organic C flux, carbonate C flux, and opal flux in the western part of the Japan Sea during the last 10 m.y. in order to reconstruct millennial-scale variability and million year–scale evolution of Asian summer monsoon, winter monsoon, Westerly Jet, subpolar front, surface productivity, and deepwater ventilation
Drilling, coring, and downhole measurements program:	Triple APC to 200 mbsf; double XCB to 285 mbsf Temperature measurements: APCT-3 Orientation on first hole: FlexIt
Downhole logging program:	Standard tools: triple combo, FMS-sonic
Anticipated lithology:	Diatomaceous clay to silty clay

Site summaries (continued)

Site ECS-1B (East China Sea-Danjo Basin)

Priority:	Primary (very high)
Position:	31°40.64′N, 129°02.00′E (WGS 84)
Water depth (m)	736
Target drilling depth (mbsf):	800
Approved maximum penetration (mbsf):	800 [EPSP 2008] *Pending request to EPSP for 850P
Previous drilling in area:	Piston cores: KR07-12, St. 2, PC-01
Comments:	Jurisdiction: Japan EEZ Potential hazards: typhoon season (June to October)
Survey coverage (track map, seismic profile):	High-resolution seismic reflection: • Primary line(s) KY07-04, Line 7 • Crossing lines(s): KY07-04, Line 8 Deep-penetration seismic reflection: • Primary line(s): KR07-12, st2-1-2 (Fig. **AF21**) • Crossing line(s): KR07-12, st2-5-6 (Fig. **AF22**) Seismic grid: • (MCS) KR07-12, Lines st2-1-2, st2-3-4, st2-5-6 • (SCS) KY07-04, Line 1, 2a, 2b, 3, 4, 5, 7, 8 3.5 kHz: KR07-12, Line st2-1-2, Line st2-5-6 Swath bathymetry: KR07-12, Line st2-1-2, Line st2-5-6 (Fig. **AF23**)
Objectives (see text for complete details):	High-resolution reconstruction of SSS and SST in the southern part of the East China Sea during the last 3–5 m.y.
Drilling, coring, and downhole measurements program:	Triple APC to 200 mbsf; single XCB to 800 mbsf; single XCB to 600 mbsf Temperature measurements: APCT-3 Orientation on first hole: FlexIt
Downhole logging program:	Standard tools: paleo combo, FMS-sonic, and possibly VSI
Anticipated lithology:	Diatomaceous clay to silt

Site summaries (continued)

Site YB-3 (Yamato Basin, Japan Sea)

Priority:	Alternate
Position:	38°37.00'N, 134°32.00'E (WGS 84)
Water depth (m)	2874
Target drilling depth (mbsf):	200
Approved maximum penetration (mbsf):	200 [EPSP 2008] *Pending request to EPSP for 250
Previous drilling in area:	Redrill of ODP Site 797
Comments:	Old site name: JS-9 Jurisdiction: Japan EEZ Potential hazards: typhoon season (June to October)
Survey coverage (track map, seismic profile):	High-resolution seismic reflection: • Primary line(s): KR07-12, Line St8-1-2 (SP518) (Fig. **AF24**) • Crossing lines(s): KR07-12, Line St8-3-4 (SP375) (Fig. **AF25**) 3.5 kHz: KR07-12: Line St8-1-2, Line St8-3-4 Swath bathymetry: KR07-12, Line St8-1-2, Line St8-3-4 (Fig. **AF26**)
Objectives (see text for complete details):	High-resolution reconstruction of dust flux, as well as other paleoceanographic records, in the southern part of the Japan Sea during the last 4 m.y.
Drilling, coring, and downhole measurements program:	Triple APC to 200 mbsf Temperature measurements: APCT-3 Orientation on first hole: FlexIt
Downhole logging program:	Standard tools: triple combo, FMS-sonic
Anticipated lithology:	Diatomaceous clay to silt

Site summaries (continued)

Site ECS-1A (East China Sea-Danjo Basin)

Priority:	Alternate
Position:	31°38.30′N, 128°56.60′E (WGS 84)
Water depth (m)	746
Target drilling depth (mbsf):	200
Approved maximum penetration (mbsf):	*Pending request to EPSP for 500
Previous drilling in area:	Piston cores: KR07-12, St. 2, PC-01
Comments:	Jurisdiction: Japan EEZ Potential hazards: typhoon season (June to October)
Survey coverage (track map, seismic profile):	Seismic single-channel survey: • Cross section of Seismic line 1 (Fig. **AF27**) • Cross section of Seismic line 4 (Fig. **AF28**) High-resolution seismic reflection: • Primary line(s) KY07-04, Line 7; Crossing Lines(s): KY07-04, Line 8 Deep-penetration seismic reflection: • Primary line(s): KR07-12, st2-1-2; Crossing Lines(s): KR07-12, st2-5-6 Seismic grid: • (MCS) KR07-12, Lines st2-1-2, st2-3-4, st2-5-6 • (SCS) KY07-04, Line 1, 2a, 2b, 3, 4, 5, 7, 8 3.5 kHz: KR07-12, Line st2-1-2, Line st2-5-6 Swath bathymetry: KR07-12, Line st2-1-2, Line st2-5-6 (Fig. **AF29**)
Objectives (see text for complete details):	High-resolution reconstruction of SSS and SST in the southern part of the East China Sea during the last 3–5 m.y.
Drilling, coring, and downhole measurements program:	Triple APC to 200 mbsf Temperature measurements: APCT-3 Orientation on first hole: FlexIt
Downhole logging program:	Standard tools: paleo combo, FMS-sonic
Anticipated lithology:	Diatomaceous clay to silt

Figure AF1. Bathymetry and site track map, proposed Site JB-3.

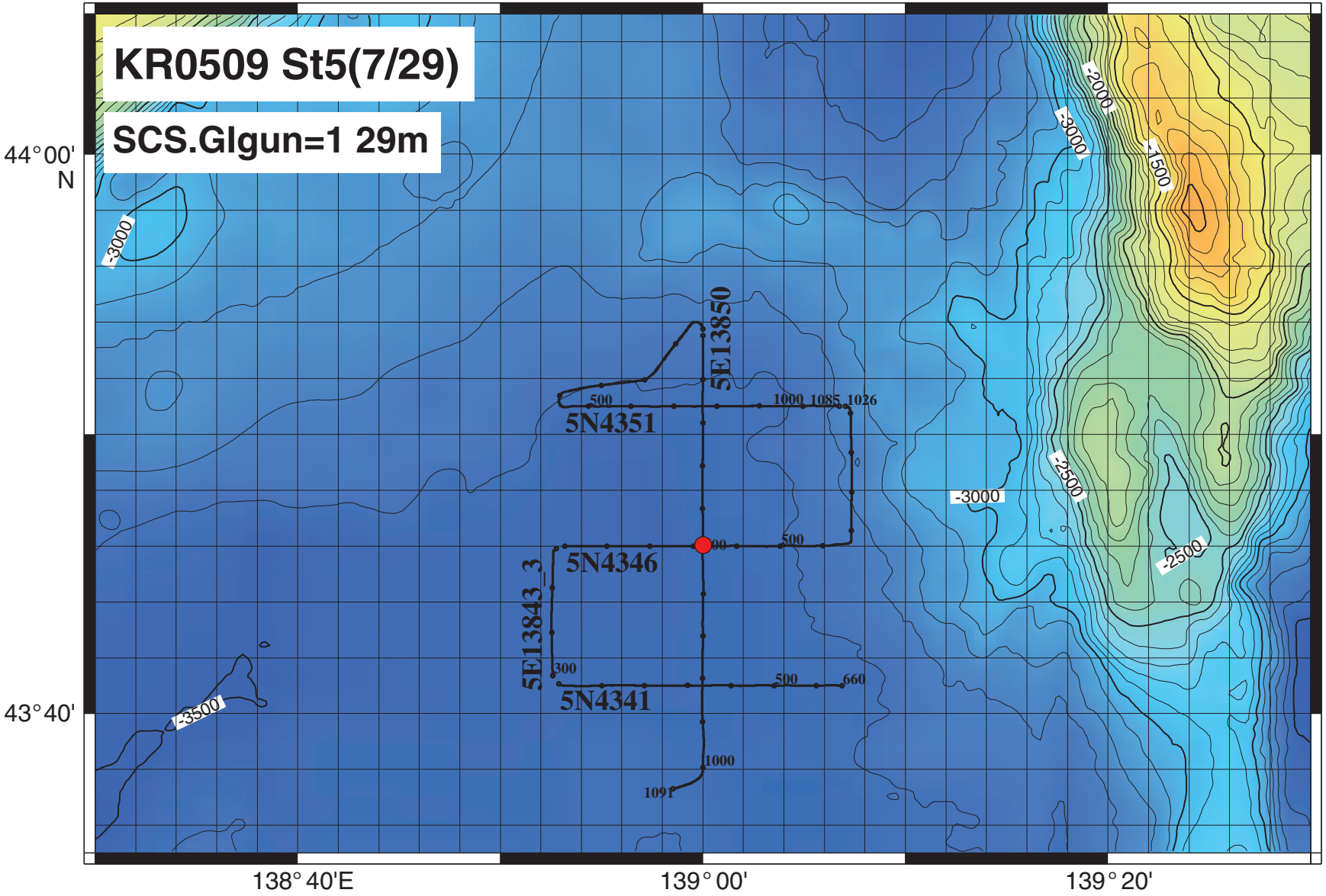

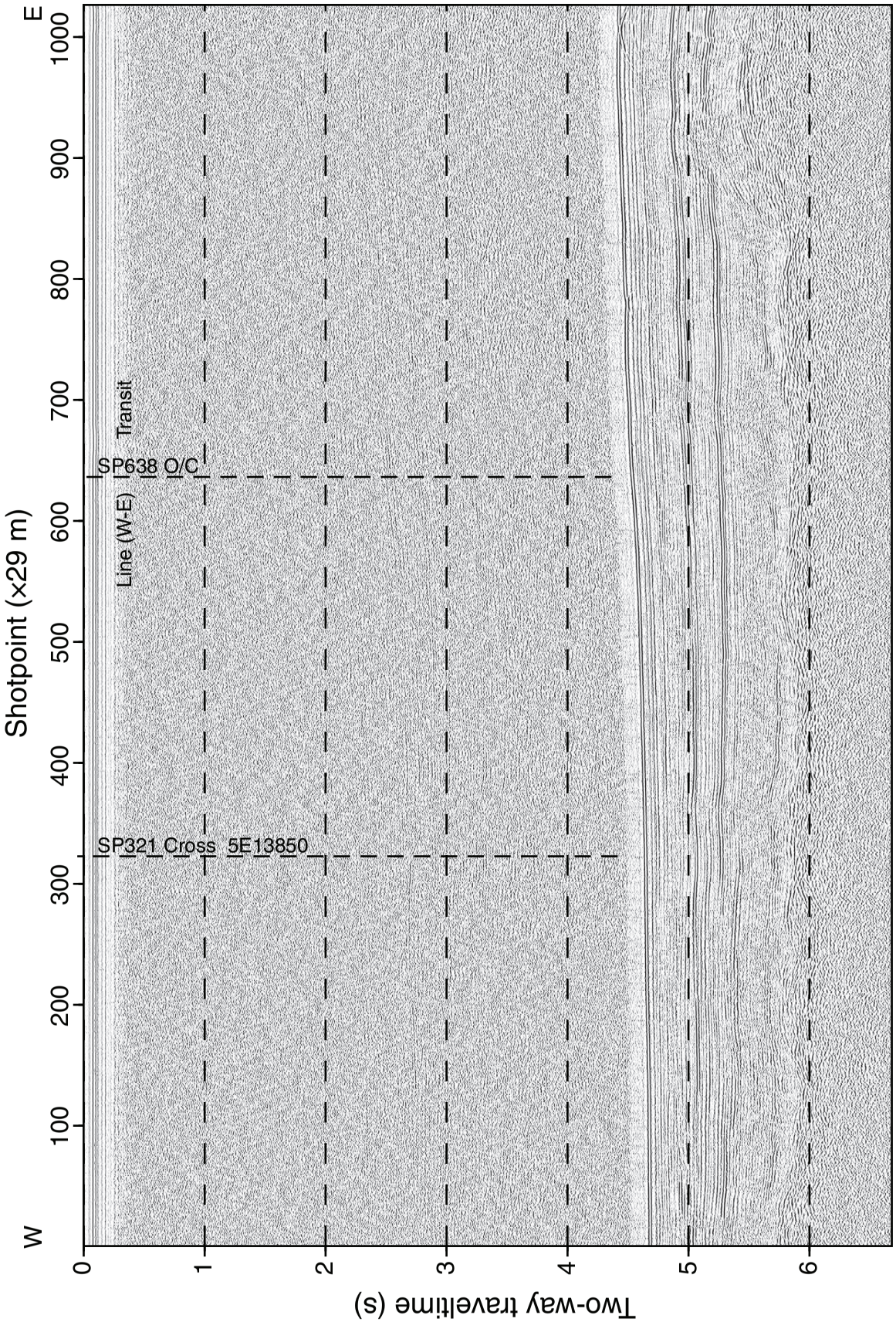

Figure AF2. Seismic crossing Line 5E13850, proposed Site JB-3. SP = shotpoint.

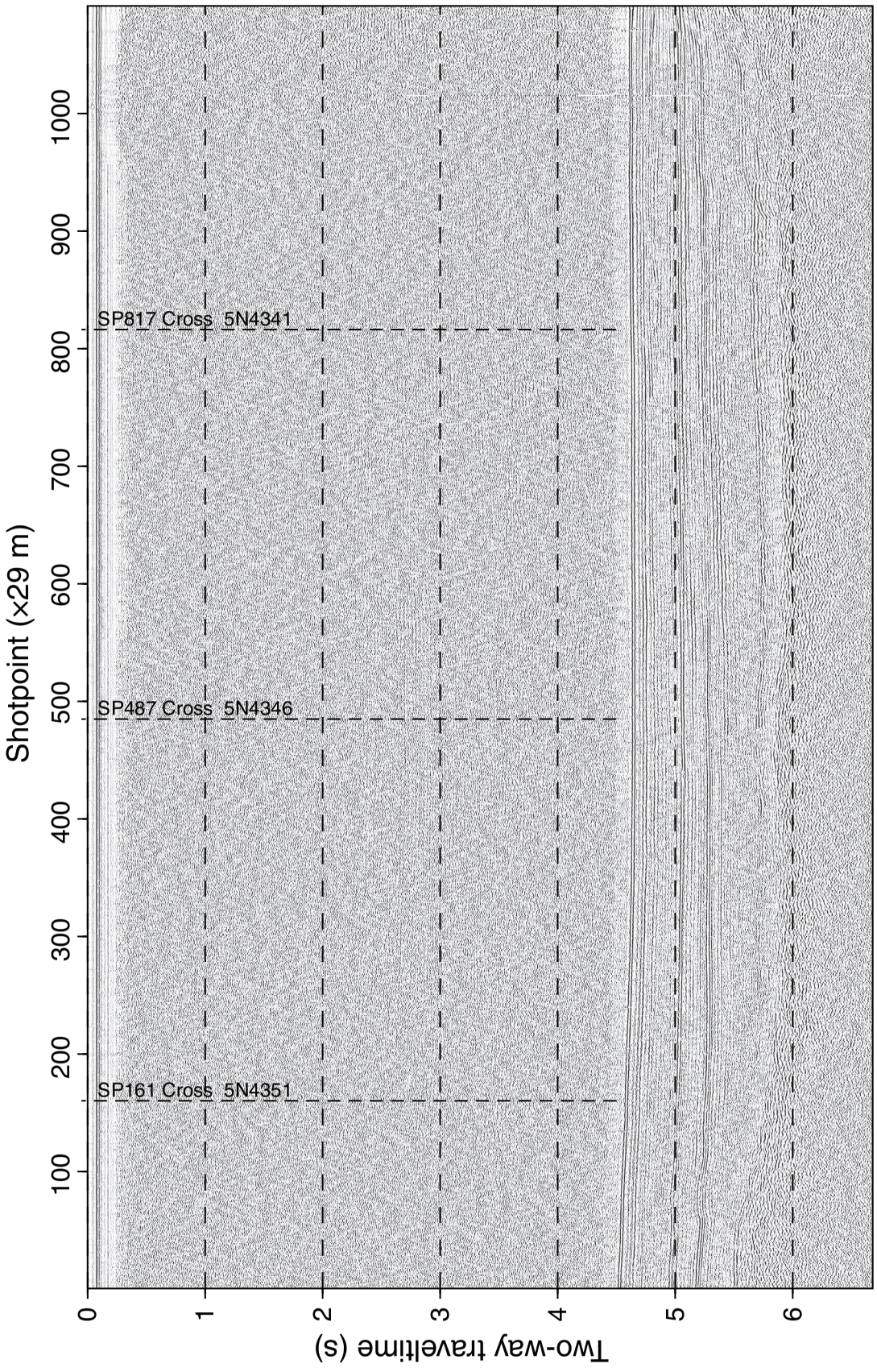

Figure AF3. 3.5 kHz seismic Line 5N4346, proposed Site JB-3. SP = shotpoint.

Figure AF4. Bathymetry and site track map, proposed Site JB-2.

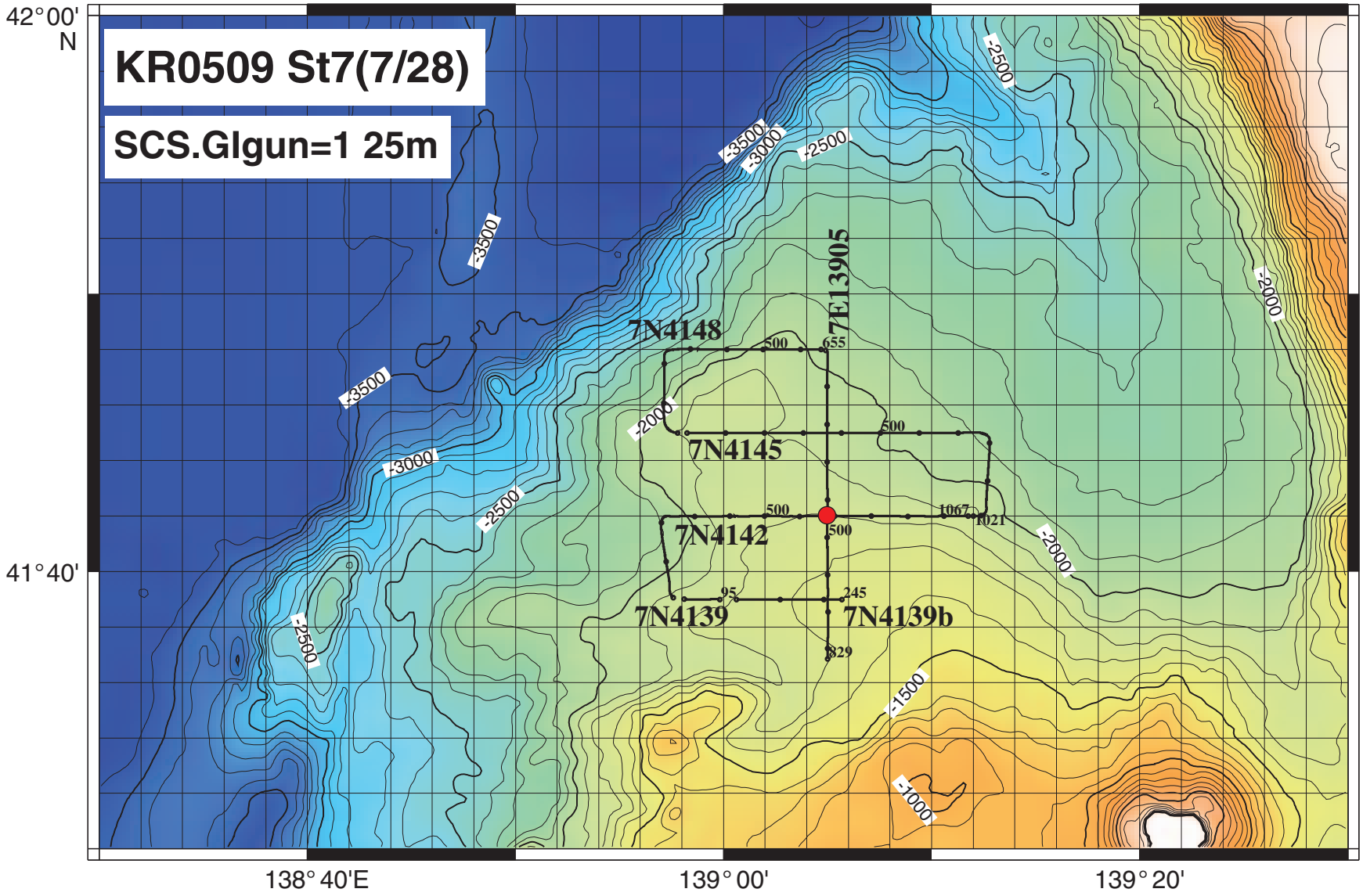

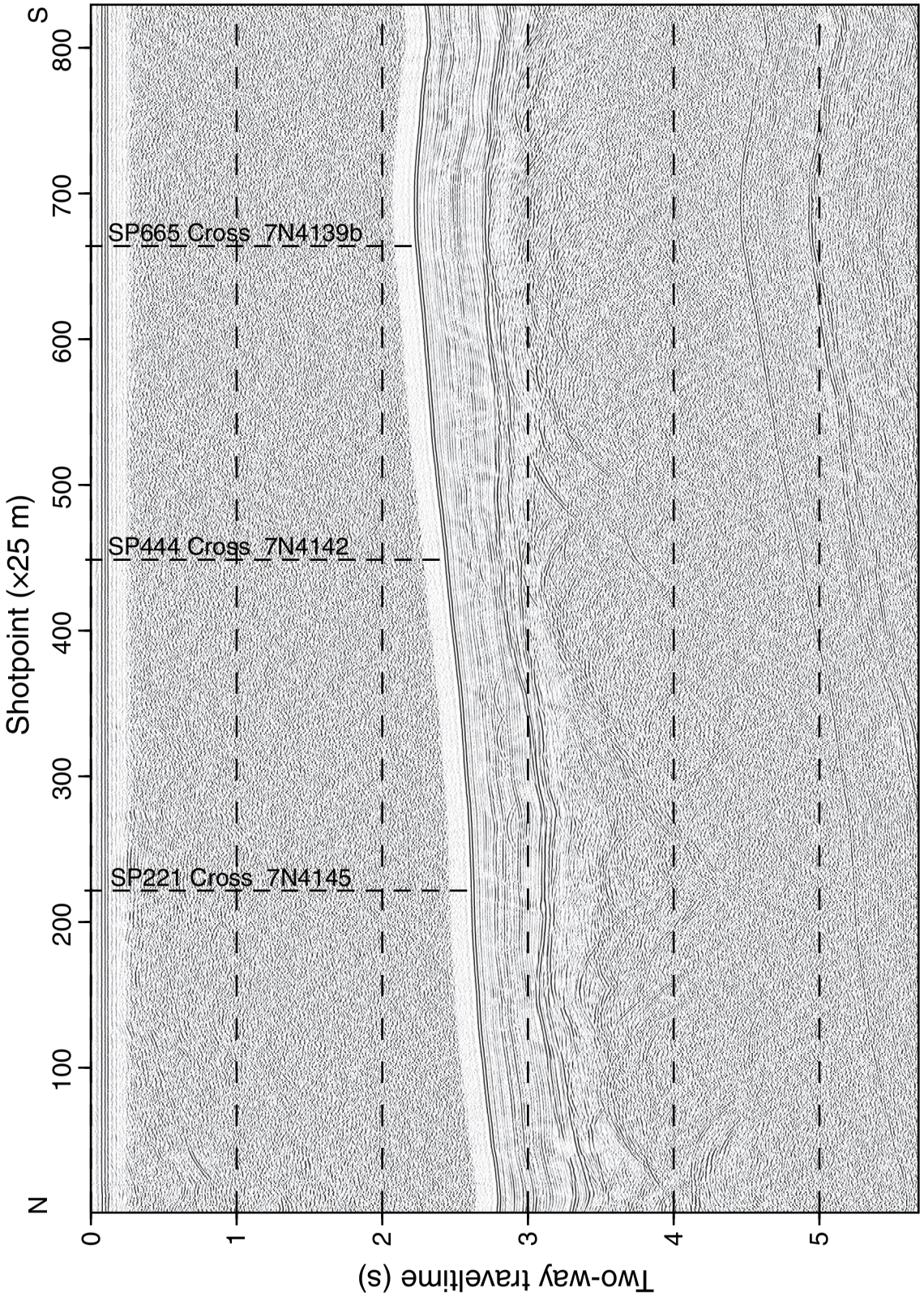

Figure AF5. Primary seismic Line 7E13905, proposed Site JB-2. SP = shotpoint.

Figure AF6. Seismic crossing Line 7N4142, proposed Site JB-2. SP = shotpoint.

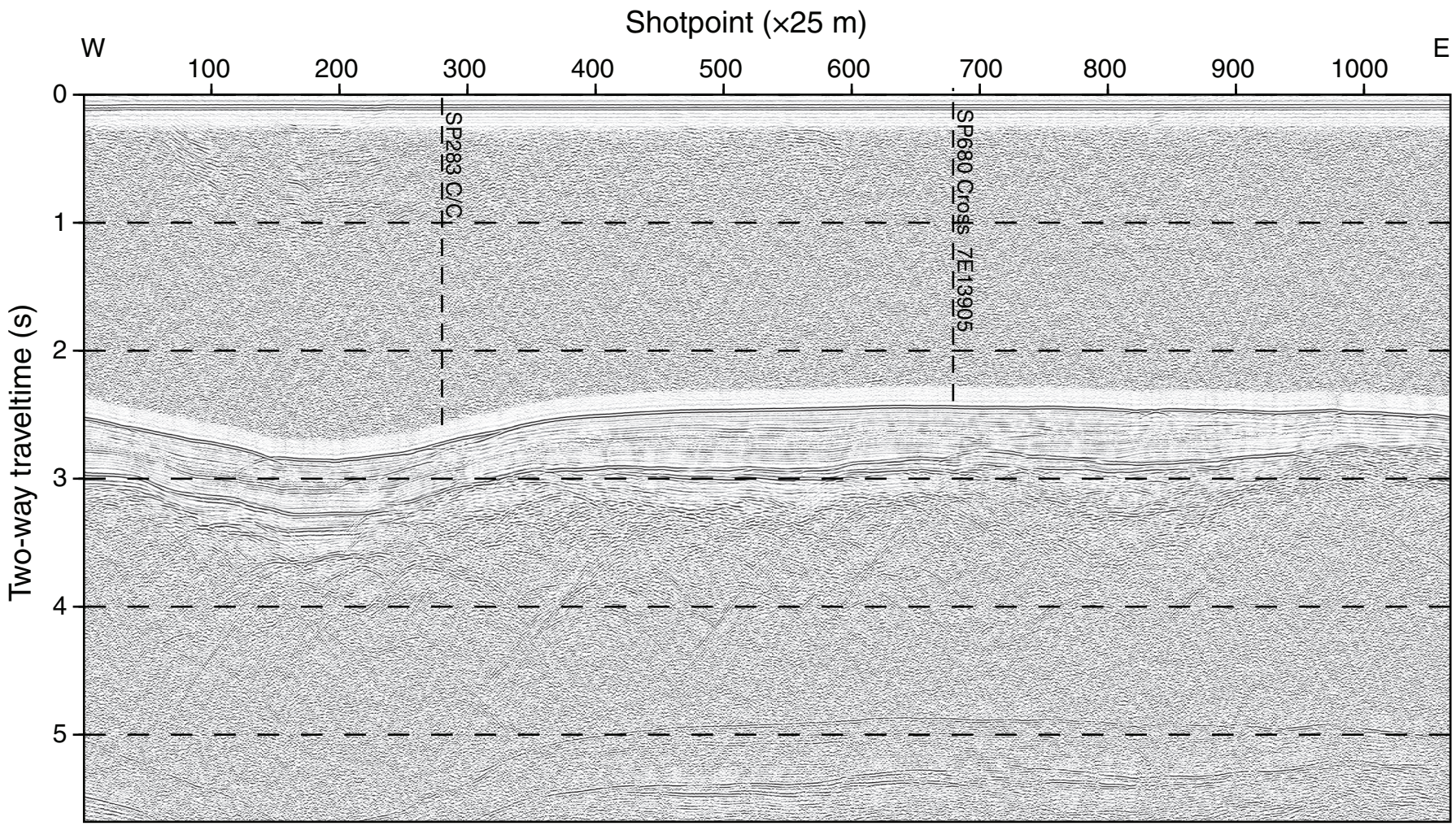

Figure AF7. Bathymetry and site track map, proposed Site JB-1.

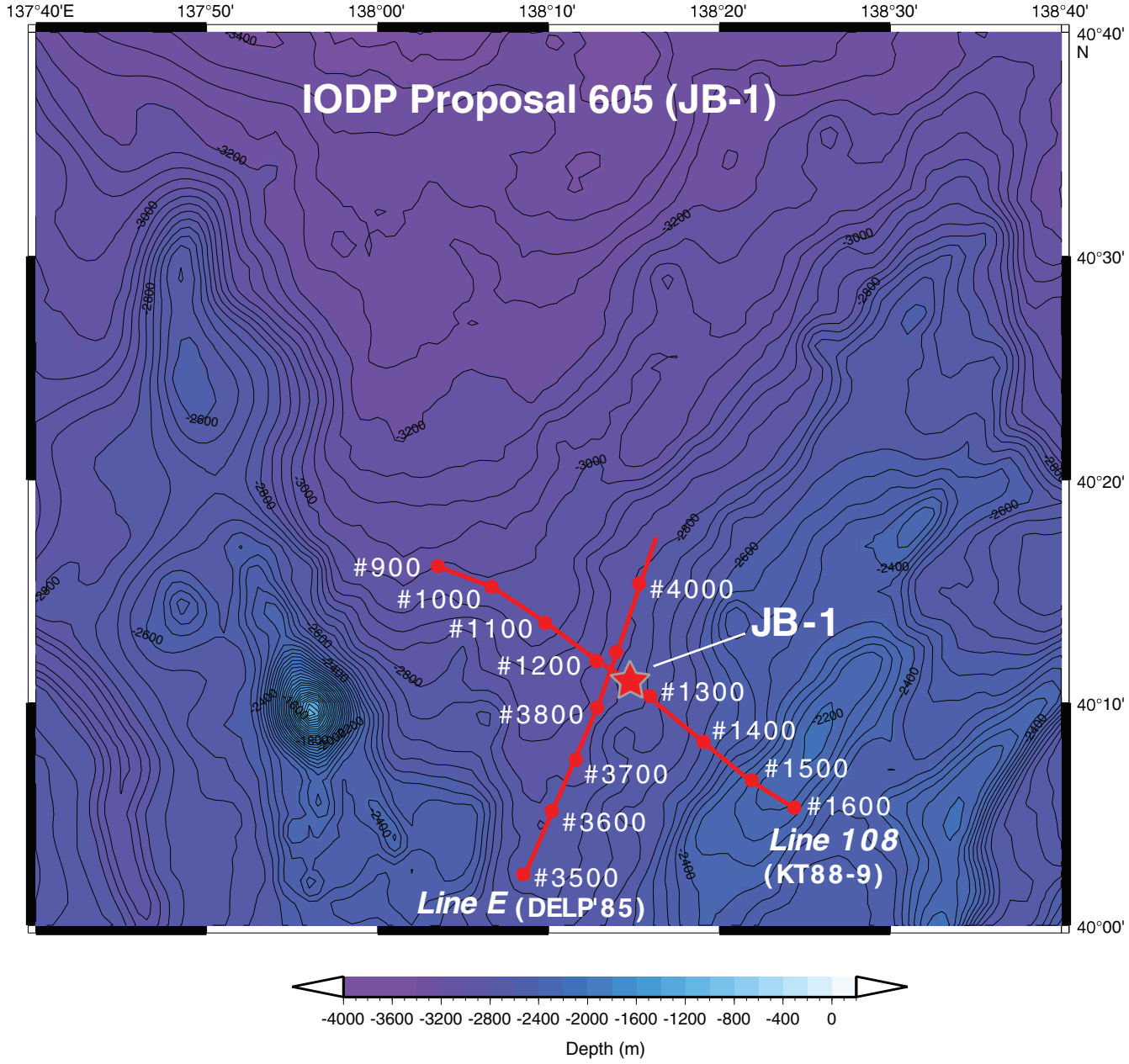

Figure AF8. Primary seismic Line 108, proposed Site JB-1.

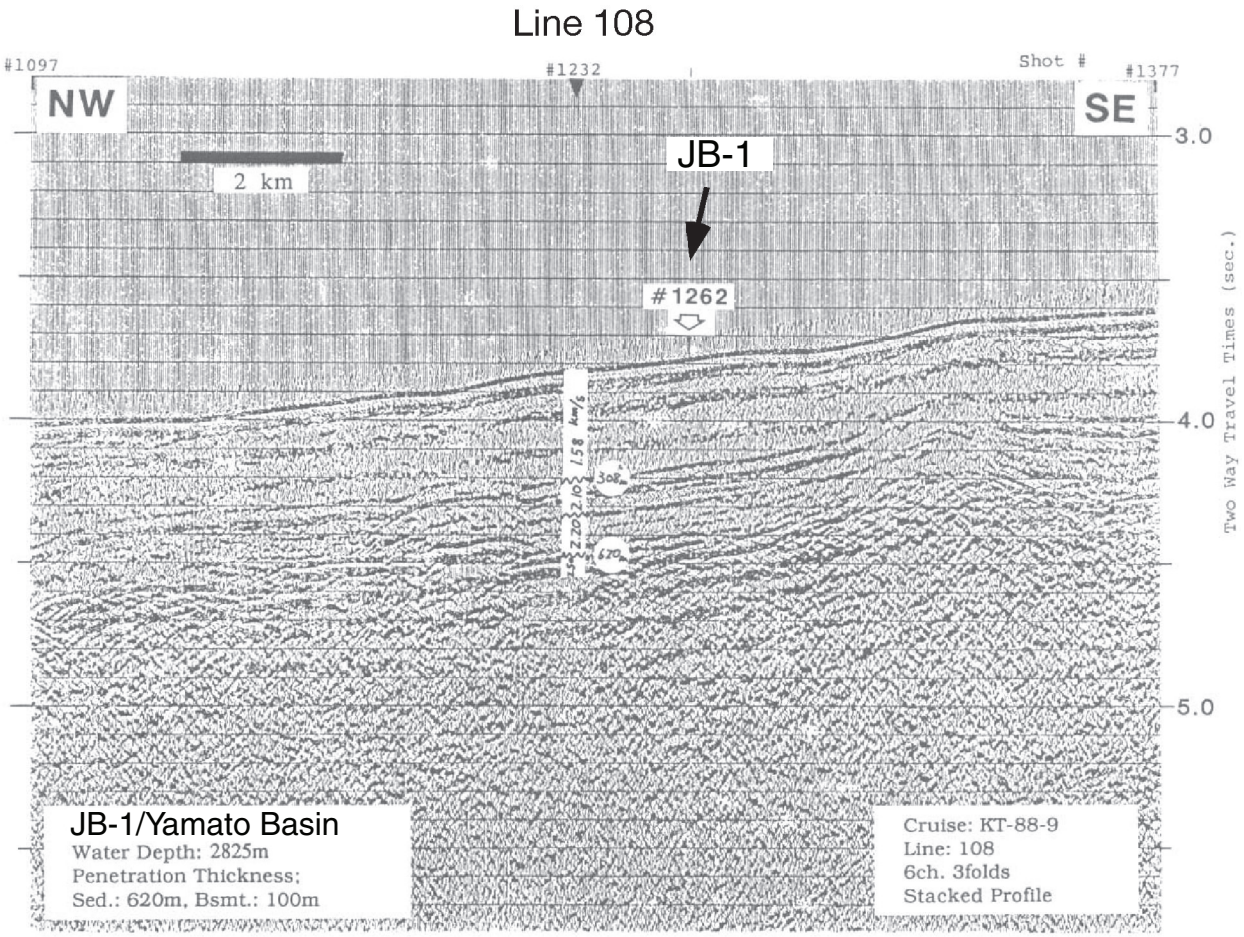

Figure AF9. Seismic crossing Line E, proposed Site JB-1.

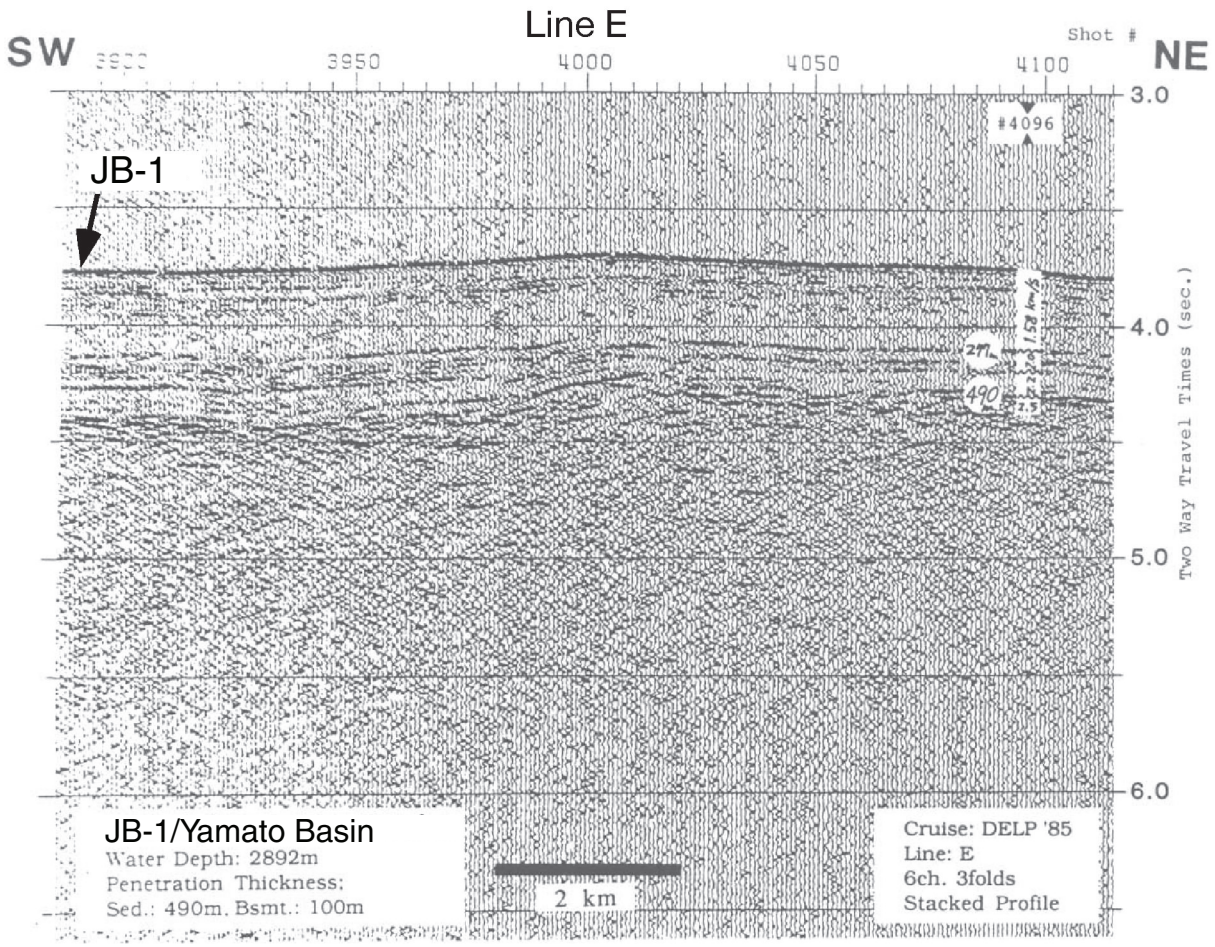

Figure AF10. Bathymetry and site track map, proposed Site YR-1.

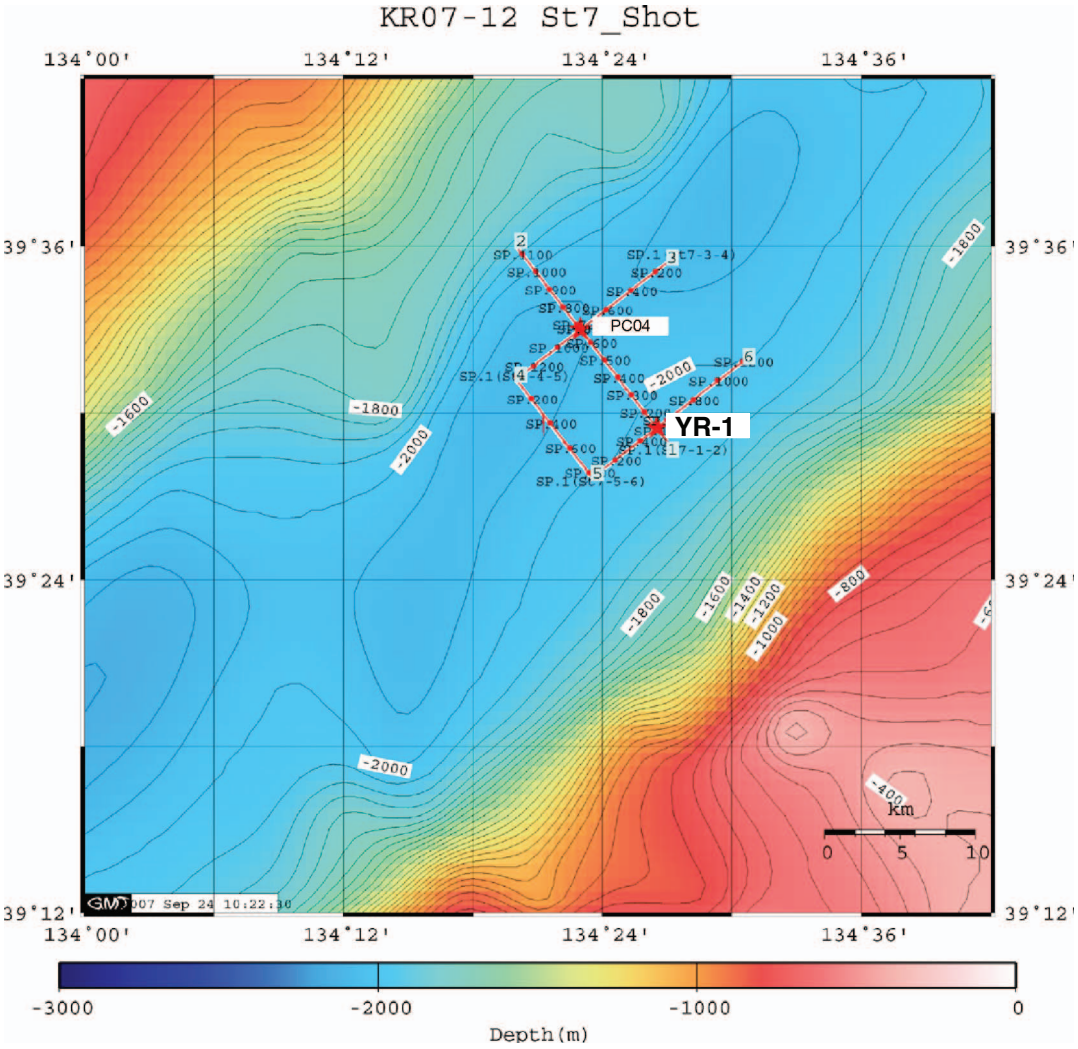

Figure AF11. Primary seismic Line St7 1-2, proposed Site YR-1.

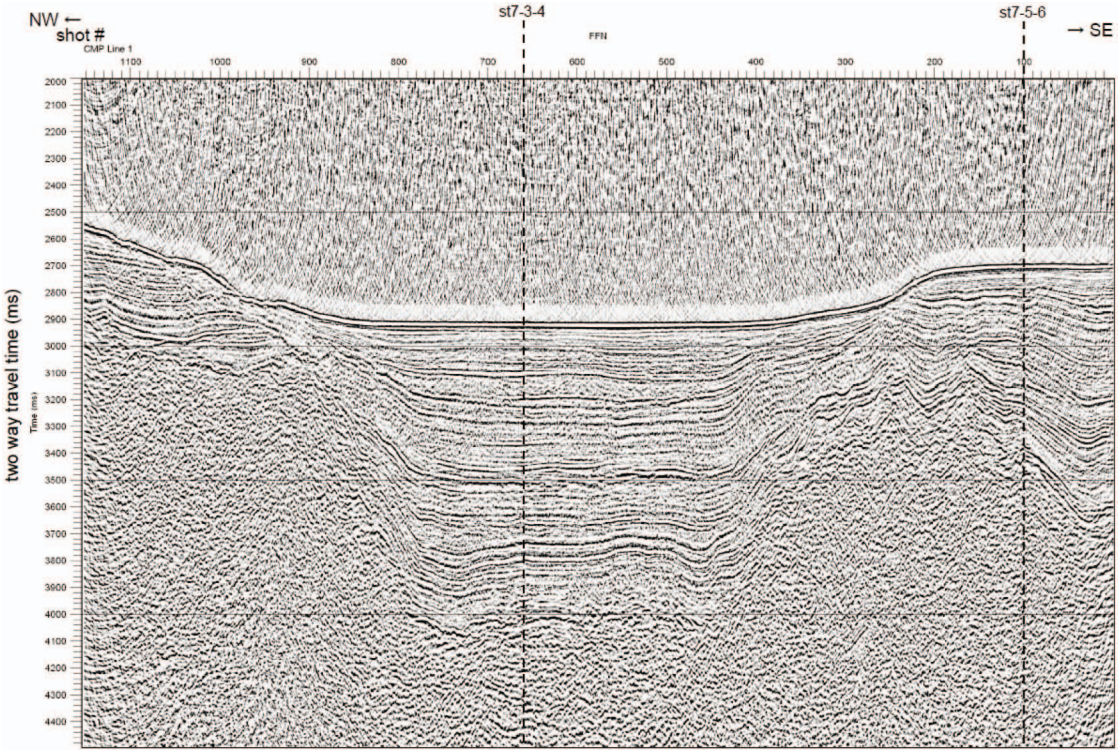

Figure AF12. Seismic crossing Line 5-63, proposed Site YR-1.

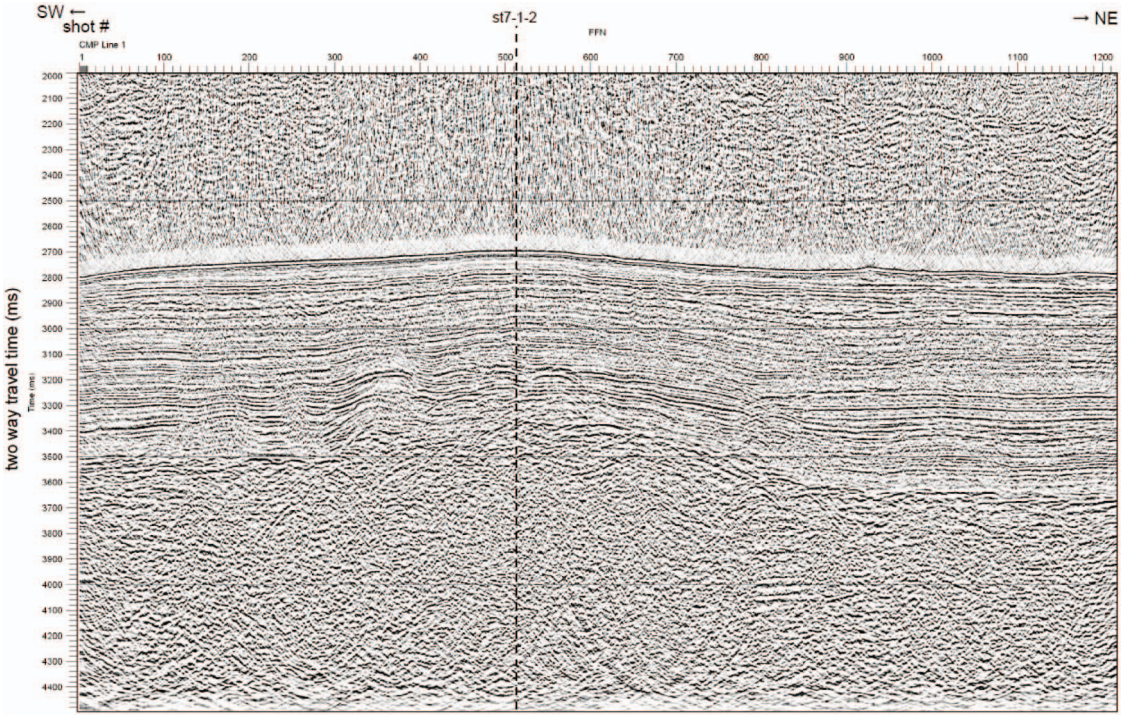

Figure AF13. Primary seismic Line JS-2, proposed Site YB-2.

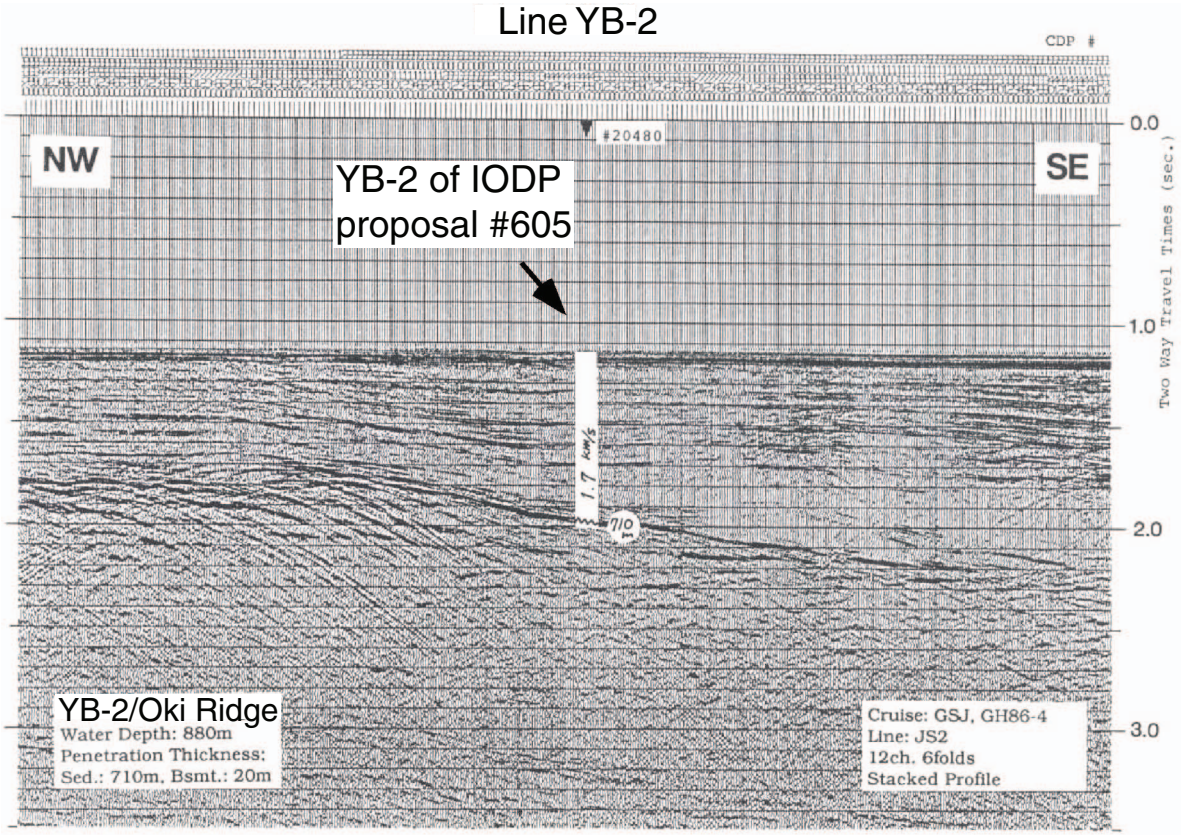

Figure AF14. Track map, proposed Site YB-2.

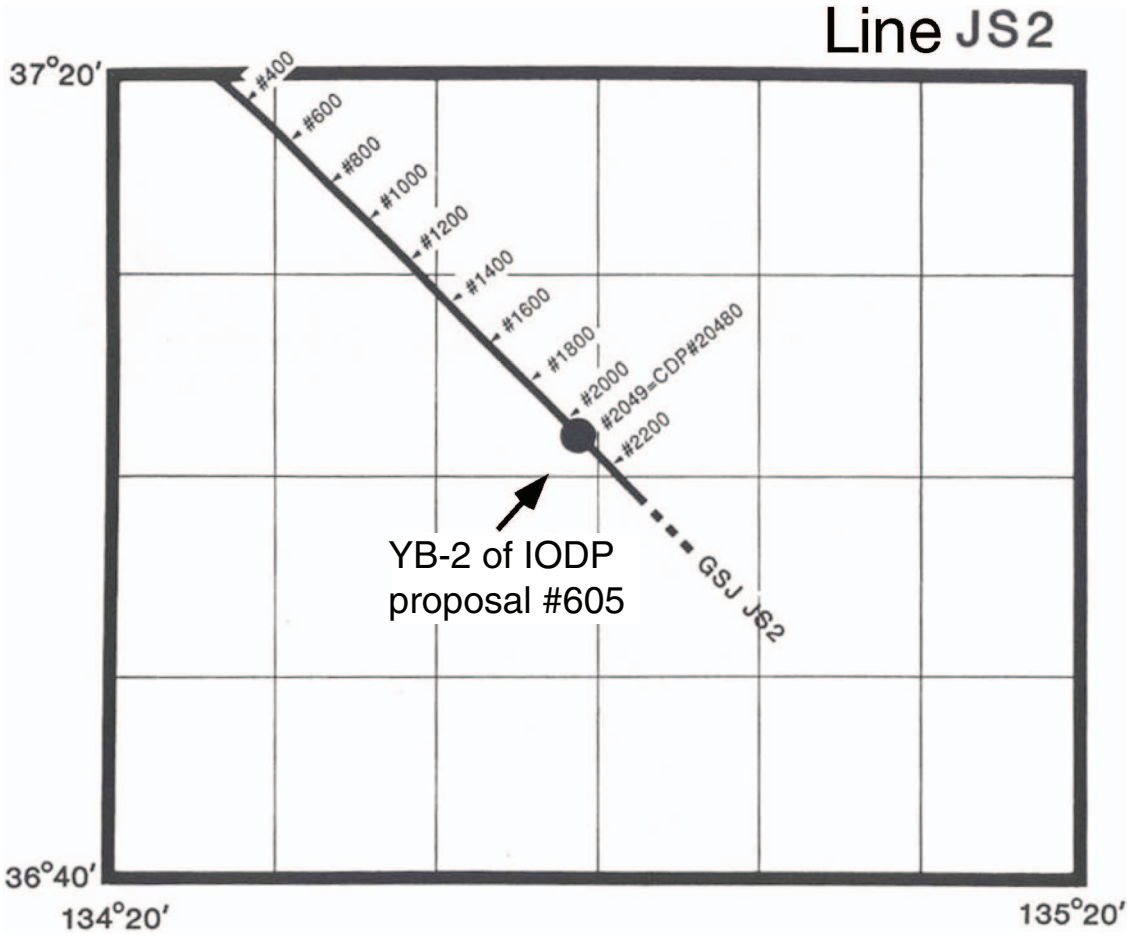

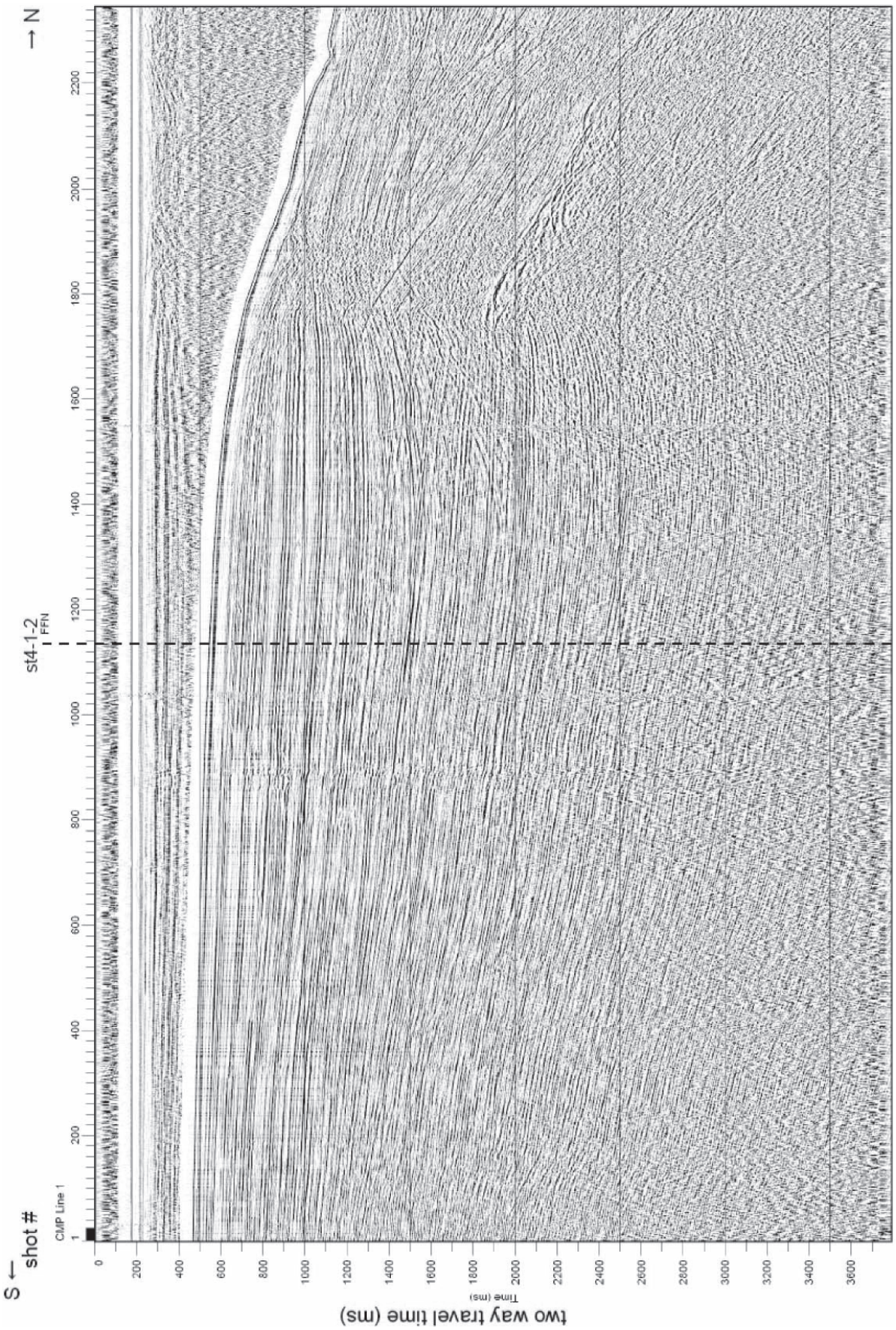

Figure AF15. Primary seismic Line 3-4-3, proposed Site YB-1.

Figure AF16. Crossing seismic Line 1-2-3, proposed Site YB-1.

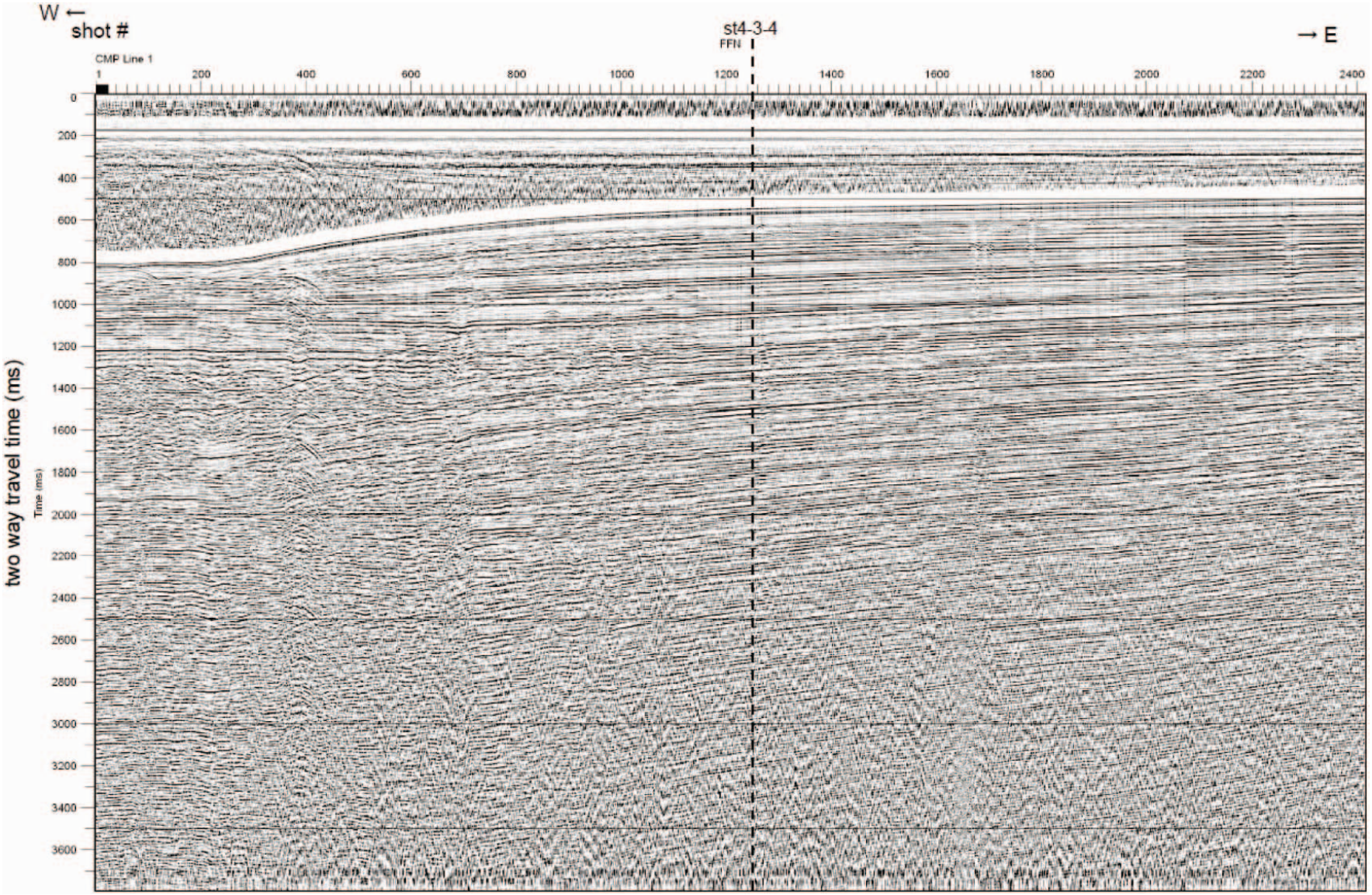

Figure AF17. Bathymetry and site track map, proposed Site YB-1.

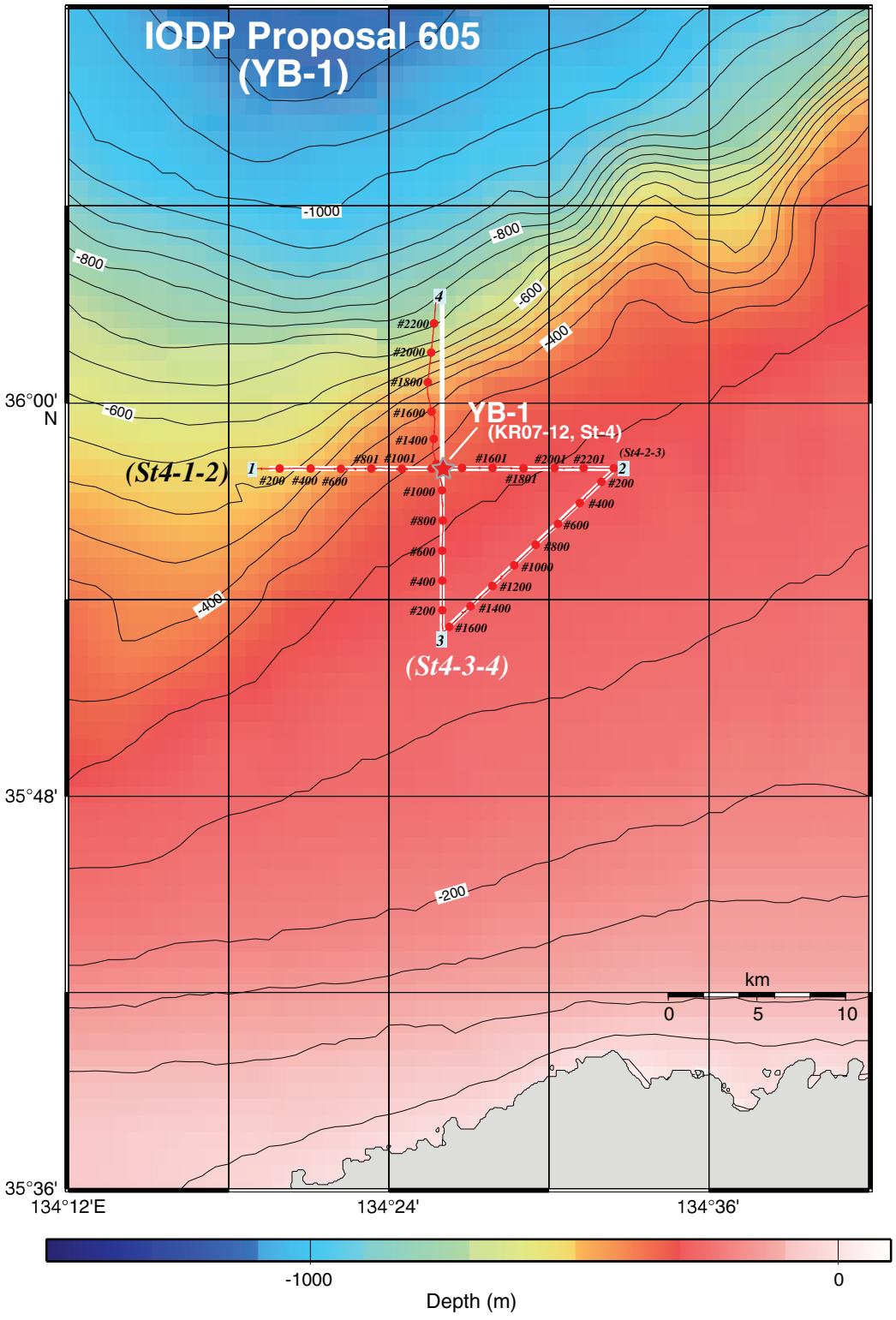

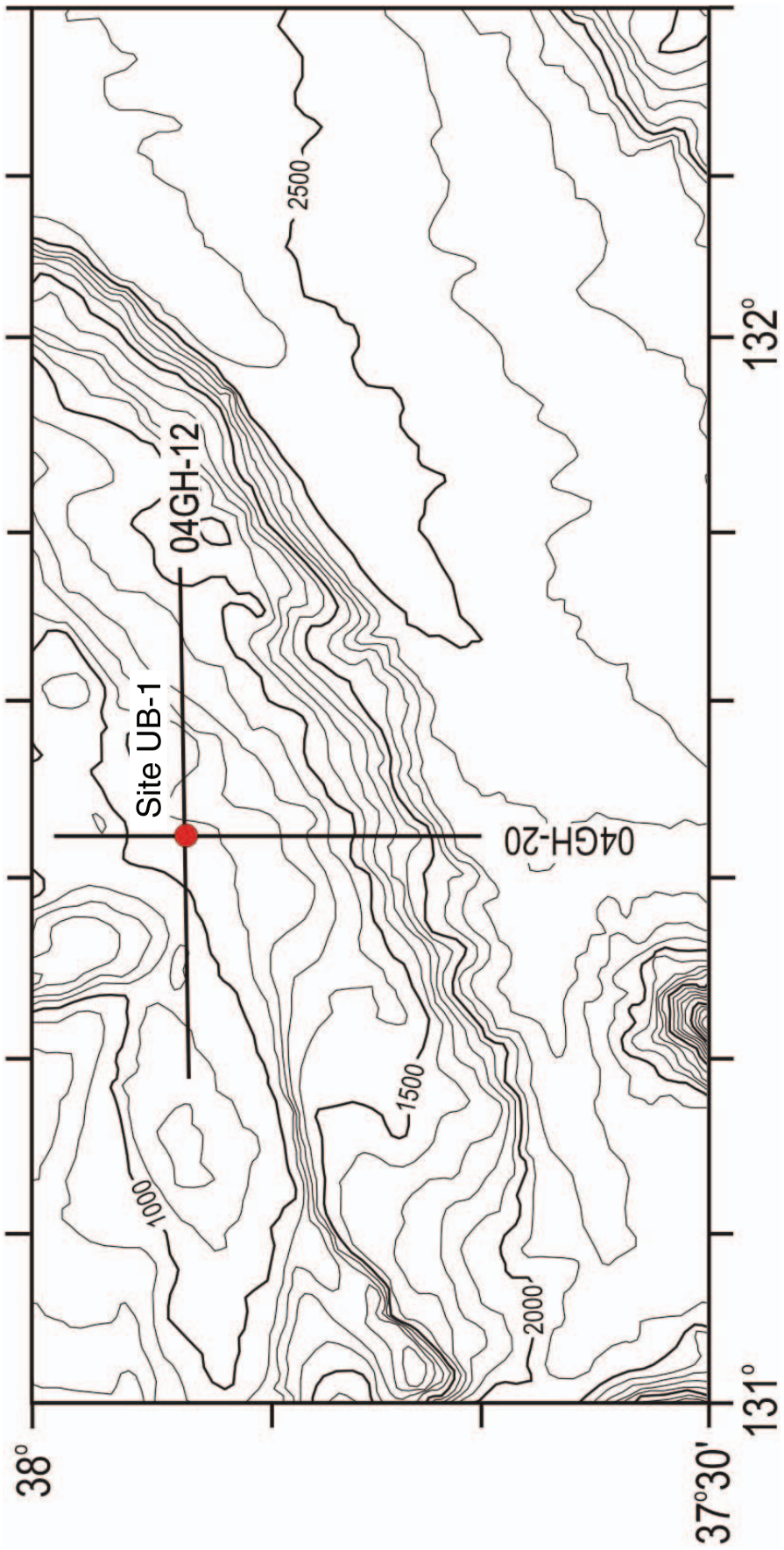

Figure AF18. Bathymetry and site track map, proposed Site UB-1.

Figure AF19. Primary seismic Line 04GH-12, proposed Site UB-1.

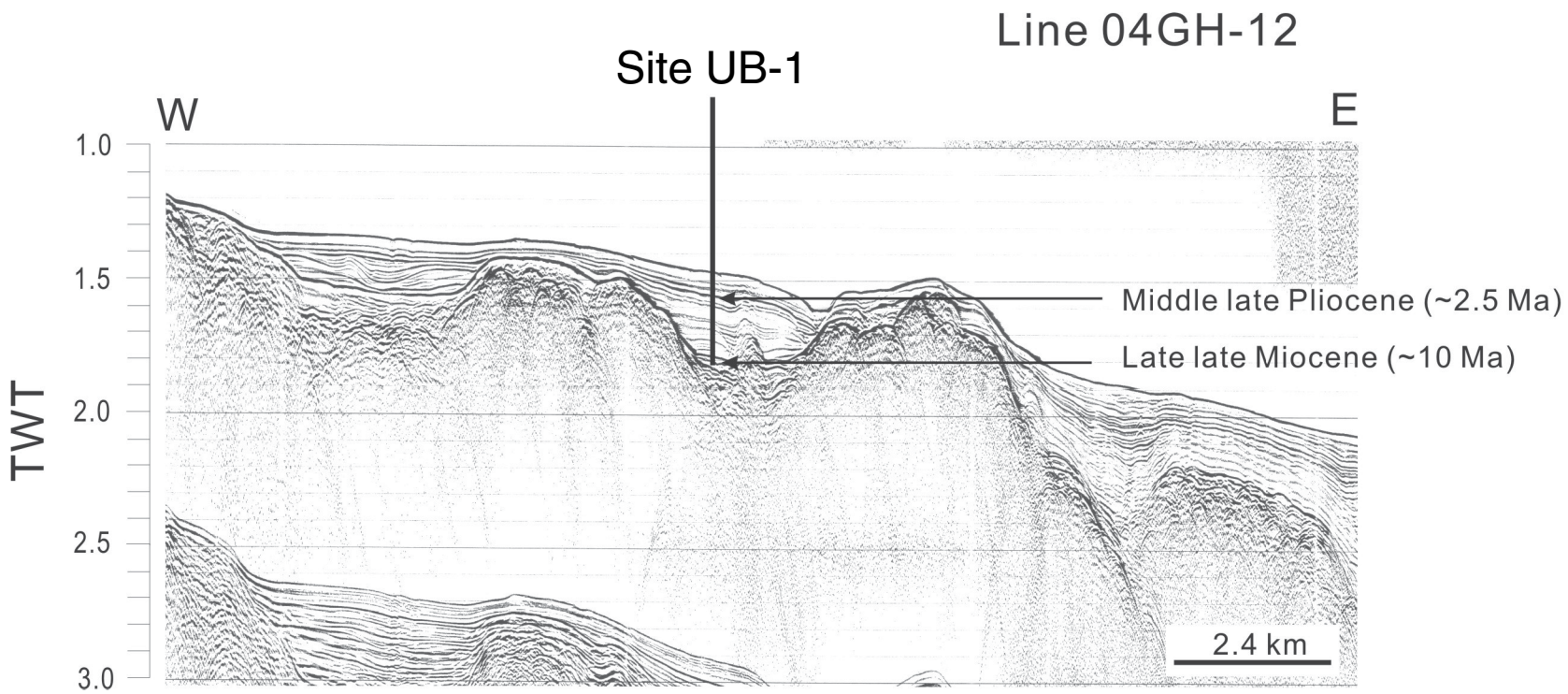

Figure AF20. Crossing seismic Line 04GH-20, proposed Site UB-1.

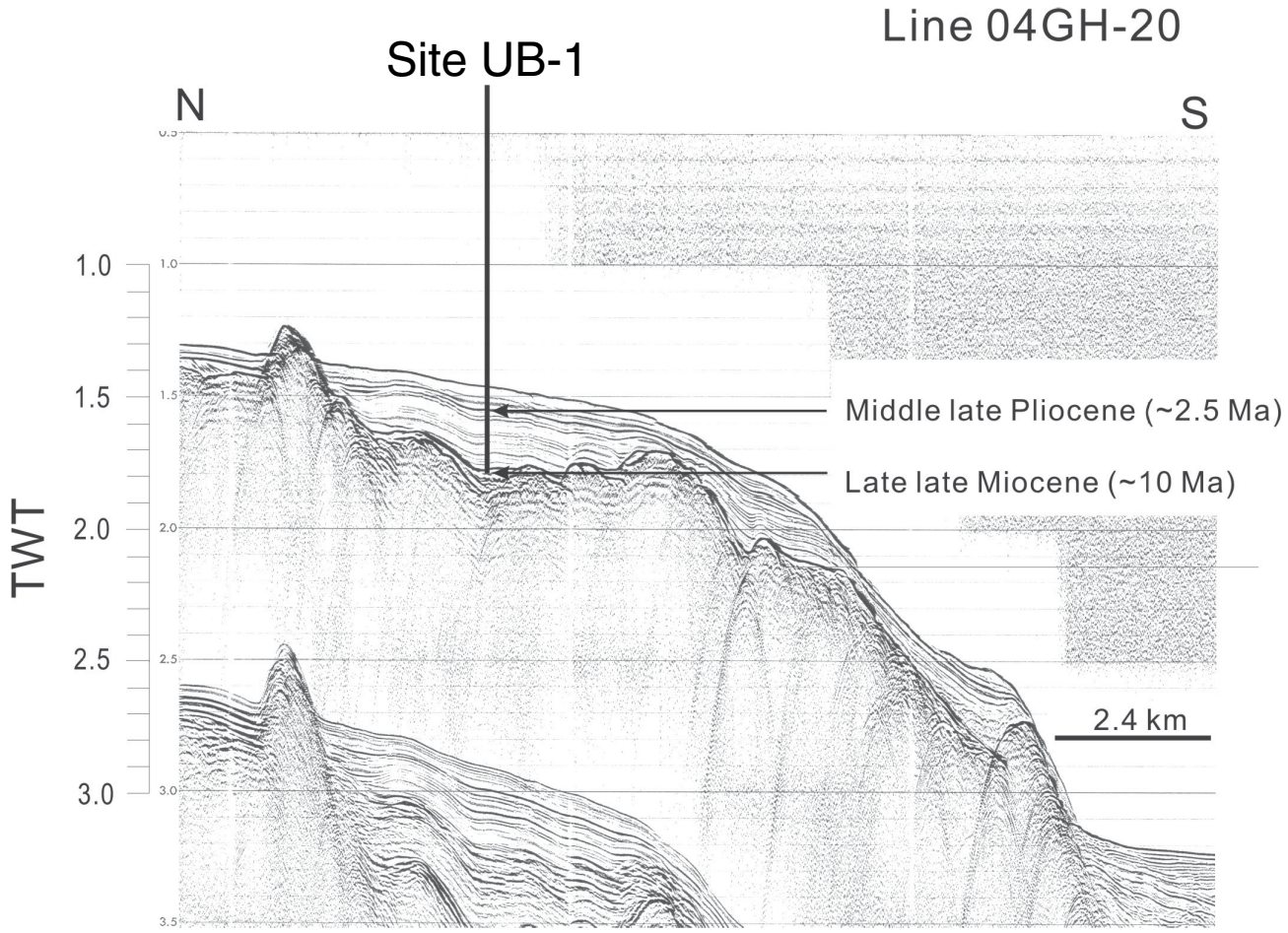

Figure AF21. Primary seismic Line St2-1-2, proposed Site ECS-1B.

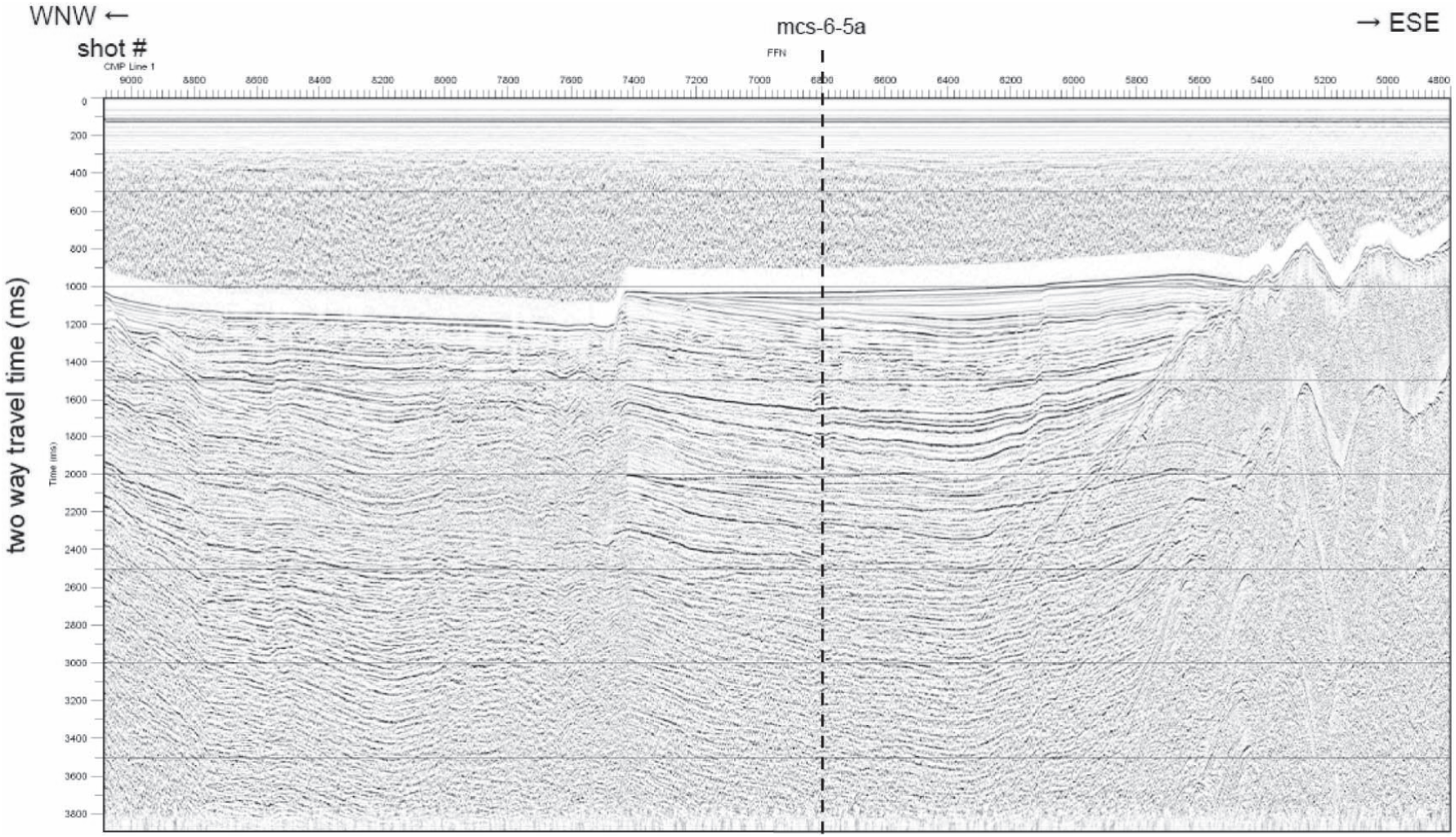

Figure AF22. Crossing seismic Line St2-5-6, proposed Site ECS-1B.

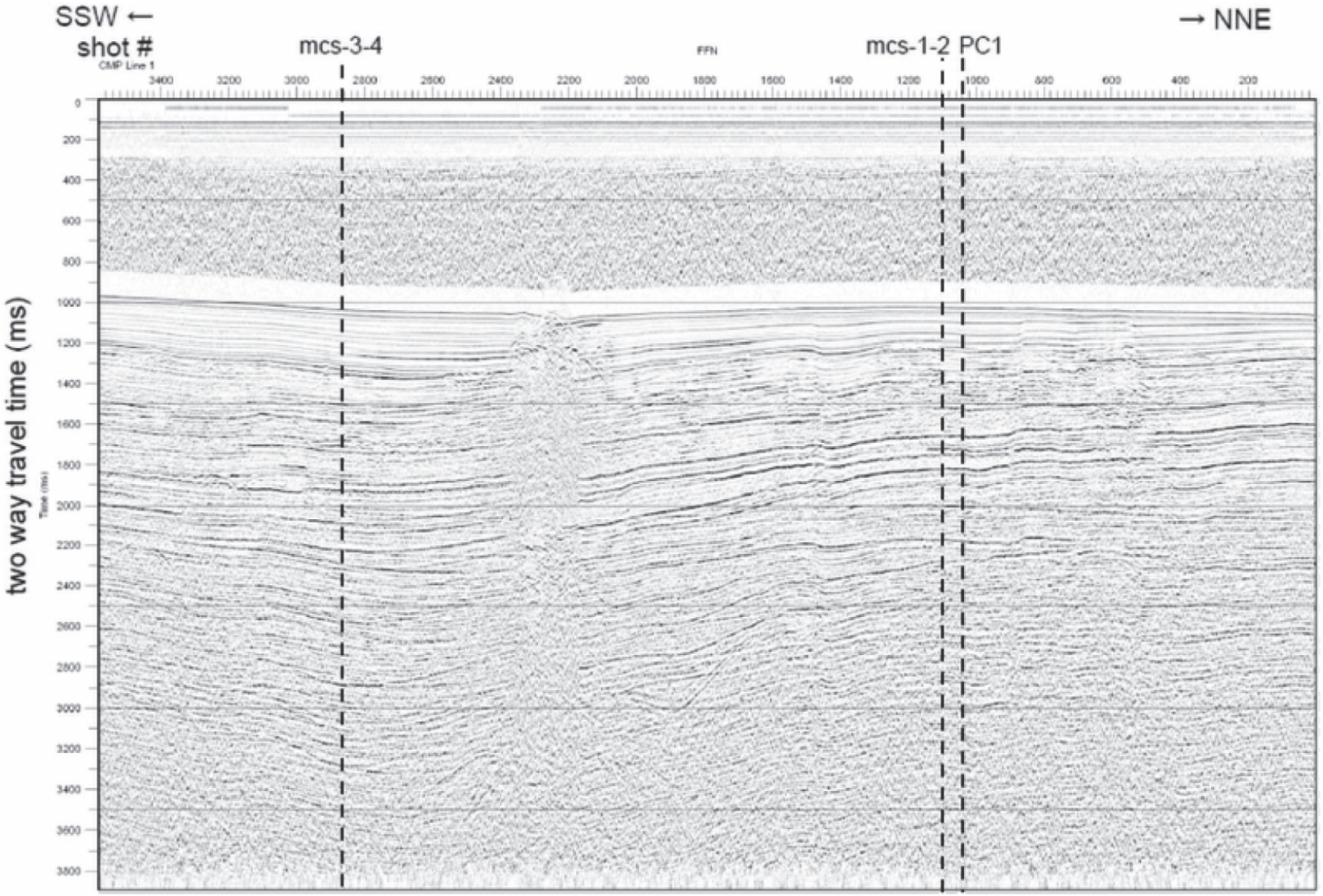

Figure AF23. Bathymetry and site track map, proposed Site ECS-1B.

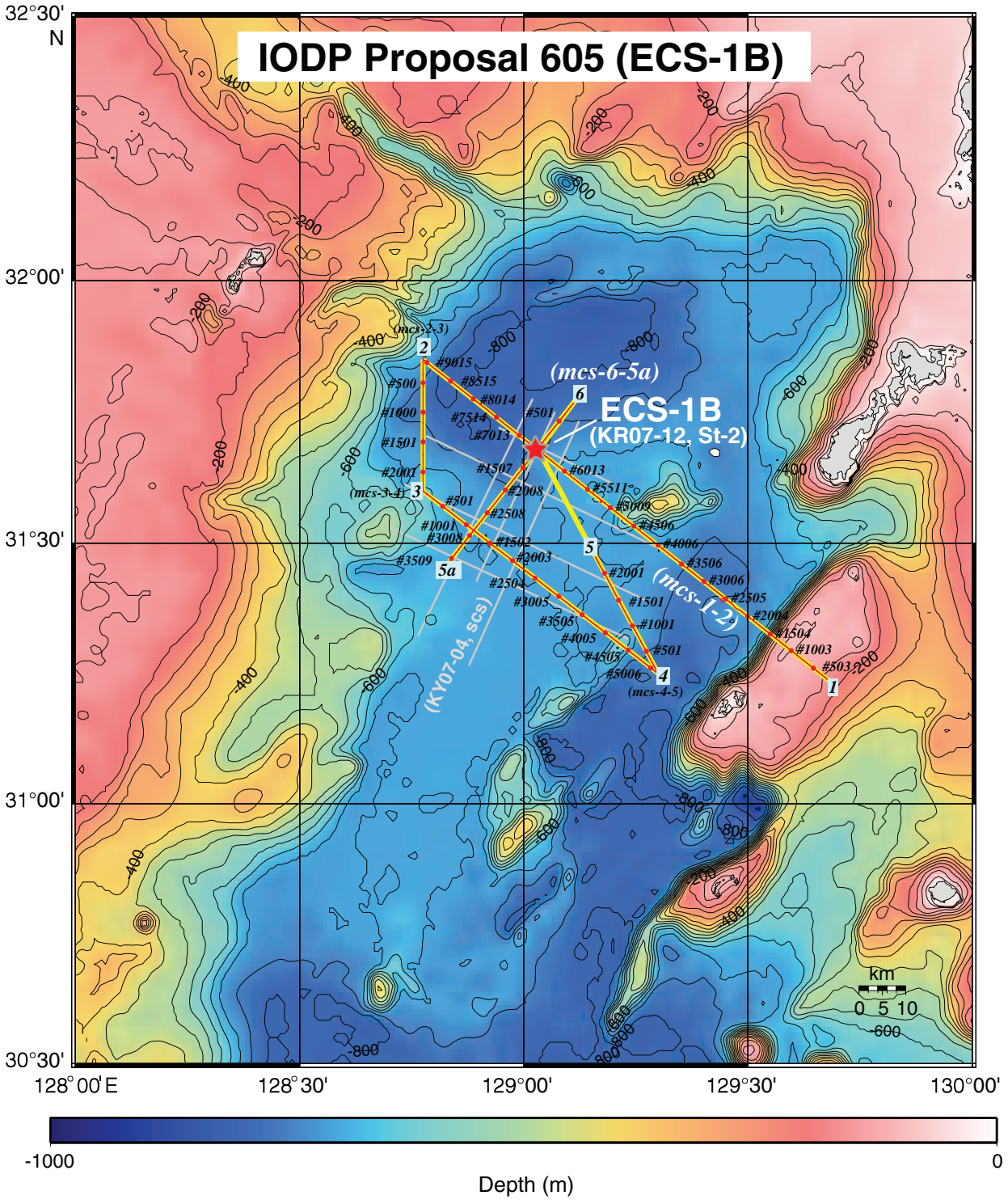

Figure AF24. Primary seismic Line St8-1-2, proposed Site YB-3.

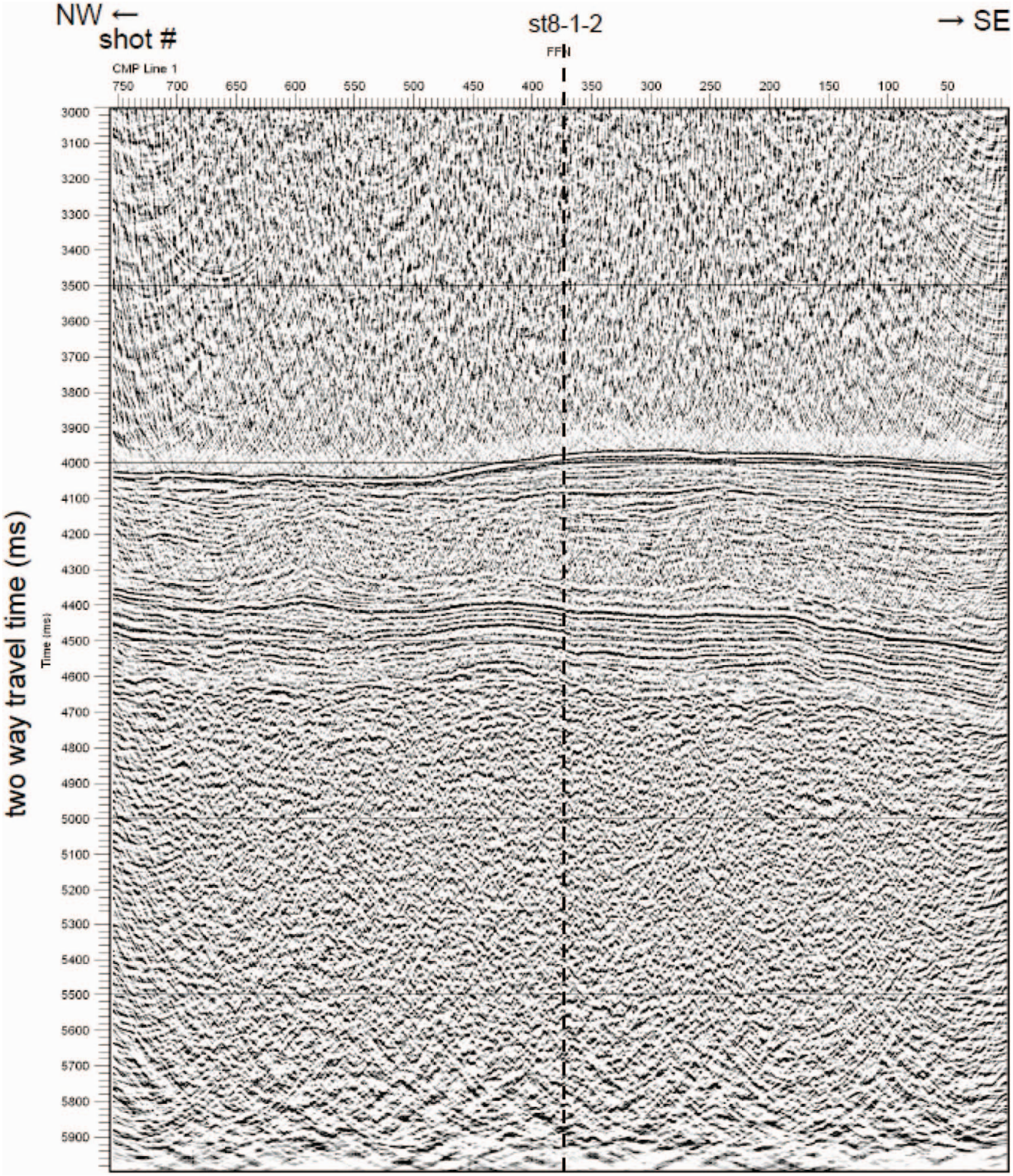

Figure AF25. Crossing seismic Line St8-3-4, proposed Site YB-3.

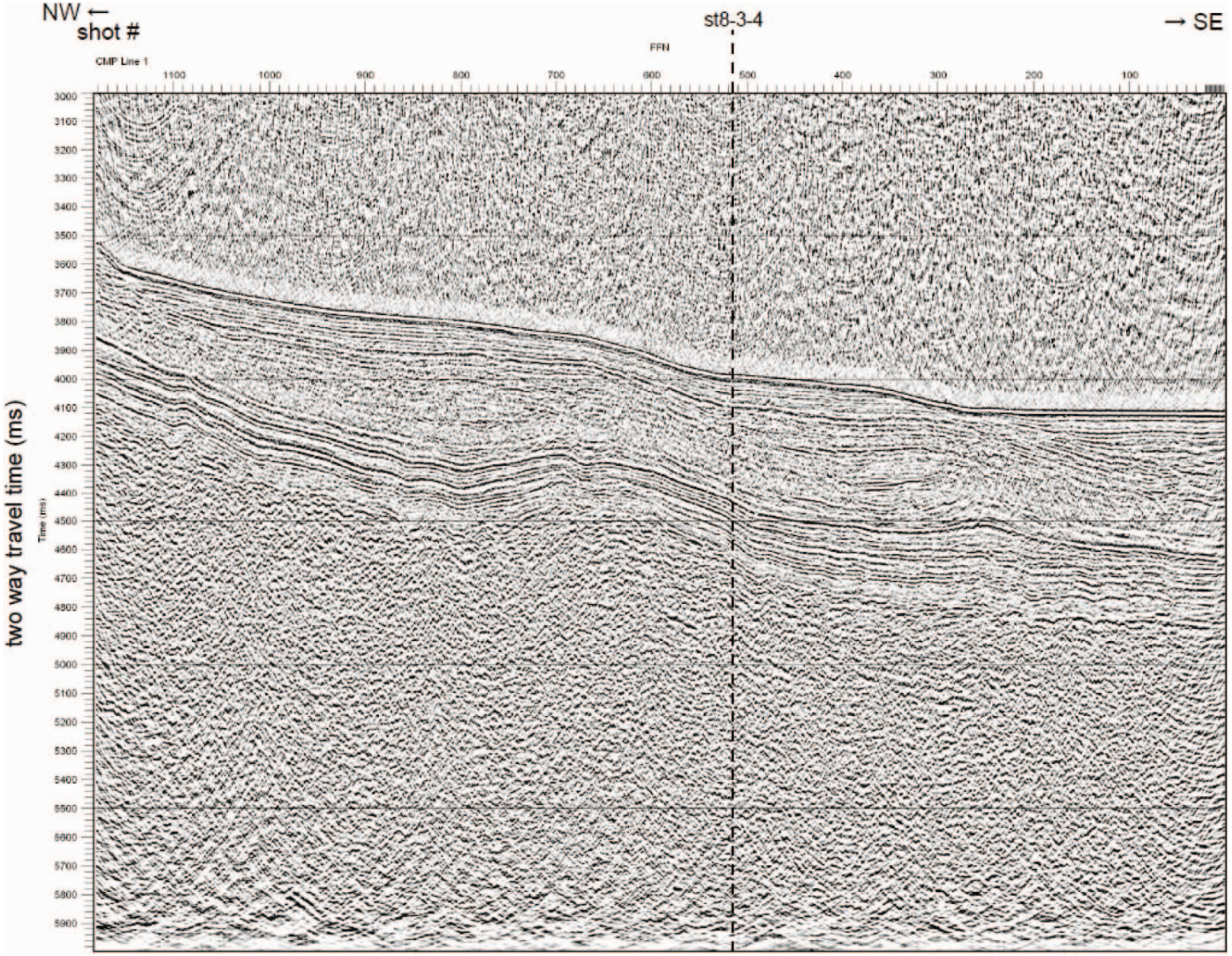

Figure AF26. Bathymetry and site track map, proposed Site YB-3.

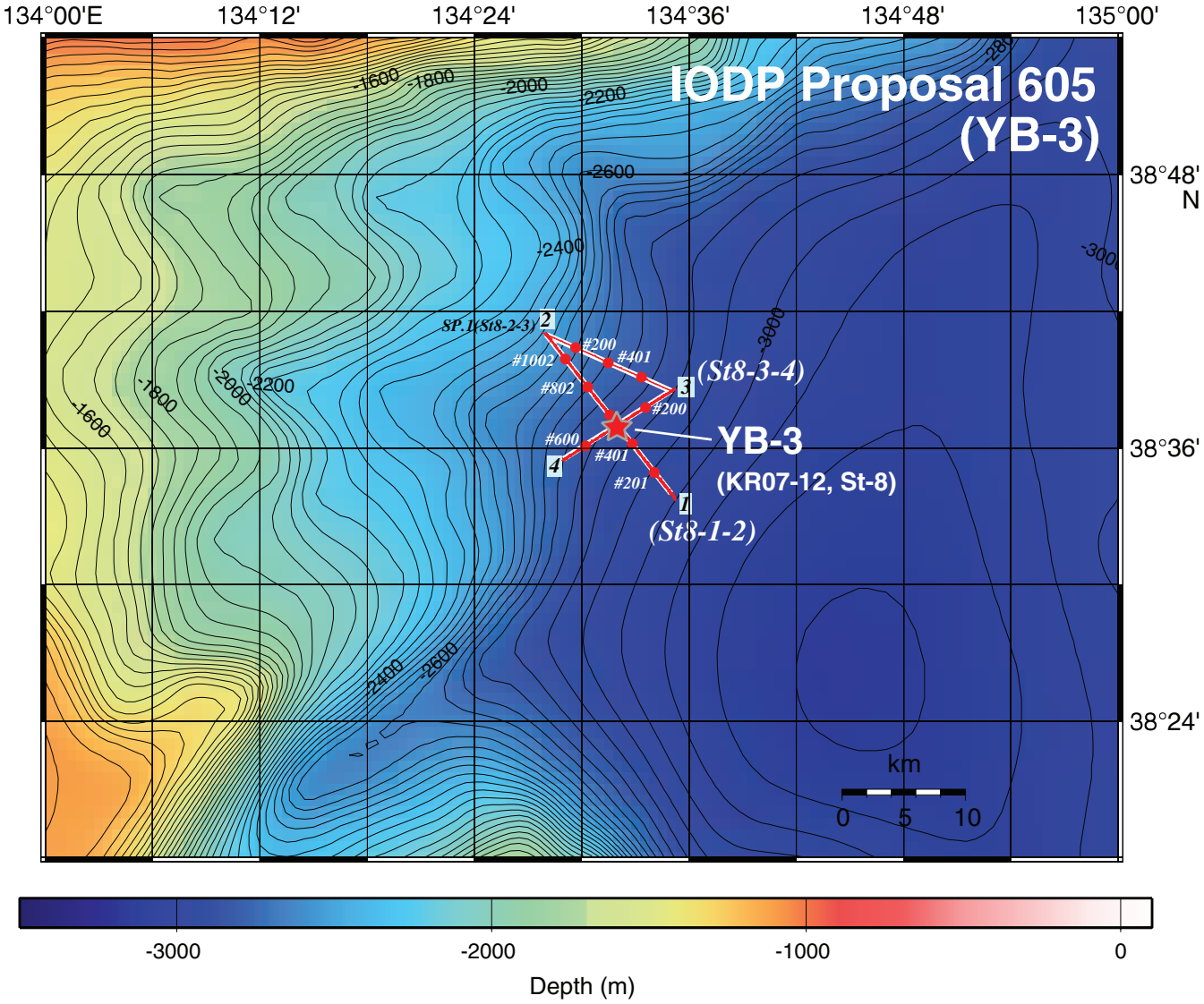

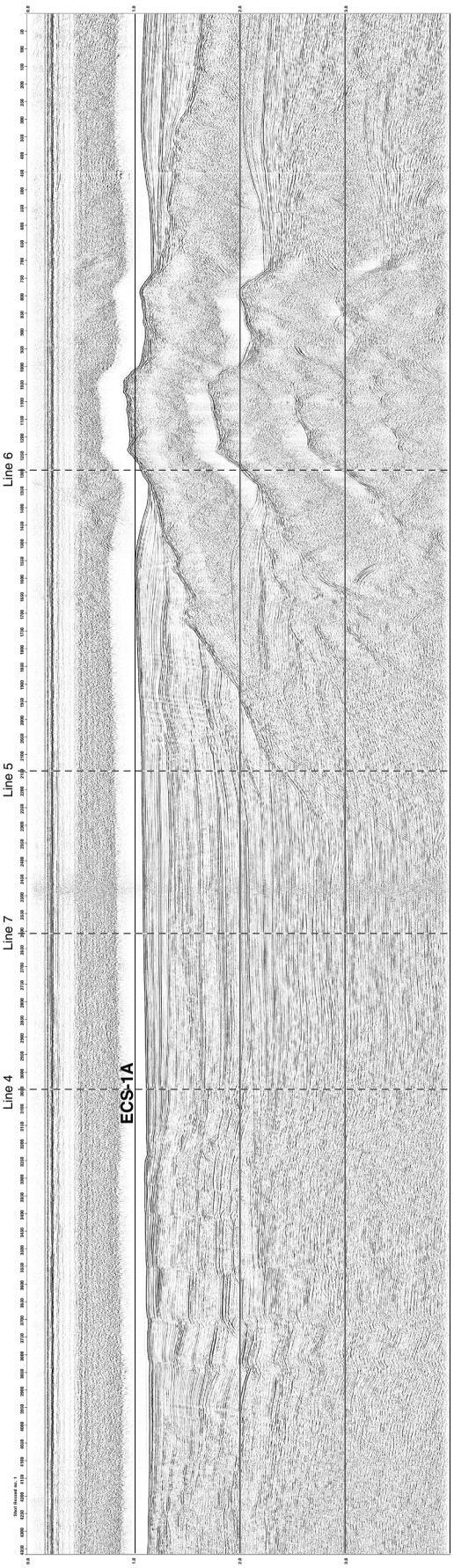

Figure AF27. Cross-section of seismic Line 1, proposed Site ECS-1A.

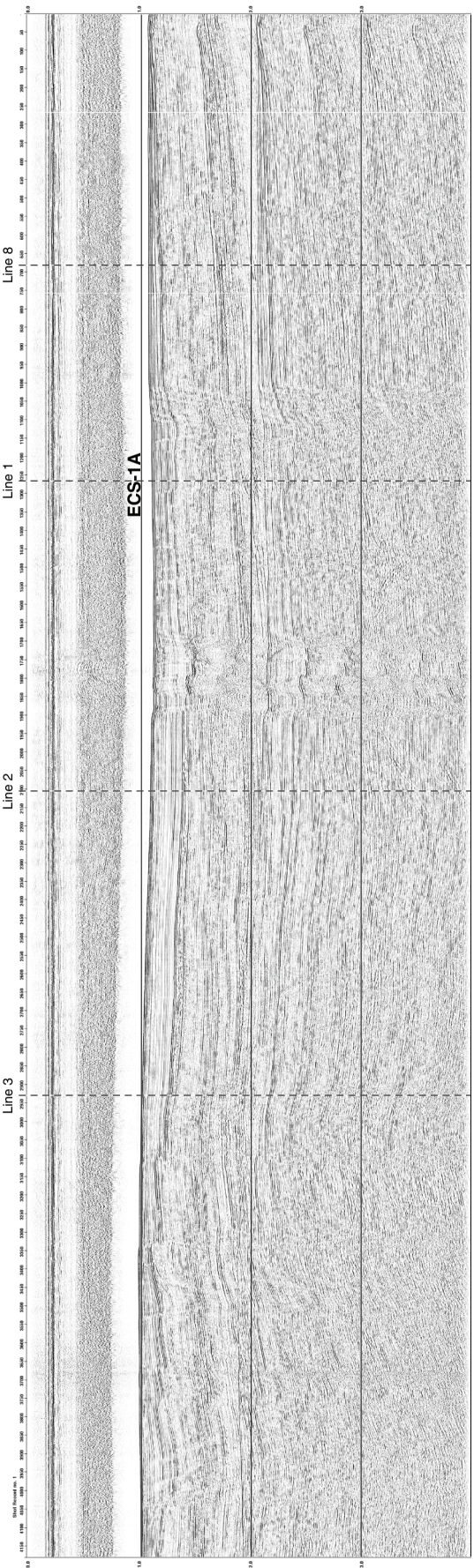

Figure AF28. Cross-section of seismic Line 4, proposed Site ECS-1A.

Figure AF29. Bathymetry and site track map, proposed Site ECS-1A.

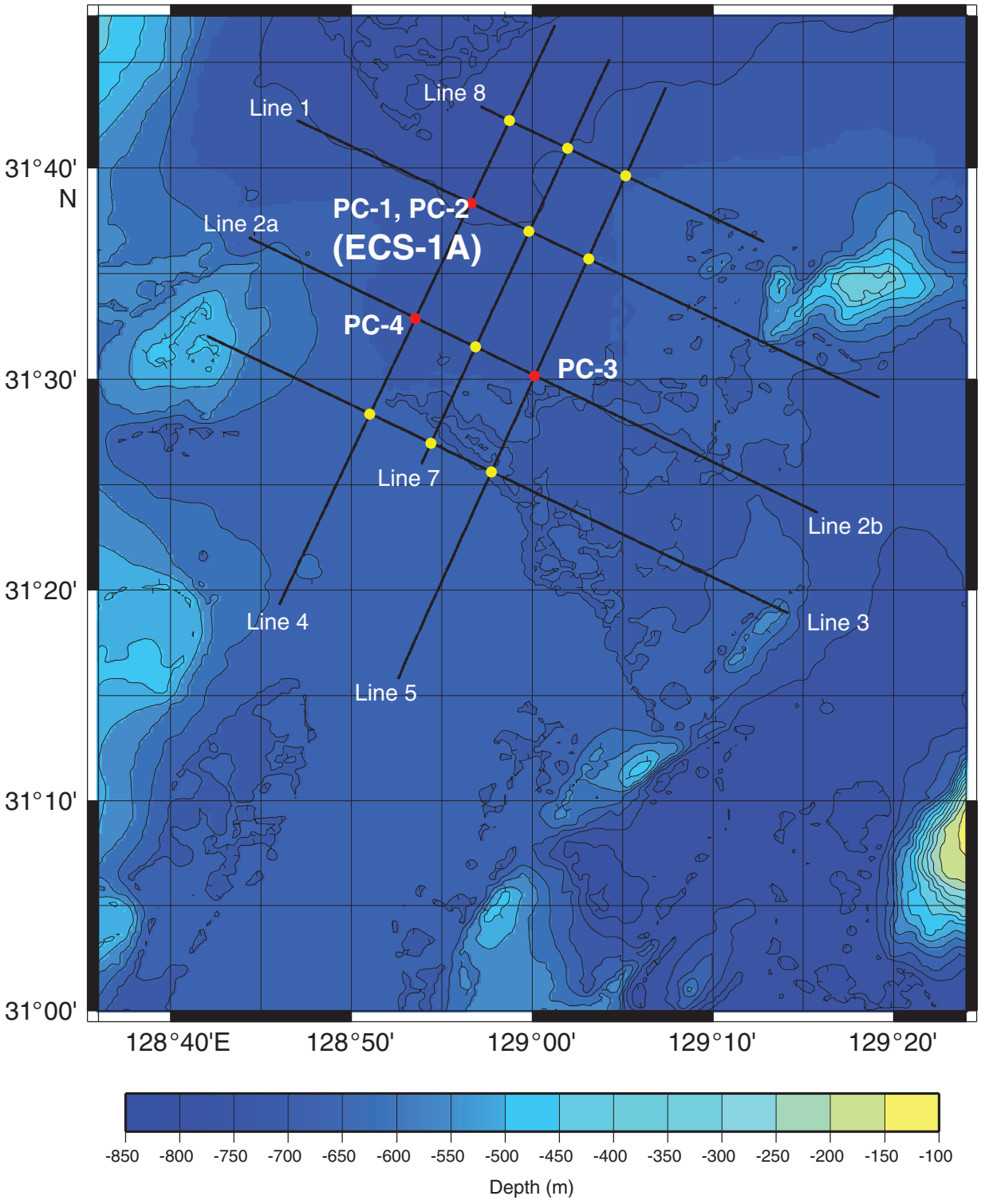

Scientific participants

The current list of participants for Expedition 346 can be found at **iodp.tamu.edu/scienceops/expeditions/asian_monsoon.html.**